MODELING AND PERFORMANCE IMPROVEMENTS OF A PRESSURE COMPENSATED AXIAL PISTON PUMP

A THESIS SUBMITTED TO
THE GRADUATE SCHOOL OF NATURAL AND APPLIED SCIENCES
OF
MIDDLE EAST TECHNICAL UNIVERSITY

BY

OKAN AYDOĞAN

IN PARTIAL FULFILLMENT OF THE REQUIREMENTS
FOR
THE DEGREE OF MASTER OF SCIENCE
IN
MECHANICAL ENGINEERING

MAY 2018

Approval of the thesis:

MODELING AND PERFORMANCE IMPROVEMENTS OF A PRESSURE COMPENSATED AXIAL PISTON PUMP

submitted by **OKAN AYDOĞAN** in partial fulfillment of the requirements for the degree of **Master of Science in Mechanical Engineering, Middle East Technical University** by,

Prof. Dr. Halil KALIPÇILAR _____
Dean, Graduate School of **Natural and Applied Sciences**

Prof. Dr. M. A. Sahir ARIKAN _____
Head of Department, **Mechanical Engineering**

Prof. Dr. R. Tuna BALKAN _____
Supervisor, **Mechanical Engineering Dept., METU**

Examining Committee Members

Assoc. Prof. Dr. Yiğit YAZICIOĞLU _____
Mechanical Engineering Dept., METU

Prof. Dr. R. Tuna BALKAN _____
Mechanical Engineering Dept., METU

Assoc. Prof. Dr. M. Metin YAVUZ _____
Mechanical Engineering Dept., METU

Assist. Prof. Dr. Ulaş YAMAN _____
Mechanical Engineering Dept., METU

Prof. Dr. Yücel ERCAN _____
Mechanical Engineering Dept., TOBB ETÜ

Date: **31.05.2018**

I hereby declare that all information in this document has been obtained and presented in accordance with academic rules and ethical conduct. I also declare that, as required by these rules and conduct, I have fully cited and referenced all material and results that are not original to this work.

Name, Last name : Okan AYDOĞAN

Signature :

ABSTRACT

MODELING AND PERFORMANCE IMPROVEMENTS OF A PRESSURE COMPENSATED AXIAL PISTON PUMP

AYDOĞAN, Okan

M.Sc., Department of Mechanical Engineering

Supervisor: Prof. Dr. R. Tuna BALKAN

May 2018, 94 Pages

Analysis of internal dynamics of a pressure compensated axial piston pump has an importance to predict the pump characteristics. In order to accomplish this mission physical model is developed to simulate pump pressure-flow characteristics for a given set of system parameters in Matlab/Simulink environment. The pump is modeled as two main groups, namely, pumping section, and compensation section. Pistons are orderly nested in cylinder block around shaft axis in the pump. In the pumping section model, multi-piston models arranged with a phase shift according to the piston number, $2\pi/N$. The model includes leakages from these pistons. Forces on individual pistons are used to model the instantaneous hydraulic torque acting on the swash plate. Individual flow rates generated by movements of the pistons determine the instantaneous delivery flow of the pump. The pressure compensation section consists of a three-way valve, a bias actuator, a control actuator, and a swash plate. Dynamics of these components are also modeled in detail. Hence, the developed

model represents a handy computational tool to get pump dynamics for various system parameters.

An experimental setup is built to measure discharge pressure and delivery flow of the pump. In order to adjust discharge pressure of the pump, pump outlet port is loaded with an adjustable needle valve which covers the entire working range. Simulation results obtained by using the developed model are compared with experimental results to verify the model. Using this model, various configurations are further examined to obtain their effects on oscillations of pressure and flow.

The aim of this work is to obtain performance improvements related with geometric dimensioning of pump internal parts. Three different configurations obtained by setting the angle of kidney-shaped flow passage area on the valve plate are used in the physical model to investigate their influence on the pump dynamics, especially leakages, and oscillations in pressure, flow, and torque. Smoother pressure transitions in piston chamber are obtained by utilizing line to line porting valve plate as opposed to using the original valve plate. The improvement in piston chamber pressure eliminates flow peaks when the piston aligns with the delivery port. As a result of this improvement, the oscillation amplitude of delivery flow is reduced. This improvement also reduces the hydraulic torque on swash plate due to pumping action. Even, lower torques are obtained by utilizing a smaller trap angle than the angles used in both original valve plate and line to line porting valve plate. Hence, the control actuator areas can be reduced for the same working pressure, resulting in lower package volumes for the pump.

Keywords: Swash Plate, Flow Oscillation, Torque Oscillation

ÖZ

BASINÇ KOMPANZASYONLU EKSENEL PİSTONLU BİR POMPANIN MODELLENMESİ VE PERFORMANS İYİLEŞTİRİLMESİ

AYDOĞAN, Okan

Yüksek Lisans, Makina Mühendisliği Bölümü

Tez Yöneticisi: Prof. Dr. R. Tuna BALKAN

Mayıs 2018, 94 Sayfa

Basınç kompanzasyonlu eksenel pistonlu bir pompanın iç dinamiklerinin analizi bu pompanın karakteristiği öngörebilmek için öneme sahiptir. Bu misyonu başarmak amacıyla set halinde verilen sistem parametrelerinin uygulandığı pompanın basınç–debi karakteristiğinin benzetimi için Matlab/Simulink ortamında fiziksel bir model geliştirilmiştir. Pompa, basınçlandırma bölümü ve dengeleme bölümü olmak üzere iki ana grup olarak modellenmektedir. Pistonlar, pompanın içinde mil eksenin etrafında silindir bloğu içinde düzenli yuvalanmaktadır. Basınçlandırma bölümü modeli, piston sayısına göre bir faz farkı, $2\pi/N$, ile düzenlenmiş birçok piston modelini içermektedir. Model bu pistonlara ait sızıntıları kapsamaktadır. Pistonların üzerindeki kuvvetler, eğim plakasına uygulanan anlık hidrolik torkun modellenmesi için kullanılmaktır. Pistonların hareketine bağlı meydana gelen ait tekil debiler, pompa anlık debi karateristiğini belirlemektedir. Basınç dengeleme bölümü üç yollu valf, değiştirme eyleyicisi, kontrol eyleyicisi ve eğim plakasından meydana gelmektedir. Bu elemanların dinamikleri detaylı bir şekilde incelenmektedir.

Dolayısıyla geliştirilen model, farklı sistem parametreleri için pompa dinamiğini elde etmek için kullanışlı bir hesaplama aracını temsil etmektedir.

Pompanın çıkış basıncının ve çıkış debisinin ölçümü için bir test düzeneği kurulmuştur. Çalışma basıncının ayarlanması için pompanın çıkış portu, tüm çalışma aralığını ayarlayabilecek bir kısma valfiyle yüklenir. Geliştirilen modelden elde edilen benzetim sonuçlarıyle test sonuçları modeli doğrulamak amacıyla karşılaştırılmıştır. Ayrıca bu model kullanarak farklı konfigürasyonların basınç ve debi salınımları elde edilerek farklılıkların etkileri incelenmiştir.

Bu çalışmanın amacı pompanın iç elemanlarını geometrik ölçülendirilerek performans iyileştirmelerinin elde edilmesidir. Fiziksel modele valf plakası üzerindeki kavisli kanal şeklindeki akış alanı açısı ayarlanarak elde edilen üç farklı konfigürasyon uygulanarak bunların pompa dinamiğine, özellikle kaçaklar ve basınç, debi ve tork salınımları, etkileri incelenmiştir. Piston odasındaki daha düzgün basınç geçişleri, orijinal valf plakasının aksine uçtan uca valf plakasında elde edilir. Piston basınç odasında elde edilen bu iyileştirme pistonun basma portu ile aynı eksene geldiği anda oluşan debi tepesini yok etmiştir. Bu gelişmenin bir sonucu olarak, çıkış debisi salınım genliği azalır. Bu iyileştirme ayrıca basınçlandırma hareketi sonucu oluşan eğim plakası üzerinde hidrolik torku düşürür. Hatta, her iki uçtan uca valf plakası ve orijinal valf plakasında kullanılan açılardan daha düşük geçiş açıları uygulanarak daha düşük torklar elde edilir. Dolayısıyla kontrol eyleyici alanları aynı çalışma basıncı için azaltılabilir; bu da pompa için daha düşük paket hacimlerine olanak tanır.

Anahtar Kelimeler: Eğim Plakası, Debi Salınımı, Tork Salınımı

To my family

ACKNOWLEDGEMENTS

First of all, I would like to express my sincere appreciation to my thesis supervisor Prof. Dr. R. Tuna BALKAN for his guidance throughout my thesis study.

I would like thank to Prof. Dr. Bülent E. PLATİN, Mr. Celal SELAMOĞLU, and Mr. Şeref SET for their guidance and affords throughout the study. It was a pleasure and honor to work with them.

The support of the Scientific and Technological Research Council of Turkey (TÜBİTAK) should be acknowledged for funding me with National Scholarship Program for MSc Students.

I wish to express my sincere thanks to my family.

Finally, I would like to express my gratitude to my beloved wife Ms. Elif AYDOĞAN for her patience, support, and understanding throughout my Master's Science student life.

TABLE OF CONTENTS

LIST OF TABLES

TABLES

LIST OF FIGURES

FIGURES

NOMENCLATURE

a	Distance between pistons spherical joint turning plane and swash plate in x-z plane	2.8	mm
Ap	Pumping piston area	23	mm^2
b	Distance between swivel axis and swash plate in x-z plane	2	mm
BSA	Kidney area of cylinder block	7.6	mm^2
c	Distance between pistons spherical joint turning plane and swash plate plane in x-y plane	3	mm
c_{rs}	Radial clearance between spool and sleeve	3.10^{-3}	mm
c_{rpc}	Radial clearance between bias actuator and cylinder	5.10^{-3}	mm
c_{spc}	Radial clearance between control actuator and cylinder	5.10^{-3}	mm
C_d	Discharge coefficient	0.65	-
C_v	Port velocity coefficient	0.98	-
d	Distance between swash plate axis and swash plate plane in x-y plane	2	mm
d_b	Diameter of bias piston	8.5	mm
d_c	Diameter of control piston	6.25	mm
d_d	Hole diameter through the piston	0.4	mm
d_{obr}	Hole diameter at side curved wall of rate piston	1.3	mm
d_p	Diameter of pumping piston	5.4	mm
d_{sp}	Diameter of spool land	1.84	mm

h_K	Radial clearance between cylinder block and piston	15.10^{-3}	mm
h_B	Radial clearance between cylinder block and valve plate	6.10^{-3}	mm
h_G	Radial clearance between swash plate and slipper	6.10^{-3}	mm
H	Radial clearance between ball and socket	1.10^{-3}	mm
I	Mass moment of inertia of yoke assembly with respect to the swivel axis	3.8	$kg.mm^2$
k_b	Stiffness of bias actuator spring	14	N/mm
k_{sp}	Stiffness of spool spring	20	N/mm
l_d	Length of the hole inside the pumping piston	5	mm
LR	Distance of the axes of the bores of bias actuator and control actuator from swivel axis	15	mm
m_b	Mass of bias actuator	5	g
m_c	Mass of control actuator	7	g
m_p	Mass of pumping piston	2	g
m_{sp}	Mass of spool	4	g
N	Number of pumping pistons	9	-
o_d	Initial overlap among control spool and sleeve	1	mm
P_a	Atmospheric pressure	1	bar

P_c	Drain pressure	5	bar
P_r	Reservoir pressure	1	bar
P_s	Suction port pressure	5	bar
r_{bi}	Inner radius of the kidney port on cylinder block	9	mm
r_{bo}	Outer radius of the slot on valve plate	10.5	mm
r_G	Inner radius of slipper pad	1.8	mm
r_o	Outer radius of ball joint on pumping piston	3	mm
r_p	Metering radius of spool	1.3	mm
R	Piston pitch radius of valve plate	10	mm
R_{bi}	Inner radius of the slot on valve plate	9.5	mm
R_{bo}	Outer radius of the kidney port on cylinder block	11	mm
R_G	Outer radius of slipper pad	3.3	mm
V_{cb}	Minimum volume of the bias actuator	150	mm^3
V_{cc}	Minimum volume of the control actuator	50	mm^3
V_{md}	Volume between delivery port of the pump and load	1	dm^3
x_{bmax}	Maximum geometric displacement limit of bias actuator	4.7	mm
x_{cmax}	Maximum geometric displacement limit of control actuator	4.7	mm
δ	Indexing angle	0.18	rad

δ_b	Pre-compression of bias actuator spring	0.9	mm
δ_{sp}	Pre-compression of spool spring	1.6	mm
δ_1	Half of the closed angle of the socket	2	rad
δ_2	Half of the open angle of the ball joint to the socket inlet	0.2	rad
β	The bulk modulus of hydraulic fluid @ 35C°	1.42	GPa
α_0	Swash plate angle at rest	0.28	rad
η	Secondary swash plate angle	0.04	rad
μ	Dynamic viscosity of hydraulic fluid @ 35C°	0.017	Pa.s
ρ	The mass density of the hydraulic fluid @ 35C°	850.5	kg/m^3
ψ	The angle of a kidney-shaped flow passage on the cylinder block	0.51	rad
ψ'	The angle of a kidney-shaped non-flow passage on the cylinder block	0.93	rad
ω	The angular speed of cylinder block		rad/s
f_b	Viscous friction force due to the leakage on bias actuator		N
f_{cp}	Viscous friction force due to the leakage on control actuator		N
F_{spring}	Bias actuator spring force		N
FB	The total force on the bias actuator		N
FCP	The total force on the control actuator		N
F_{aK_i}	Inertia force acting on the i^{th} pumping piston		N
F_{AK_i}	The total force on the i^{th} pumping piston		N
F_{DK_i}	Pressure force acting on the i^{th} pumping piston		N
F_{TK_i}	Viscous friction force due to the leakage at the pumping piston and cylinder		N

l_k	Length of the fluid column inside the cylinder block	m
N	The rotational speed of the shaft	rpm
Q_{si}	Volumetric suction flow at the i^{th} piston	m^3/s
Q_{di}	Volumetric delivery flow at the i^{th} piston	m^3/s
Q_d	Total volumetric flow to the delivery manifold	m^3/s
Q_s	Total volumetric flow from the suction manifold	m^3/s
Q_{lt}	Volumetric leakage flow through the three-way actuator to the reservoir	m^3/s
Q_{lkb}	Volumetric leakage flow through the clearance between bias actuator and sleeve	m^3/s
Q_{lkc}	Volumetric leakage flow through the clearance between control actuator and sleeve	m^3/s
Q_L	Volumetric flow through to the load	m^3/s
Q_{si}	The volumetric flow between the suction port and i^{th} cylinder	m^3/s
Q_{SB}	Volumetric leakage flow inward and outward direction between the cylinder block and valve plate	m^3/s
Q_{SG}	Volumetric leakage flow through the clearance between rate piston and cylinder	m^3/s
Q_{SK}	Volumetric leakage flow across the annulus between pumping piston and cylinder block	m^3/s
Q_{SPHERE}	Volumetric leakage flow across the ball and socket joint	m^3/s
P_d	Pump discharge pressure	Pa
P_{pi}	i^{th} piston chamber pressure	Pa
P_{ccm}	Control actuator chamber pressure	Pa
P_{bcm}	Bias actuator chamber pressure	Pa

V_i	The instantaneous volume of the piston chamber	m^3
x_b	Bias actuator displacement	m
x_c	Control actuator displacement	m
x_i	Displacement of the i^{th} piston from the neutral plane	m
$\dot{x}_i$	The velocity of the i^{th} piston	m
$\ddot{x}_i$	The acceleration of the i^{th} piston	m
x_{sp}	Spool displacement	m
α	Swash plate angle	rad

CHAPTER 1

INTRODUCTION

1.1 Background

Fluid power systems, which consist hydraulic systems and pneumatic systems, become an indispensable part of the high-power control applications [1]. The power density is the ratio of output power to the volume and the volume refers to the physical space that devices take up on a shop floor [2]. Power densities of the various powered devices are shown in Table 1. In order to compare the devices, output power is selected as the same. As shown in Table 1, a piston pump can produce more power than an AC Electric Motor and Diesel Engine for the same volume. Hydraulic power is generally preferred when small package volume is the requirement of the overall system, especially in aerospace industry, highway vehicle industry and in many industrial applications. With a rough expression, small package volume means less weight and inertia. The low inertia allows fast response to the system, which means that higher gains and higher bandwidths are achieved by using hydraulic actuators in servo circuits.

Maximum efficiencies of hydraulic fluid power devices (pumps and motors) are between 85% and 95%. Although the efficiencies of hydraulic fluid power devices are sufficient, the hydraulic fluid power systems work with lower efficiencies. Hydraulic systems are generally powered by a single pump for supplying different actuators and loads. If load potentials of those actuators are different, this condition causes operation non-efficient. Another major reason of low efficiency is the pressure drop across the valves.

Table 1: A comparison of power densities of three different machines [2]

Device	**Output Power [kW]**	**Volume [m^3]**	**Power Density [W / m^3]**
Diesel Engine	375	1.500	250
AC Electric Motor	375	0.690	543
Piston Pump	375	0.055	6.818

By advancing hydraulic systems, hundreds of horsepower is controlled by signals in the order of milliamp or millivolt. By the way, hydraulic systems are used under various loading conditions at high frequencies. Heat is generated in all devices due to the inefficiencies of systems. The hydraulic fluid transferred through the system works also as cooling equipment for dissipating heat produced by the system in hydraulic systems. In mobile applications, flexible routing of hydraulic power by using hoses is a good benefit with respect to the engine driven systems. Lastly, hydraulic fluid works as a lubrication element for the circuit components that hydraulic fluid takes the maintenance duty spontaneously.

On the other hand, hydraulic systems have many handicaps to limit their application areas. It is so hard to achieve zero-leak hydraulic systems. Because of this reason, hydraulic systems may not be used for cleanroom applications. Secondly, filtration is an important duty to protect valves or actuators against clogging and the hydraulic equipment against wear. Working with hydraulic system needs careful handling. This duty may be ignored by maintenance labor and the inspecting lists must be controlled strictly not to use contaminated hydraulic fluid in the hydraulic system, especially for aerospace industry. From manufacturing view, tight tolerances are needed to achieve less leakage in the actuators or hydraulic components. These tight tolerances cause high costs for the components. Lastly, hydraulic systems generally work with high levels of noise.

1.2 Previous Researches

Variable displacement axial piston pumps are used generally in aerospace, military, automotive, and mobile applications. The widespread usage of this pump in the industry has attracted researchers' attention about its dynamics in detail.

Lewis & Stern [3] described detailed approaches to formulate the transfer functions of the hydraulic components and to get the dynamic responses of the components and hydraulic circuits. Reethof [4] investigated the characteristics of positive-displacement pumps and motors at steady state. Ivantysyn and Ivantysynova [5] studied the principles, design performance, modeling, analysis, control, and testing of the hydrostatic pumps and motors. They formulated dynamic leakage equations and pressure distribution of a piston by integrating the Reynolds equation of lubrication. Watton [6] presented flow through the various leakage gaps. Most of these flow equations are related with a variable displacement pump components. In addition, he investigated the flow losses and torque losses for an axial piston machine. Manring [7] investigated the detailed design, analysis, and control of an axial piston pump. He studied component level design fundamentals, different types of controlled axial piston pumps, and performed their dynamic performance. Ma [8] presented optimization of the cross angle on the dynamics of the pump. He put forward the correlation between analysis and experimental results. Then he optimized key dynamics (flow peak and pressure pulsation) by changing the cross angle on valve plate.

In this study, a complete dynamic analysis is applied to project the discharge pressure-delivery flow characteristics of the pump. Flow, pressure, and torque characteristics are improved by applying various valve plate geometries.

1.3 Motivation and Objectives

The motivation of this work is to get performance improvements by geometric dimensioning of the pump internal parts. Examination of the boundaries related with working conditions is aimed in order to determine pressure and flow rate pulsation

limits. The objective of this thesis is to analyze the pump dynamics by producing measured and non-measured operational variables; for example, the discharge pressure peak, the pulsation of the discharge pressure, the flow peak, the torque peak on the swash plate and affordability of instantaneous total torque by control actuator are predicted by these simulations. The performances of the different pump configurations are investigated by utilizing various parameters at the physical model.

1.4 Thesis Outline

The content of this thesis is an investigation of dynamics of the pressure compensated axial piston pump including interior parts, such as bias actuator, control actuator, swash plate, valve plate, etc. Firstly, leakage paths are examined in order to determine the dominant path. Volumetric efficiency can be improved especially by decreasing the dominant leakage path. Secondly, dynamics of the bias actuator, the control actuator, the three-way valve, pumping pistons, the valve plate, and the swash plate are inspected. Case studies are done to improve the performance of the pump, such as torque peak, torque oscillations, pressure peak, pressure oscillations, flow peak, flow oscillations, etc. A coupled model is developed in Matlab/Simulink environment to model pump. Then, measured experimental results and simulated results are compared to cross-check the model. Finally, case studies are inspected to visualize the improvements on pressure-flow characteristics.

CHAPTER 2

VARIABLE DISPLACEMENT SWASH PLATE PUMPS

Pumps or motors, whose working principle is related with displacement volume, are called as displacement machines. These displacement machines work under different phenomena. These displacement machines are classified as, piston machines, gear machines, screw machines, vane machines, and other machines. These machines are named via the component constitutes the displacement. The main distinction between piston machines and other machines is the direction of the motion. The piston machines working phenomena rely on translational motion of the displacement component. The displacement component performs rotary motion at the gear machines, screw machines, and vane machines. The piston type machines are classified as, axial piston machines and radial piston machines. The difference between axial piston machine and radial piston machines is motion of the pistons. In axial piston machines, pistons work parallel to the each other. In radial piston machines, the pistons are arranged around the driving shaft. Motion of each piston is perpendicular to the shaft axis. The axial piston type machines are classified as, swash plate machines and bent axis machines according to the principle of generation of the piston stroke. The piston stroke is generally produced due to the support of the piston on the swash plate machines [5].

In swash plate pump usage market, pressure compensated axial piston pumps are utilized usually due to their simplicity and cost-effectiveness. In this thesis, the internal dynamics and the pressure-flow characteristics of a pressure compensated axial pump is examined in detail.

2.1 Types of Variable Displacement Swash Plate Pumps

Variable displacement pumps have an adjustable swept volume. Variable displacement volume is useful for control systems. Employing a variable displacement pump is more energy efficient because flow and pressure closely adapt to the load. Favorable efficiency (higher than 90%) can be achieved by employing swash plate pumps; which leads to low operating costs.

Swash plate angle, α, of a variable displacement axial piston pump is controlled by a control actuator. This control actuator is powered by a signal that can be hydraulic, mechanical or electrical. Desired displacement volume can be accomplished by energizing the control piston.

There are several types of displacement/pressure control mechanisms. Some of these mechanisms are explained in following sections.

2.1.1 Pressure Compensated Axial Piston Pump

Pressure compensator mechanism limits the discharge pressure to the rated discharge pressure, like a relief valve. When discharge pressure is below the compensator setting pressure, the pump is at full stroke in other words displacement volume is at most as shown in Figure 1. When the hydraulic discharge pressure reaches the rated discharge pressure, displacement volume is maintained to the minimum level as shown in Figure 2. The discharge pressure-delivery flow characteristic curve of a typical pressure compensated axial piston pump is shown in Figure 3. When the load is at the minimum level, maximum delivery flow occurs. When the pump is pressurizing the hydraulic system up to compensator setting pressure, flow decreases due to volumetric losses. Volumetric losses increase with increasing discharge pressure. It is possible to operate at various discharge pressure magnitude up to rated pressure. Spring losses occur while the discharge pressure is between maximum full-flow pressure and rated discharge pressure. The pump maintains rated discharge pressure with the minimum delivery flow until the load drops.

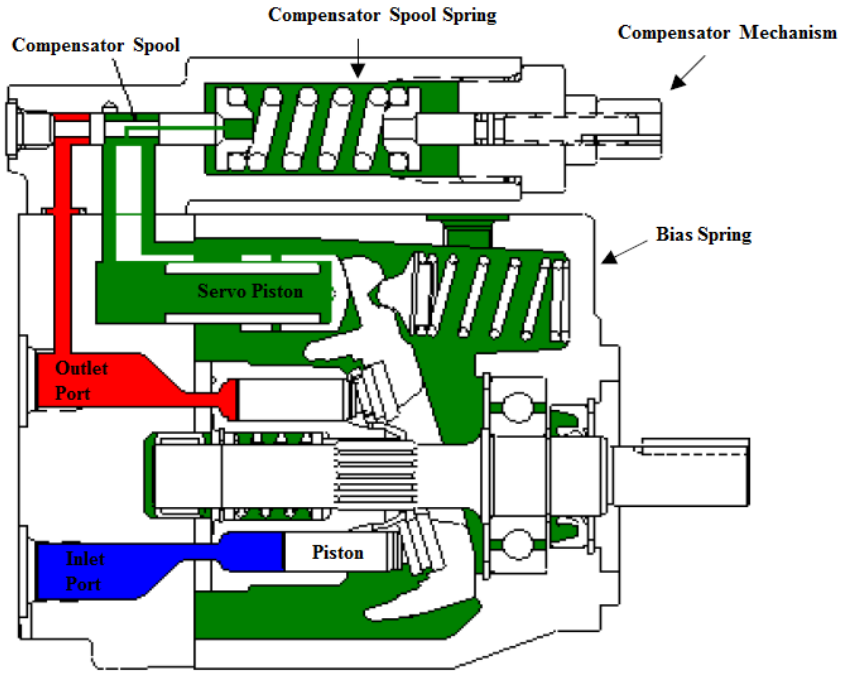

Figure 1: Swept volume of a pressure compensated axial piston pump while discharge pressure is lower than the maximum full-flow pressure [9]

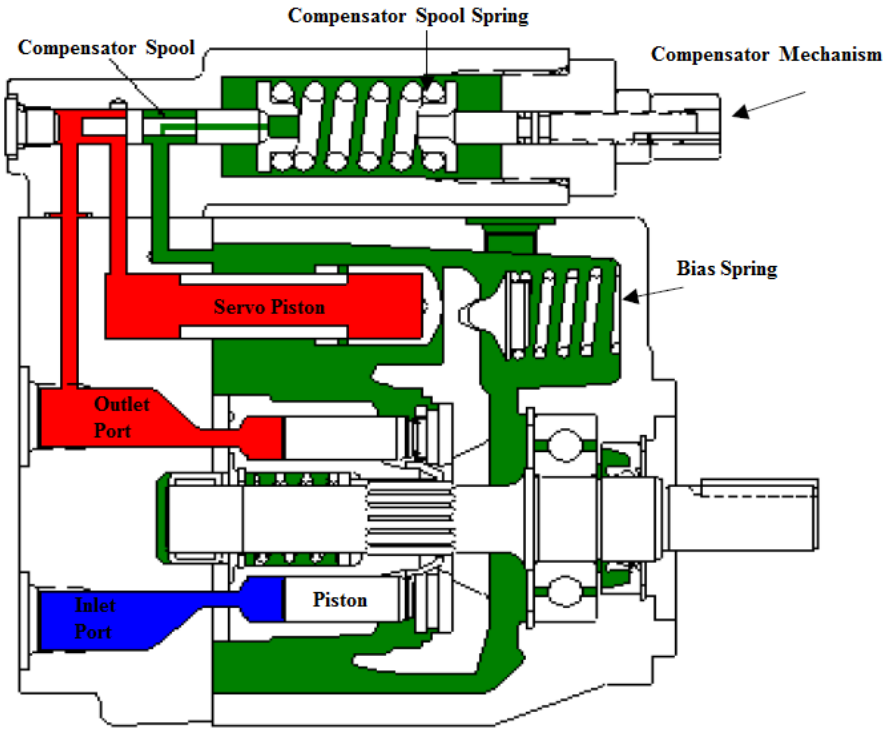

Figure 2: Swept volume of a pressure compensated axial piston pump while discharge pressure is equal to the rated pressure [9]

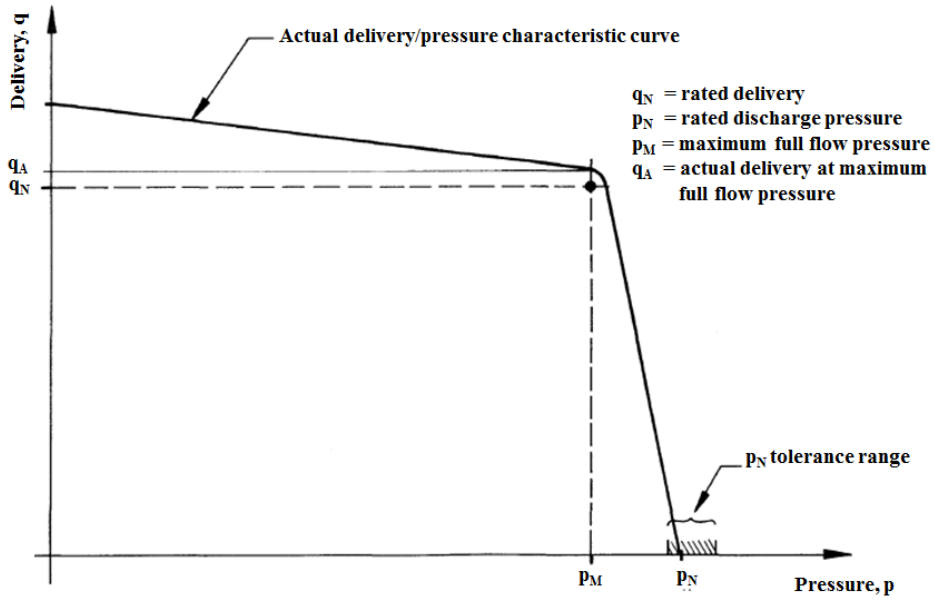

Figure 3: The discharge pressure-delivery flow characteristic curve of a typical pressure compensated axial piston pump [10]

2.1.2 Remote Pressure Compensated Axial Piston Pump

Using a remote pressure compensator is another way to control the pump displacement according to the actual need of the flow for various pressure magnitudes which are determined by a remotely installed pilot valve. When the system pressure is reached to the relief valve setting pressure, control piston adjusts the swash plate angle to the minimum value. The pump maintains the relief valve setting pressure until load drops. The difference between standard pressure compensator and remote pressure compensator is that pressure limiter adjustment is controlled with an external relief valve in remote pressure compensator.

2.1.3 Load-Sense Controlled Axial Piston Pump

Load-sense control is another way of controlling the adjustment of the swash plate angle. Pump discharge pressure is synchronized to the system demand at a pressure which is little above the system demand. This adjustment is triggered by sensing the system maximum hydraulic load, then adjusting the displacement volume to cope with the system maximum hydraulic load. When there is no load, pump works at full

displacement. When there is a load, the pump discharge pressure increases until it overcomes the differential spring force and shifts the control actuator to adjust the displacement volume as seen in Figure 4.

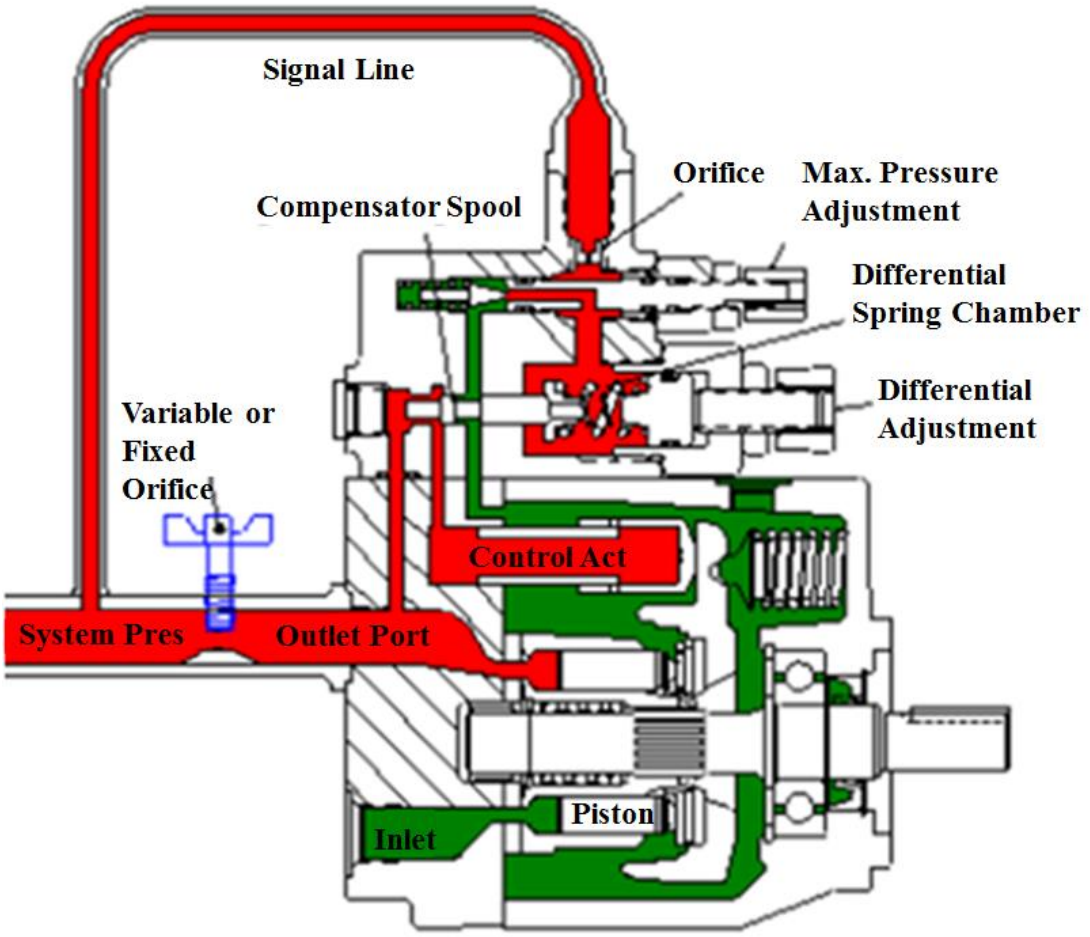

Figure 4: Load-sense controlled axial piston pump configuration [9]

The pump carries a displacement level, which keeps the pressure drop constant across the hydraulic load. This pressure drop is equal to the differential spring load. Discharge flow increases when the hydraulic load decreases, or vice versa. For a unique hydraulic load, pump delivery flow does not vary with respect to the varying driveshaft speed. Because load-sense control maintains a constant pressure drop across the orifice, the load-sense pump will maintain the same delivery flow various driveshaft speeds. When the hydraulic load reaches the maximum set pressure, control actuator adjusts the displacement volume to the minimum. The discharge

pressure-delivery flow characteristic curve of a typical load-sense controlled axial piston pump is shown in Figure 5.

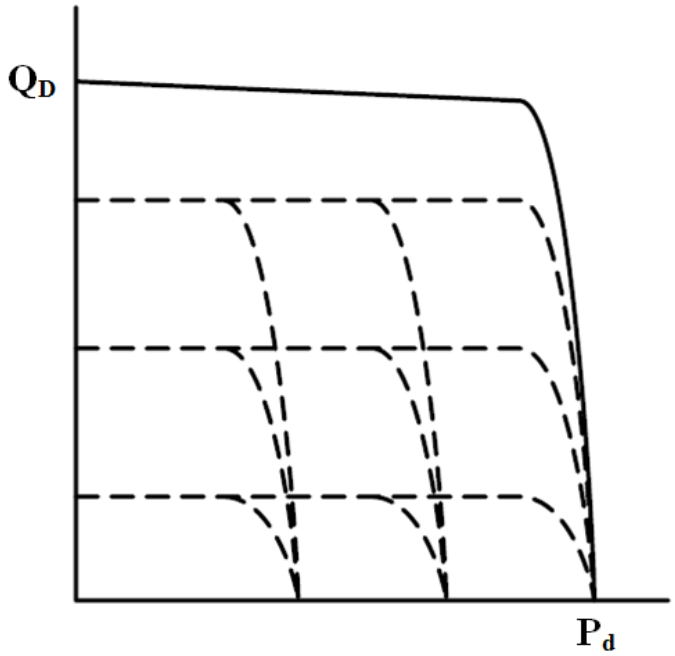

Figure 5: The discharge pressure-delivery flow characteristic curve of a typical load-sense controlled axial piston pump [11]

2.1.4 Torque Controlled Axial Piston Pump

Torque control is another way to control the adjustment of the swash plate angle. This type of control is beneficial when the available power for the hydraulic system is limited. The intent of this type of pump control is to use the available input power most efficiently. Torque limiter control adjusts the displacement volume as the hydraulic load changes, to maintain a constant required torque. The discharge pressure-delivery flow characteristic curve of a particular torque controlled axial piston pump is shown in Figure 6. Various delivery flows are seen for a particular pressure (ex. 250 bar) with respect to the changing supply input power.

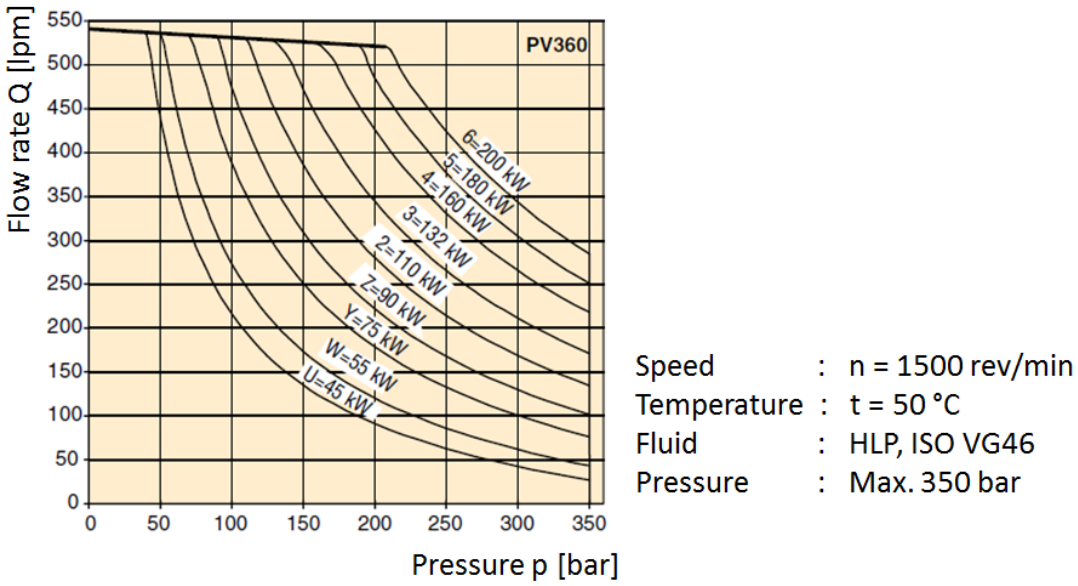

Figure 6: The discharge pressure-delivery flow pressure characteristic curve of a torque controlled axial piston pump [11]

2.1.5 Proportional Controlled Axial Piston Pump

Another control option is the proportional displacement control. At this type of control, displacement volume is proportional to the input voltage or input current. Discharge pressure does not have an effect on the determination of the displacement volume. Discharge pressure can be controlled by employing a pressure transducer with the pump. A linear variable displacement transducer (LVDT) measures the swash plate angle, so the displacement volume is measured with respect to this feedback signal. A pressure compensator also exists in this type of pumps. This pressure compensator limits the rated discharge pressure.

Proportional control gives chance to switch the pressure and tank ports by changing the direction of the displacement volume. As seen in Figure 7, direction and magnitude of displacement volume vary with respect to the changing direction and magnitude of the current. These types of pumps are suitable to use for hydrostatic drives in closed circuits. Displacement volume and shaft speed determine the flow magnitude up to set pressures of relief valves. Pump protects itself by using two relief valves on each pressure ports. This type of pumps can be controlled by

proportional hydraulic/electronic control units or mechanical servomechanisms. With the help of electronic control units, discharge flow can be determined precisely by well-adjusting displacement volume. By changing current direction and magnitude, flow direction and flow magnitude can be determined so smoothly. EP3 and EP4 denote that various powering options.

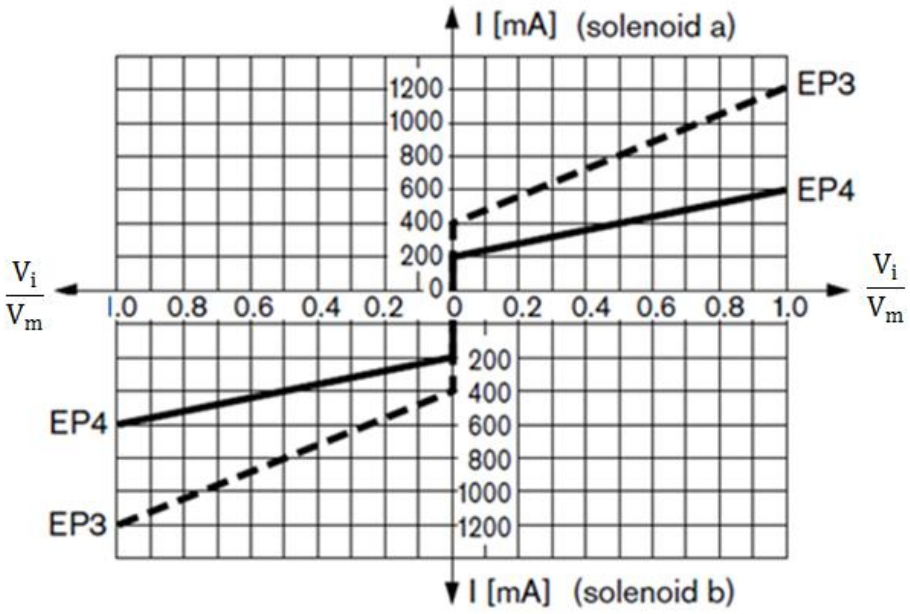

Figure 7: Displacement volume vs input current of a pump [12]

CHAPTER 3

PRESSURE COMPENSATED AXIAL PISTON PUMP PRIMARY SUB-COMPONENTS AND MODELING

In the previous chapter, general information is given about variable displacement axial piston pumps. Mechanics and discharge pressure-delivery flow relations are given in this chapter in component level.

3.1 Definition of the Pump Primary Mechanisms

Hydrostatic pumps are a component of hydraulic circuits that have been used widely in the aircraft industry, industrial and mobile applications. Several researches are made for sizing the critical components to design the response of the pump and overall hydraulic system recently. Kim et al [13], Schoneau et al [14], and Manring [7] have published documents related with the dynamics of the swash plate variable displacement pumps.

Typical configuration of a pressure compensated axial piston pump is given in Figure 8. Several pistons, generally odd number, are nested in cylinder block around x-axis. Pistons are connected to the slipper with ball and socket joint. This slipper-piston assembly is connected to a circular shaped plate, retainer. Circular shaped plate is connected to the swash plate with a connection that gives permission to the revolute motion around the x-axis. Inclination degree of swash plate around z-axis, α, is a variable to determine displacement volume. This angle is named as swash plate angle that varies with respect to the system dynamics. Inclination degree of swash plate around y-axis, η, is also a parameter to determine the displacement volume. This inclination angle is named as secondary swash plate angle that is constant. The swash

plate-piston mechanism is assembled with cylinder block. This assembly gives permission to the translational motion of the pistons. Cylinder block is located against a valve plate and connected to the shaft with involute spline. As the cylinder block is driven around x-axis, each piston is forced to rotate around x-axis by cylinder block. Pistons cross over the intake port and discharge port. Because of the swash plate angle, α, and the secondary swash plate, η, pistons do oscillatory motion in and out of the cylinder block.

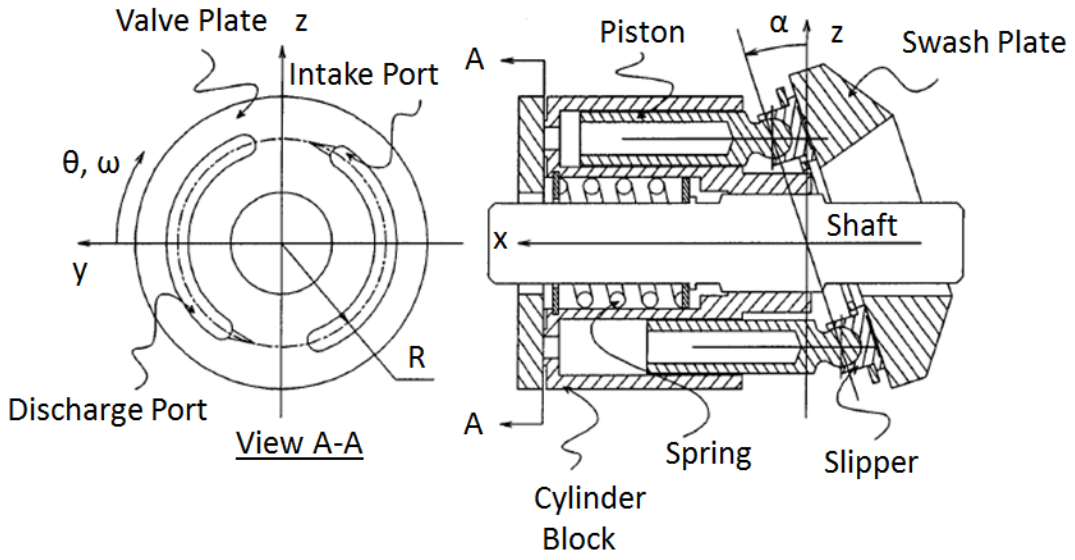

Figure 8: General pump configuration [15]

In order to explain the working mechanism of the pump in detail, a piston in the cylinder block considered. When the fluid-filled chamber is at the maximum level in cylinder block for a piston, this position is named as the top dead center, TDC. When the fluid-filled chamber is at the minimum level in cylinder block for a piston, this position is named as the bottom dead center, BDC. This means that piston is ready to suck fluid to fill its volume up to TDC. After piston passes the TDC position, fluid-filled chamber tends to decrease volume. The fluid, which is in the closed chamber, is pressurized by this motion of the piston. Then, piston discharges fluid until it reaches to the BDC. This process explains one complete cycle for one piston. This motion is completed in every cycle, so pump working frequency can be calculated by shaft frequency multiplied by the piston number.

The displacements of a piston at BDC and TDC positions are nearly equal when swash plate angle, α, equals to the minimum and secondary swash plate angle, η, becomes driver angle for displacement volume. This condition occurs when the pump is working at rated discharge pressure. Because of the secondary swash plate angle in the x-y plane as shown in Figure 11, piston gets minimum chamber volume at the mid position of the delivery port in y plane.

Secondary swash plate angle, η, is used to limit the minimum displacement volume. Pressure compensation mechanism needs a minimum volume (approximately 4% of ΔV_{max}) to maintain a stable operation. Also, the pump needs this minimum volume for self-lubrication [5]. This secondary swash plate angle, η, is provided to decrease the excessive noise and to improve efficiency of the pump [16].

Swept volume is explained as the total displacement of the pumping pistons in previous researches. This condition is valid when the pumping piston is connected to the delivery port at BDC and when the piston is connected to the suction port at TDC. If these conditions are not satisfied, the pump could not use suction and discharge potentials efficiently. Although many researches have been published related with pumps, little attention is mentioned about the importance of this condition. Efficient use of suction and discharge potentials of the pump may be satisfied in the experiments of these researchers, otherwise the definition of the swept volume includes an error related with the potential swept volume and actual swept volume. It is important to mention that when chamber volume starts to increase, the piston must be closed to the delivery port to prevent backflow from delivery line. Similarly, when chamber volume starts to decrease, the piston must be closed to the suction port to prevent backflow to the suction line.

The pressure compensation mechanism consists of a three-way valve, bias actuator, bias spring, and control actuator. The control mechanism of a typical pressure compensated pump is shown in Figure 9. Swash plate angle, α, is controlled by the forces of the control actuator and bias actuator. The displacement volume is altered by the adjustment of the swash plate angle, α. When pump discharge pressure gets higher than maximum full-flow pressure, valve spool moves towards the valve

spring. By this actuation, flow is oriented through the control actuator chamber. Hence pressure is built up inside the control actuator chamber. This pressurized fluid powers the control actuator to rotate the swash plate mechanism against the bias actuator force constituted by the bias spring.

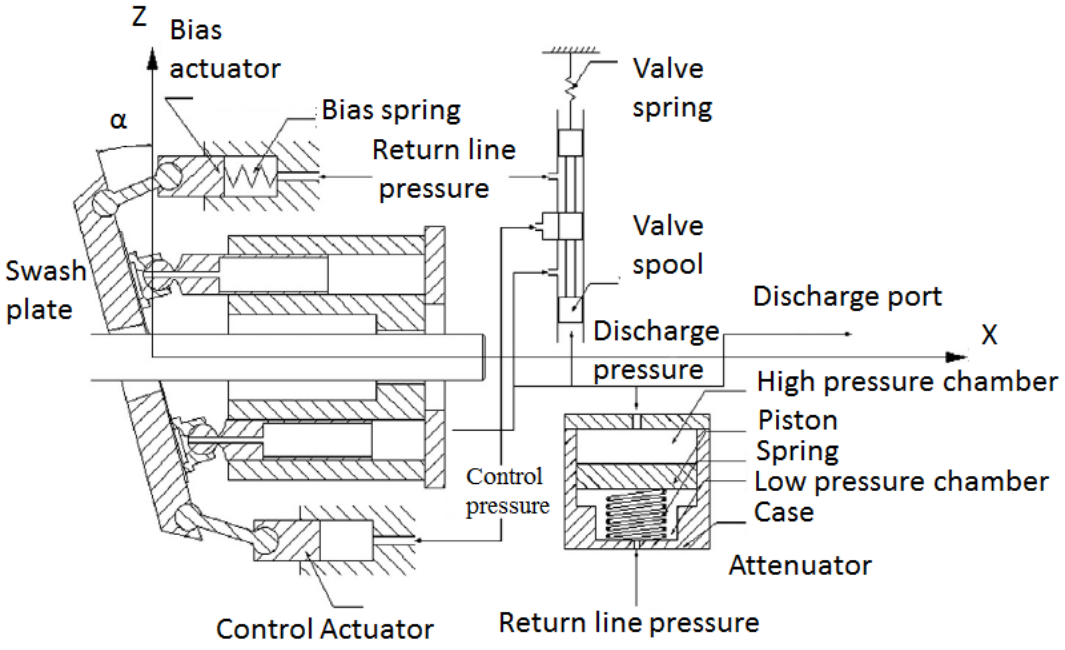

Figure 9: A cross-sectional view of the pressure controlled axial-piston pump [17]

The adjustment of pressure compensation mechanism tends to de-stroke swash plate mechanism when the discharge pressure is higher than maximum full-flow pressure. In contrary view, bias actuator tends to stroke swash plate mechanism when hydraulic system pressure falls down lower than the maximum full-flow pressure.

3.2 Sub-component Kinematics and Pump Modeling

3.2.1 Kinematics of the Piston-Slipper Assembly

Displacement of a piston at x-direction is shown in x-z plane in Figure 10 and x-y plane in Figure 11. The pump has N number pistons and these pistons are equally spaced in the cylinder block. In Matlab/Simulink model, these pistons are modeled completely similar to a phase shift. All variables (piston displacement, piston

velocity, flow, leakage, pressure, etc.) are similar for each piston for a particular angle, θ, in y-z plane by assuming the pump is in the steady-state and components of the pump are identical.

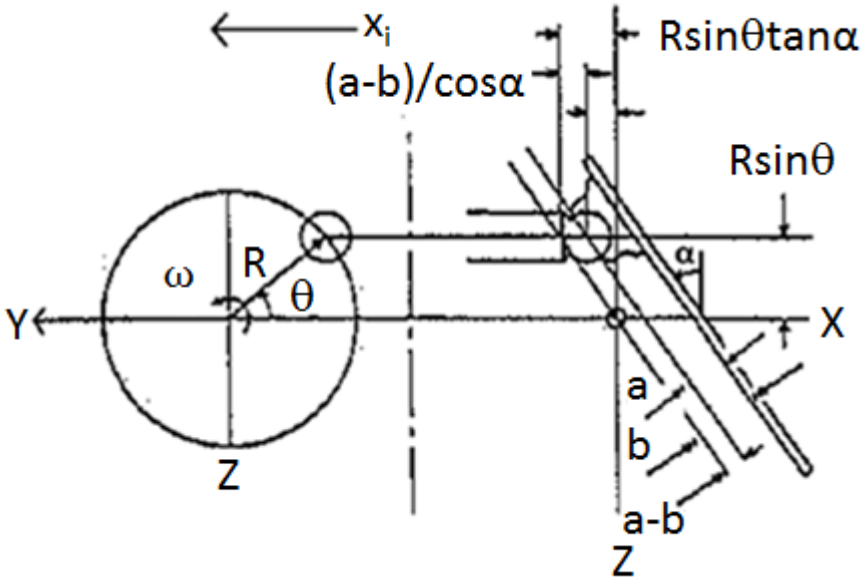

Figure 10: Piston geometry in the x-z plane [14]

Displacement of the i^{th} piston in the x-direction is given in Equation 1 with respect to the varying angular position of the piston, θ, in y-z plane and swash plate angle, α, in the x-z plane. The perpendicular distance from piston-slipper ball joint to swash plate is defined as "a" in the x-z plane. The perpendicular distance from swash plate to the swivel axis is defined as "b" in the x-z plane. Pitch radius of the cylinder block is defined as R.

$$x_i = \frac{a - b}{\cos \alpha} + R \sin(\theta) \tan(\alpha) \tag{1}$$

Displacement of the i^{th} piston in the x-direction is given in Equation 2 with respect to the varying angular position of the piston, θ in the y-z plane and constant secondary swash plate angle, η in the x-y plane. The perpendicular distance from swivel axis to

swash plate is defined as c in the x-y plane. The perpendicular distance from piston-slipper ball joint to the swash plate is defined as d in the x-y plane.

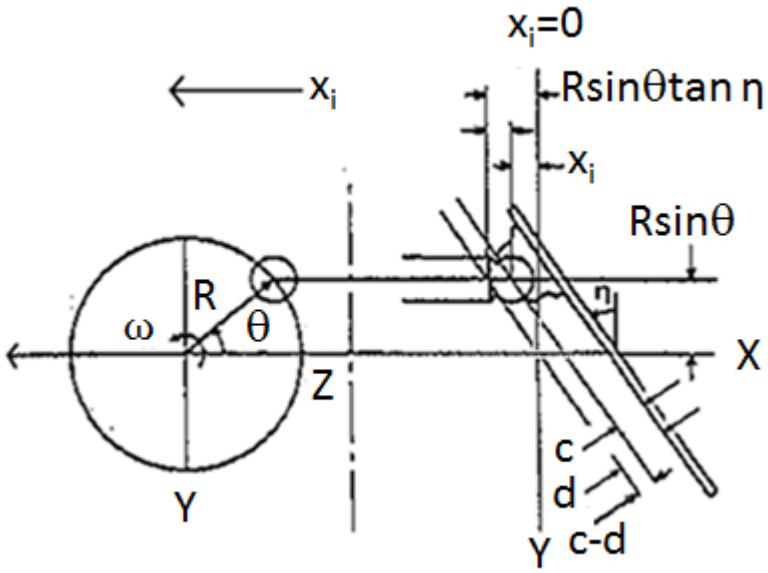

Figure 11: Piston geometry in the x-y plane [14]

$$x_i = \frac{c - d}{\cos\eta} + R\sin(\theta)\tan(\eta) \tag{2}$$

In order to express the total displacement of the i^{th} piston in Equation 3, it is needed to equalize these two motions phases. So phase difference, $\pi/2$, between these two motions are added into Equation 2 with considering the direction of the motion.

$$x_i = \frac{a - b}{\cos\alpha} + \frac{c - d}{\cos\eta} + R\tan(\alpha)\sin(\theta) + R\tan(\eta)\sin\left(\theta + \frac{\pi}{2}\right) \tag{3}$$

The velocity of the i^{th} piston in the x-direction is given in Equation 4 with respect to the constant angular speed of the cylinder block, ω, varying angular position of piston, θ, in the y-z plane, varying swash plate angle, α in the x-z plane and constant secondary swash plate angle, η, in x-y plane. ($\dot{\theta} = \omega$)

$$\dot{x}_i = (a-b)\frac{\sin(\alpha)\,\dot{\alpha}}{\cos^2(\alpha)} + R\tan(\alpha)\cos(\theta)\,\omega + R\frac{\sin(\theta)\,\dot{\alpha}}{\cos^2(\alpha)} + R\cos\left(\theta+\frac{\pi}{2}\right)\tan(\eta)\,\omega \tag{4}$$

Acceleration of the i^{th} piston in the x-direction is given in Equation 5 with respect to the constant angular speed of the cylinder block, ω, varying the angular position of piston, θ, in y-z plane, varying swash plate angle, α in x-z plane and constant secondary swash plate angle, η, in x-y plane. ($\dot{\theta} = \omega$)

$$\ddot{x}_i = \left\{\frac{1+2\tan^2(\alpha)\dot{\alpha}^2}{\cos(\alpha)} + \frac{\sin(\alpha)\,\ddot{\alpha}}{\cos^2(\alpha)}\right\}(a-b) + \left\{\frac{2R\dot{\alpha}^2\sin(\alpha)}{\cos^3(\alpha)} + \frac{R\ddot{\alpha}}{\cos^2(\alpha)} + R\tan(\alpha)\omega^2\right\}\sin(\theta) + \frac{2R\dot{\alpha}^2\,\omega}{\cos^2(\alpha)}\cos(\theta) - R\sin\left(\theta+\frac{\pi}{2}\right)\tan(\eta)\,\omega^2 \tag{5}$$

3.2.2 Leakage Flow Modeling of the Pump

Different from the discharge flow of the pump, continuous leakage flows occur in the pump while the pump is working. Although these leakage paths help to the pump for self-lubrication, in analytical view these leakages decrease the pump volumetric efficiency, η_v, as seen in Equation 6 [18].

$$\eta_v = \frac{Q_d}{V_d\,\omega} \tag{6}$$

where,

Q_d: delivery flow (m^3/s)

V_d: displacement volume (swept volume) (m^3)

ω : angular velocity of the shaft (rad/s)

While defining the leakage relations, following assumptions are made;

- The hydraulic fluid inertia is negligible,
- The hydraulic fluid is Newtonian,
- The hydraulic fluid is incompressible with nobody forces,
- Pressure gradient exists only along the direction of the flow,
- Eccentricity about piston and sleeve is neglected.

3.2.2.1 Leakage around a Piston

The leakage flow equation between pumping piston and cylinder block is given in Equation 7 by considering steady flow in annulus between piston and sleeve, minus flow related with the movement of the piston as shown in Figure 12. Piston and cylinder block eccentricity is assumed as zero. Instantaneous leakage flow path length is denoted as l_k which is depended to the varying x_i. Clearance between piston and cylinder block is denoted as h_K. Diameter of the pumping piston is denoted as $d_{p.}$ Pressure inside the i^{th} chamber and pump drain line is denoted as P_i and P_c, respectively.

$$Q_{SK} = \frac{\pi d_p h_K^3}{12\mu l_k}(P_i - P_c) - \frac{\pi d_p h_K \dot{x}_i}{2} \tag{7}$$

Bergada et al. [19] made detailed research about leakages inside the pump in previous studies. They presented leakage flow equation around a piston including the effects of the grooves cut on the piston.

Blackburn [4] presented steady flow in the annulus by including eccentricity. The flow rate is increased 2.5 times the value of the concentric cylinders, assuming the same pressure drop.

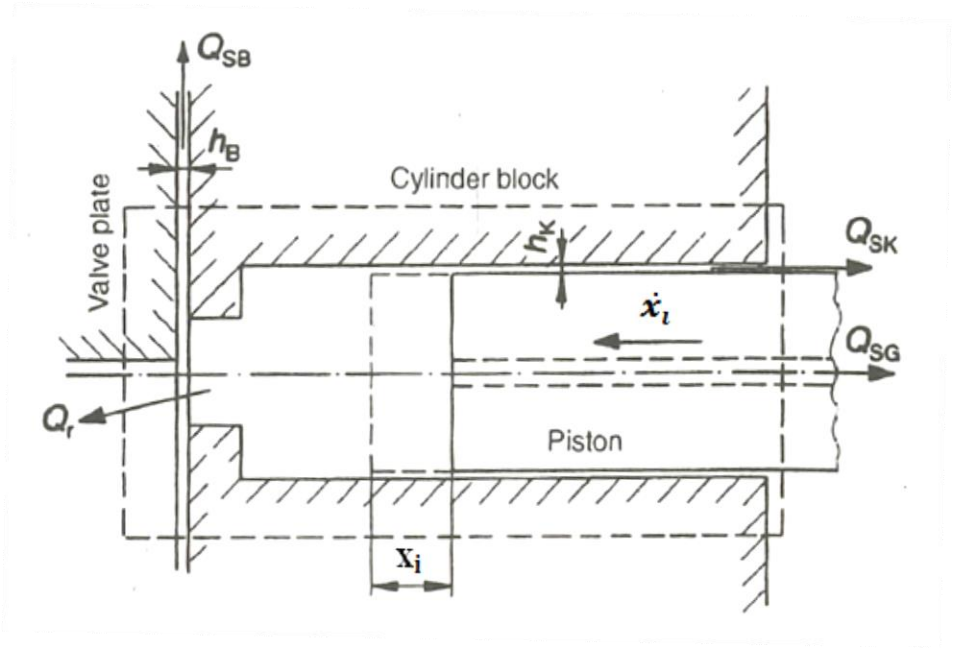

Figure 12: Control volume for the analysis of pressure development in the cylinder [5]

3.2.2.2 Leakage Flow between Cylinder Block and Valve Plate

Flow rate in radial flow conditions is defined in Equation 8 by integrating Reynolds equation in radial direction. The fluid film thickness is shown as h_B in Figure 12.

$$Q_{radial} = \frac{\pi {h_B}^3}{6\mu \ln(r_{out}/r_{in})}(P_i - P_c) \tag{8}$$

Fully circumferential flow is considered through formulating Equation 8. While the pump is operating, the kidney-shaped flow passage area on the cylinder block is pressurized. Equation 8 is modified with respect to the angular dimension of the kidney-shaped flow passage in Equation 9. Cylinder block slotted port angle, ψ, is denoted as by referencing cylinder block center line as shown in Figure 13. Inner radii of kidney port on valve plate and cylinder block are denoted as R_{bo} and r_{bo}, respectively.

$$Q_{\text{opening angle}} = \frac{\psi\, h_B^3}{12\mu \ln(R_{bo}/r_{bo})}(P_i - P_c) \tag{9}$$

These leakages occur in radially inward and outward directions as seen in Figure 13. Total leakage for the piston is defined in Equation 10. Inner radii of kidney port on valve plate and cylinder block are denoted as r_{bi} and R_{bi}, respectively. Although, the film thickness varies with respect to the surface flatness and hydrodynamic bearing conditions, for simplicity constant fluid film thickness is considered. This film thickness is sufficient to prevent metal to metal contact between the cylinder block and valve plate [20].

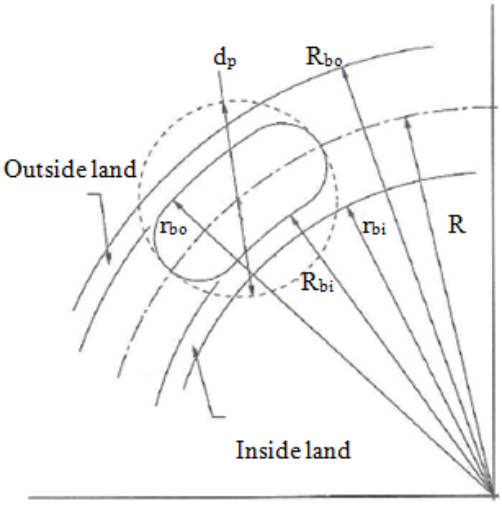

Figure 13: Kidney port and manifold geometry [7]

$$Q_{SB} = \frac{\psi h_B^3}{12\mu}(P_i - P_c)\left[\frac{1}{\ln(R_{bo}/r_{bo})} + \frac{1}{\ln(R_{bi}/r_{bi})}\right] \tag{10}$$

3.2.2.3 Leakage through the Slipper and Swash Plate

Flow rate in radial flow conditions is defined in Equation 8. Gap height between the slipper and swash plate is defined as h_G in Figure 14. Outer radius and inner radius of the slipper is defined as R_G and r_G, respectively. The pressure inside the slipper is

defined as P_G. Leakage flow rate through the slipper and swash plate is defined in Equation 11.

$$Q_{radial} = \frac{\pi h_G^3}{6\mu \ln(R_G/r_G)}(P_G - P_c) \tag{11}$$

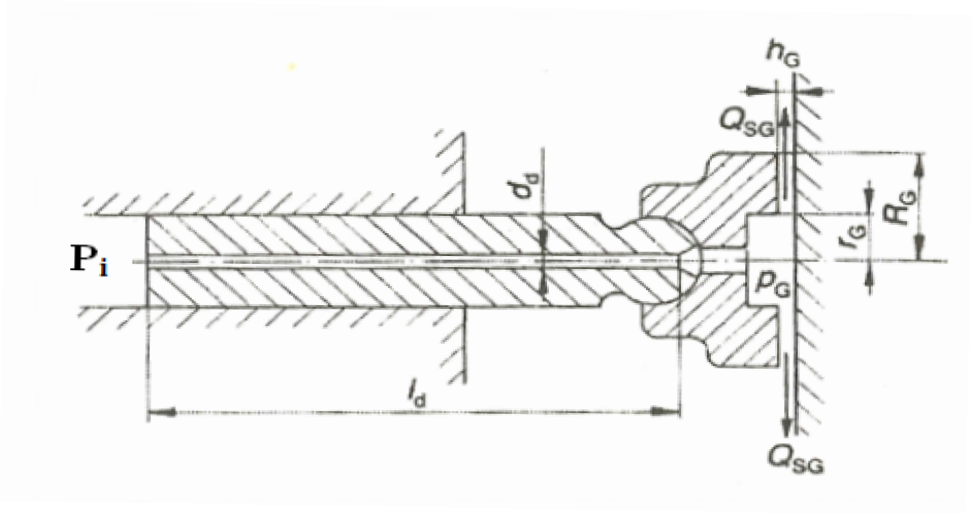

Figure 14: Scheme for the determination of flow rate between slipper and swash plate [5]

Steady flow through the pipe is defined in Equation 12. d_d is the hole diameter inside the piston. Hole length is defined as l_d. P_G is the pressure inside the slipper.

$$Q_{pipe} = \frac{\pi d_d^4}{128\mu l_d}(P_i - P_G) \tag{12}$$

Equation 11 and Equation 12 are substituted to present flow rate (Q_{SG}) between slipper and swash plate by considering zero leakage across the ball and socket joint [5]. Slipper spin is not taken into account in Equation 13. Although h_G varies depending on the pump operating conditions, in this formulation this term is assumed as constant for simplicity. Several researches have been done related with slippers. In these researches, it is investigated that gap height is related with tilt angles, rotational

speed, facing surfaces flatness, machine working condition (pumping or motoring), etc.

$$Q_{SG} = \frac{\pi h_G^3 d_d^4}{\mu \left(6 d_d^4 \ln(R_G/r_G) + 128 h_G^3 l_d\right)} (P_i - P_c) \quad (13)$$

3.2.2.4 Ball and Socket Joint Leakage

Spherical journal bearing characteristics have been studied by different researchers. These researches generally focus on friction torque characteristics of spherical journal bearings. Meyer transformed Reynolds equation in spherical coordinates [21]. This transformation gives permission to get pressure distribution on the spherical bearing and fluid film thickness. Manring studied about volumetric flow-rates and load carrying capacity characteristics of the various socket geometries experimentally [22]. Although non-traditional spherical socket design, which is explained in the article [22], and conical socket design permits higher load capacity than classical design, measured bearing leakage at these various socket geometries is higher than classical design.

Bearing leakage is defined in Equation 14. This equation is valid for non-rotational motion between ball and socket, steady-state flow conditions, and ball and socket are concentric [19]. H is the clearance between ball and socket geometry. The radius of the ball is defined as r_o as shown in Figure 15.

$$Q_{SPHERE} = \frac{(P_i - P_c)\pi \left(r_o \frac{H^3}{6} + \frac{H^4}{12}\right)}{\mu \left(r_o + \frac{H}{2}\right) \ln\left(\frac{\tan(\delta_2/2)}{\tan(\delta_1/2)}\right)} \quad (14)$$

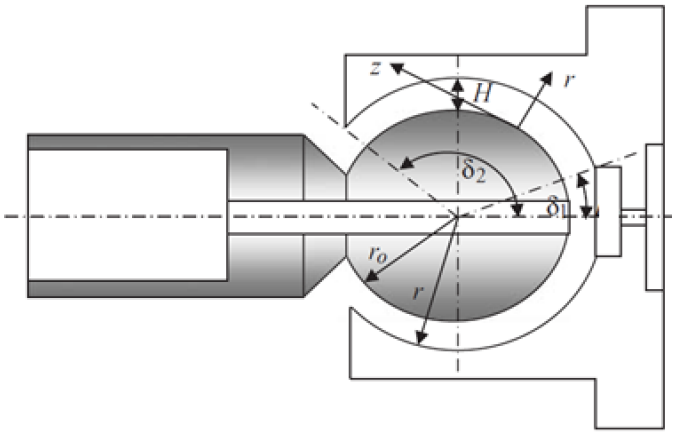

Figure 15: Ball and socket geometry (clearance exaggerated) [6]

In Equation 14, it is shown that variation in the clearance between ball and socket is effective on the maximum limit of this bearing leakage to a high degree. For an example, in order to limit piston leakage, Eaton firm suggests that maximum translational motion of the piston with respect to the fixed shoe plate must not exceed 0.005 inches for industrial 220 series piston pump [23] as shown in Figure 16.

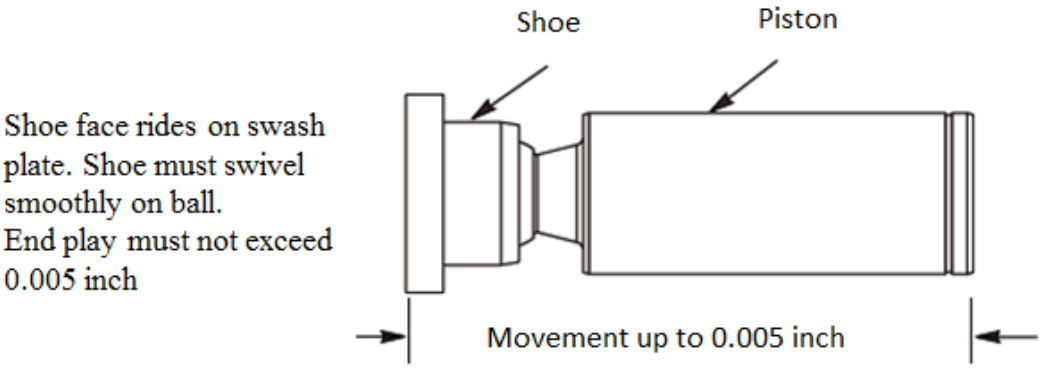

Figure 16: Ball and socket movement [23]

3.2.3 Valve Plate Geometry and Valve Plate Timing

A non-over centered valve plate is shown in Figure 17. These types of valve plates are utilized when the direction of shaft rotation and direction of swash plate angle do not change to the opposite direction. The valve plate shown in Figure 17 could be used for clockwise rotation (view on the valve plate) due to slot geometries at zone 3,

and zone 8. Zone 4 and zone 5 show suction port. Zone 1 and zone 9 show discharge port.

Differently, the suction port and the discharge port can twist at over center pumps by the changing direction of swash plate angle. In this type of pumps, zone 4, and zone 5 are similar to the zone 1, and zone 9. The geometry shown at zone 1 and zone 9 is named as $Q_{web.}$ These webs are used to strengthen the valve plate. These webs are not used in the y-axis (Figure 8) at the discharge port/suction port in order not to restrict the flow while maximum flow occurs. Maximum flow occurs in this region because the maximum translational motion of a piston occurs in this region related with the swash plate angle, α.

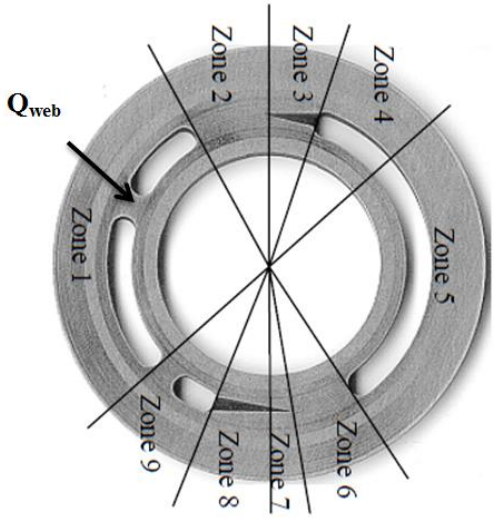

Figure 17: A non-over centered valve plate showing different geometric zones [24]

Lastly, shaft rotation direction could be changed from clockwise to the counterclockwise or vice-versa in bi-directional pumps. In addition to the over-center pumps, zone 2 and zone 6 are similar to the zone 3 and zone 8 in this type of pumps.

The valve plate of a typical non-over center pump is shown in Figure 8. The angular position of the i^{th} piston is defined in Equation 15, where ω is the angular speed of cylinder block and N is the total number of pistons. Piston, where angular position, θ, equals to zero over discharge port in the y-axis, is named as the first piston. The

angular position of the piston, θ, is defined with respect to the midpoint of the delivery port.

$$\theta = \omega t + \frac{(i-1)2\pi}{N} \tag{15}$$

Typical valve plate design is shown in Figure 18. While the pump is working, cylinder port moves, and valve plate remains stationary. Discharge area, $A_{d,}$ or suction area, A_s, of a piston at an instantaneous angular position is given in Equation 16 with a rough approach. In this equation slot angle, φ_f, is considered as zero (no slot geometry). Indexing Angle, δ, and angular dimension at BDC and TDC, ψ′, are considered as same. Variation of the flow passage area is considered as linear at transition regions.

$$\text{Piston}_{Ad\ \&\ As} = \begin{Bmatrix} A_d = BSA, A_s = 0 & -\frac{\pi}{2}+\frac{\psi'}{2}+\delta+\frac{\psi}{2} < \theta < \frac{\pi}{2}-\frac{\psi'}{2}+\delta-\frac{\psi}{2} \\ A_d = BSA\frac{(\frac{\pi}{2}-\frac{\psi'}{2}+\delta+\frac{\psi}{2})-\theta}{\psi}, A_s = 0 & \frac{\pi}{2}-\frac{\psi'}{2}+\delta-\frac{\psi}{2} < \theta < \frac{\pi}{2}-\frac{\psi'}{2}+\delta+\frac{\psi}{2} \\ A_d = 0, A_s = 0 & \frac{\pi}{2}-\frac{\psi'}{2}+\delta+\frac{\psi}{2} < \theta < \frac{\pi}{2}+\frac{\psi'}{2}+\delta-\frac{\psi}{2} \\ A_d = 0, A_s = BSA\frac{\left(\theta-(\frac{\pi}{2}+\frac{\psi'}{2}+\delta-\frac{\psi}{2})\right)}{\psi} & \frac{\pi}{2}+\frac{\psi'}{2}+\delta-\frac{\psi}{2} < \theta < \frac{\pi}{2}+\frac{\psi'}{2}+\delta+\frac{\psi}{2} \\ A_d = 0, A_s = BSA & \frac{\pi}{2}+\frac{\psi'}{2}+\delta+\frac{\psi}{2} < \theta < \frac{3\pi}{2}-\frac{\psi'}{2}+\delta-\frac{\psi}{2} \\ A_d = 0, A_s = BSA\frac{\left((\frac{3\pi}{2}-\frac{\psi'}{2}+\delta+\frac{\psi}{2})-\theta\right)}{\psi} & \frac{3\pi}{2}-\frac{\psi'}{2}+\delta-\frac{\psi}{2} < \theta < \frac{3\pi}{2}-\frac{\psi'}{2}+\delta+\frac{\psi}{2} \\ A_d = 0, A_s = 0 & \frac{3\pi}{2}-\frac{\psi'}{2}+\delta+\frac{\psi}{2} < \theta < \frac{3\pi}{2}+\frac{\psi'}{2}+\delta-\frac{\psi}{2} \\ A_d = BSA\frac{\left(\theta-(\frac{3\pi}{2}+\frac{\psi'}{2}+\delta-\frac{\psi}{2})\right)}{\psi}, A_s = 0 & \frac{3\pi}{2}+\frac{\psi'}{2}+\delta-\frac{\psi}{2} < \theta < \frac{3\pi}{2}+\frac{\psi'}{2}+\delta+\frac{\psi}{2} \end{Bmatrix} \tag{16}$$

Indexing Angle, δ, is shown in Figure 18. The angular dimension between ports is defined as ψ′ [8]. When ψ′ is bigger than ψ, this design is named as trapped volume design. When ψ′ is equal to the ψ, this design is named as line to line porting. When ψ′ is smaller than ψ, this design is named as cross porting.

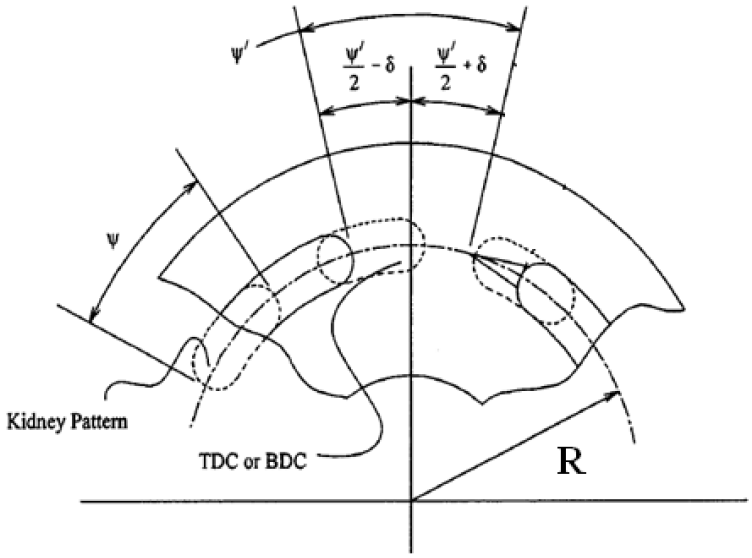

Figure 18: Trapped valve plate design [7]

A characteristic constant of the design is defined in Equation 17. Characteristic constant, φ', can be positive, negative or zero in accordance with the design parameters. When characteristic constant, φ', is positive, it means that piston is open to the suction and discharge slots while it is crossing TDC and BDC for a zero-indexed valve plate. Because of this reason, there is no possibility of cavitation for positive values of characteristic constant, φ'. On the other hand, when the characteristic constant, φ', is negative, it means that piston is closed to the suction, and discharge ports while it is crossing TDC and BDC for a zero-indexed valve plate. For this reason, designs with negative characteristic constant, φ', may cause cavitation. This condition can be seen at the trapped volume designed valve plates. Manring suggested that characteristic constant, φ', should be higher than $0.25°$ [7].

$$\varphi' = \frac{\psi - \psi'}{2} - \delta \tag{17}$$

In order to use swept volume efficiently, $\psi/2$ should be equal or higher than $(\psi'/2 - \delta)$. If this condition is not satisfied, the piston will not be fully filled at TDC. In contrary, piston chamber is closed to the delivery line while the end of the

kidney port is at $(\pi + \psi'/2 - \delta)$. In order to empty the chamber, $\psi/2$ should be equal or higher than $(\psi'/2 - \delta)$. If this condition is not satisfied, the piston will tend to jeopardize the chamber until sweeping to the BDC. It is important to consider that while piston starts to compress the chamber, the piston must be closed to the suction port. Similarly, while piston chamber starts to increase, the piston must be closed to the delivery port to prevent backflow.

In order to use swept volume efficiently and eliminate the cavitation, slots are utilized at BDC and TDC as shown in Figure 19.

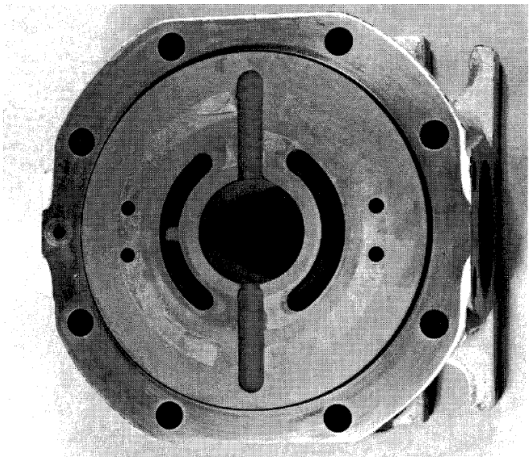

Figure 19: Valve plate of Denison Model P6W-R5B-C10-00-M2 [25]

Different types of slot geometries have been utilized to have smoother pressure rise, and drop profiles. Common slots would be summarized as a combination of flat or ramped geometries. The variation of the slot geometries is limited with the production capabilities.

Manring studied to define pressure transition of various slot geometries (constant, linear, and quadratic) at low displacements [15]. He investigated that if a short slot is needed, linearly varying slot geometry is suitable. If maximum discharge area of the slot is limited, the constant area slot geometry can be utilized. He figured out various valve plate designs (line to line, cross porting, and trapped volume design) without indexing for the same swash plate angle, α=9°, and rotational speed, n=2250 rpm, at [7]. While piston pressure is decreasing to the inlet pressure, pressure transition ($\dot{P}$ [GPa/s]) is about 95 for line to line porting, approximately 70 for cross porting, and

close to 95 for trapped volume design for the same pressure magnitude, 20 MPa, and for overlap angle, $\Delta\psi=3°$ for cross porting, and trapped volume design. While piston pressure is increasing to the discharge pressure magnitude, pressure transition, $\dot{P}$ [GPa/s]), is about 60 for line to line porting, approximately 50 for cross porting, and close to 60 for trapped volume design for the same conditions. Pressure transition is lower at cross porting comparing to the others. Lower pressure transition means lower noise and vibration. It is important to mention that internal leakage occurs from delivery port to the suction port across the pumping piston chamber in cross porting design. This means that inefficiency occurs while the pump is reciprocating. In addition to these researches, he made a comparison between trapped volume design without slot and line to line design with flat bottom constant width slot geometry [26]. This research shows that it is more efficient to use slot angular volume as trapping volume. By the view of these researches, it is easy to say that optimum valve plate design changes with respect to the applications.

Nafz et al analyzed a pressure equalization system with valve-controlled pressure recuperation chamber (PRC) and it is shown that both the efficiency and the noise emission reduction could be improved apparently [27]. Xu et al [27] investigated a non-traditional approach to noise reduction method by utilizing pressure equalization mechanism with a check valve and PRC as shown in Figure 20. Delivery flow peak, swash plate torque oscillation, and efficiency of the pump are examined in this detailed study. The major phenomenon of this study is to transfer hydraulic energy stored in BDC to the TDC. This mechanism works while the first piston is at BDC and its closed volume is jeopardized due to its shrinking volume. This energy is transferred to the piston in TDC across check valves and PRC. This energy transfer goes on one by one. The energy transfer from contrary direction is prevented by utilizing check valves. Noise reduction is shown by considering flow peak reduction and torque oscillation reduction. In addition, the total swept volume of the pump is used effectively by employing this mechanism. Flow from BDC to the PRC and PRC to the TDC decreases inefficiency because of the leakage of the piston around BDC. The pressure at the piston, which is entering the discharge port, reaches to the discharge pressure magnitude faster. Backflow from delivery line to the pump is

decreased by this way. Lastly, control actuator volume could be reduced by decreasing required de-stroking torque by decreasing maximum torque exerted on swash plate.

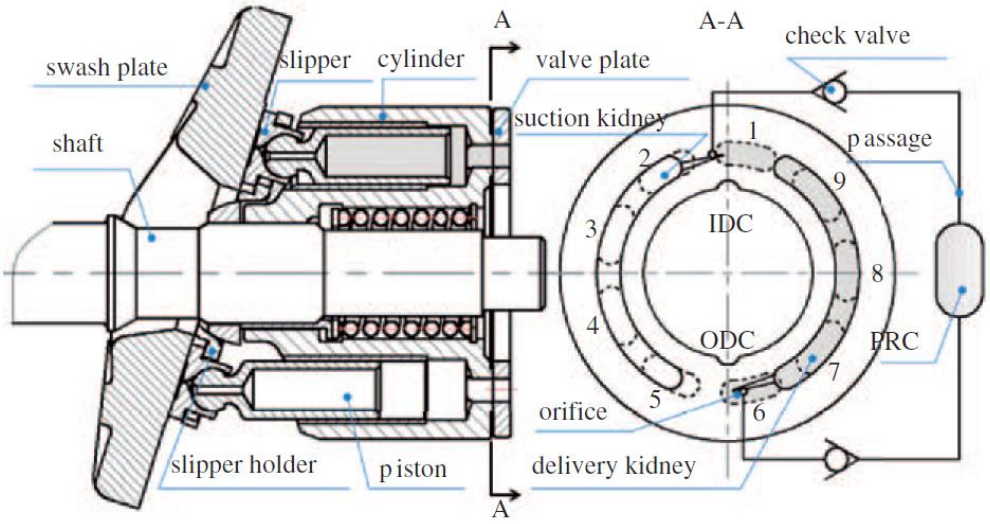

Figure 20: Schematic diagram of an axial piston pump with pressure equalization mechanism [27]

3.2.4 Speed Limitations

Three well-known speed limitations related with axial piston machines are given in the following sections. In addition to these limitations, tribology considerations between piston and cylinder block, valve plate and cylinder block, and retainer and swash plate might be examined.

3.2.4.1 Limitations Related with Cylinder Block

The pressure dynamics of a pump in a cycle is given in the previous sections. The pumping pistons should not be run at the vacuum on whole valve plate in order not to meet wear problems due to cavitation at low pressure.

Ivantysynova presented a pressure relief valve in cylinder-block to reduce pressure peaks [5]. This relief valve limits the chamber pressure on the piston in the cylinder block. By the way, pumping pistons are not jeopardized. This solution needs special

slots and space to implement valves inside the cylinder block. By the way, the force on the cylinder block may be minimized.

Manring [28] investigated the analytical equation of cylinder block tipping away from valve plate. He presented design criteria to eliminate this problem. The cylinder block spring might be designed to satisfy this criterion. The speed limit of the pump with no load condition is determined by inertial forces.

The cylinder block and the valve plate work facing one another with metal to metal contact. It is suggested to produce these components from dissimilar materials. These materials might have a different hardness to prevent adhesion. In general, the mutual faces are coated to prevent wear. These materials might have also an ability to dissipate heat in order to prevent softening.

Manring [7] presented the speed limitation equation due to the cylinder-block filling. The flow passage area and suction port pressure of pump are examined in this relation. The suction port pressure, P_s, or kidney area of the cylinder block, BSA, might be increased in order to increase the maximum speed of the pump by satisfying this equation. Decreasing the pitch radius, R, is another way to increase the maximum speed.

3.2.4.2 Limitation Related with Socket Tipping

Similar to the cylinder block tipping, there exist slipper tipping restrictions. These conditions can occur at high displacements (large inclination angles) and high shaft speeds.

Manring [29] presented the analytical criteria for slipper tipping away from retainer ring. Centrifugal inertia throws away the slippers due to rotational speed effects. The inertial forces acting on the pistons and the slippers are included in this equation.

Speed scaling results of Rexroth open-circuit machinery is shown in Figure 21. Scaling laws are utilized in order to determine speed and displacement volume limitations.

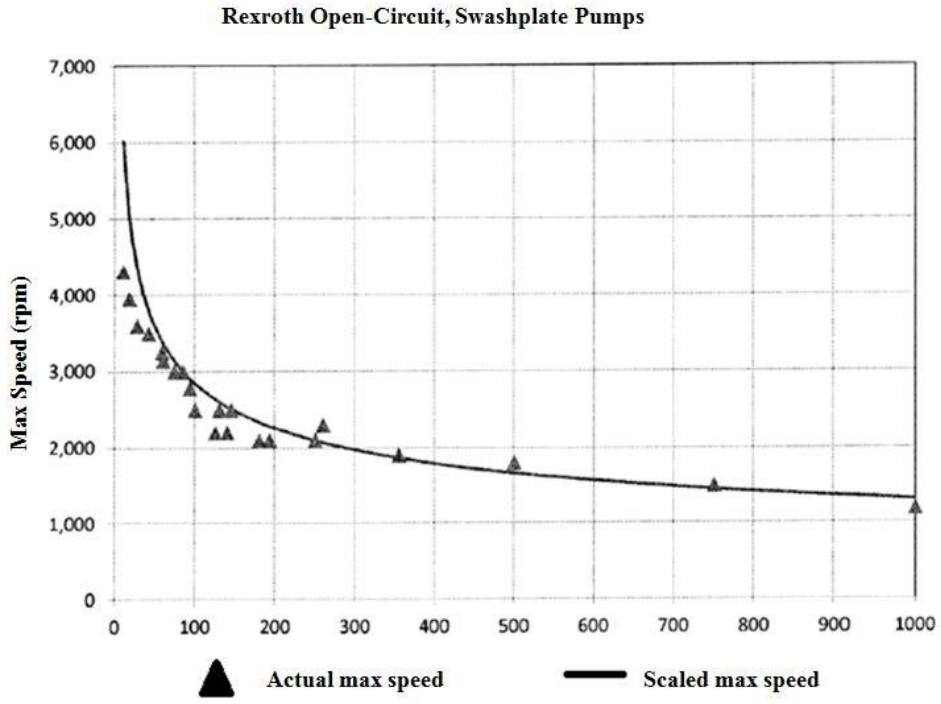

Figure 21: Rexroth open-circuit machinery [29]

3.2.5 Dynamics of the Three-Way Valve

Schematic of a three-way valve, which is utilized to control volumetric flow through to the control actuator, is shown in Figure 22. This valve contains generally a spool, sleeve, and a spring. The left side of the valve, where the spring is mounted, and left chamber side of the spool are connected to the reservoir line. The discharge pressure of the pump, P_d, is used as a hydraulic signal to control spool position, x_{sp}. This valve limits flow through to the control actuator while discharge pressure is lower than maximum full-flow pressure. Discharge pressure works against the spring force to overcome initial overlap, o_d, towards the left chamber connected with reservoir line. When the discharge pressure is higher than the spring force, the fluid flows through to the control chamber.

Although the initial overlap is constant due to the design of the valve, pre-compression of the spring is adjustable. The adjusting component of the valve is shown in Figure 4. Maximum full-flow pressure is determined by adjusting this component.

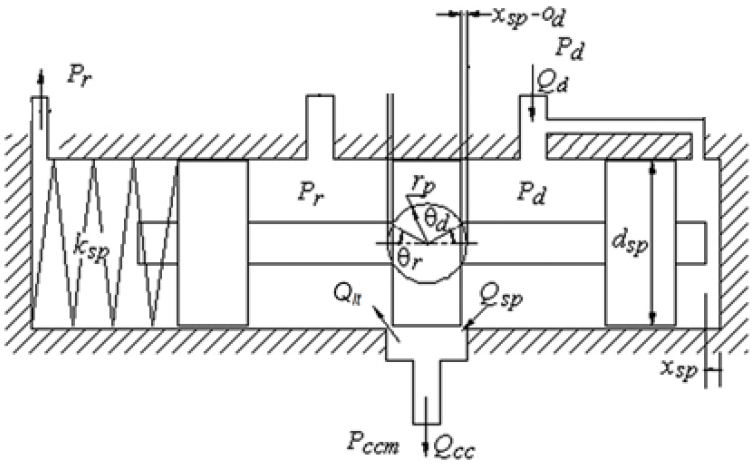

Figure 22: Schematic of a three-way valve [30]

In common usage, sealing equipment is not used to eliminate sticking forces related with the sealing equipment. This type of valve configuration causes internal leakages across the valve while discharge pressure is lower than maximum full-flow pressure.

Leakage equation between the right chamber and control chamber is considered as a steady flow in the annulus between circular shaft and cylinder with no eccentricity [4]. This yields the leakage as where P_{ccm} is the pressure in the control actuator chamber, d_{sp} is spool diameter, c_{rs} is clearance between the sleeve and spool land (o_d-x_{sp}) is column length. Equation 18 is valid while o_d is larger than $x_{sp.}$ This leakage decreases volumetric efficiency while pump discharge pressure is below maximum full-flow pressure. Leakage term related with the spool velocity is neglected.

$$Q_{sp} = \frac{(P_d - P_{ccm})\pi d_{sp} c_{rs}^3}{12\mu(o_d - x_{sp})} \tag{18}$$

By considering spool is zero-lapped, the flow rate is derived in Equation 19 while discharge pressure is between maximum full-flow pressure and rated pressure. Flow rate between the right chamber and control chamber is governed using the classical orifice equation where A_D is the opening area between spool and sleeve. Geometric relation of A_D is given in Equation 20 where θ_d is the half angle at the center of the metering port opening of the spool at the right chamber as shown in Figure 22.

$$Q_{sp} = A_D C_d \sqrt{\frac{2(P_d - P_{ccm})}{\rho}} \tag{19}$$

$$A_D = \begin{cases} r_p^2(\theta_d - \sin(2\theta_d)/2) & x_{sp} < (o_d + r_p) \\ r_p^2(\theta_d + \sin(2\theta_d)/2) & x_{sp} > (o_d + r_p) \end{cases} \tag{20}$$

Leakage flow from control actuator chamber to the reservoir port through the clearance between sleeve and spool, Q_{lt}, is valid while x_{sp} is bigger than o_d, as given in Equation 21. This yields the leakage as where spool diameter is d_{sp}, the clearance between spool and sleeve is c_{rs}, spool displacement is x_{sp}, and initial overlap between spool and sleeve is o_d. The direction of this leakage is shown in Figure 22. While o_d is bigger than $x_{sp,}$ opening area, A_R, at the left side of the metering port is big enough to discharge leakage flow coming from the right chamber. When the discharge pressure is lower than maximum full-flow pressure, the leakage flow regime at the left metering port is negligible for the analysis for a zero lapped valve.

$$Q_{lt} = \frac{(P_{ccm} - P_r)\pi d_{sp} c_{rs}^3}{12\mu(x_{sp} - o_d)} \tag{21}$$

The volumetric flow into the control actuator, Q_{cc}, is shown in Figure 22 by summing flows across the metering port. The relation is expressed in Equation 22.

$$Q_{cc} = Q_{sp} - Q_{lt} \tag{22}$$

Steady state flow produces axial force, F_1, which tends to reduce the valve opening area as shown in Figure 23. Axial force exerted on the spool is defined as

$$F_1 = 2\,C_d\,C_v\,A_D(P_d - P_{ccm})\cos\theta_j \tag{23}$$

where C_d is discharge coefficient, C_v is velocity coefficient, A_D is orifice area, and θ_j is jet angle across the orifice.

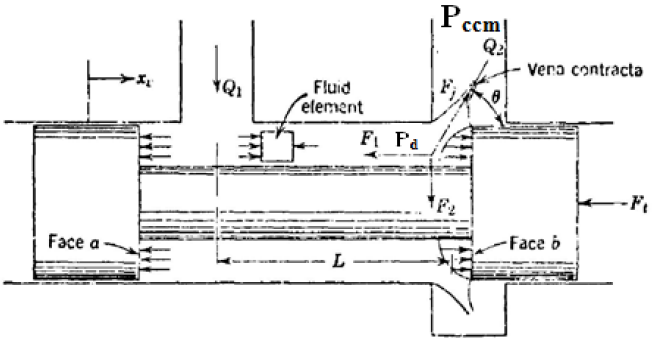

Figure 23: Flow forces on a spool valve due to flow leaving a valve chamber [31]

The equation of motion of the spool shown in Figure 22 is defined as

$$P_dA_{sp} - k_{sp}\delta_{sp} - F_1 = m_{sp}\ddot{x}_{sp} + c_{sp}\dot{x}_{sp} + k_{sp}x_{sp} \tag{24}$$

where A_{sp} is spool area, k_{sp} is spring stiffness, δ_{sp} is initial pre-compression of the spring, m_{sp} is mass of the spool, x_{sp} is spool displacement, c_{sp} is damping coefficient. Damping coefficient of the system is defined in Equation 25. The equation shows that the system works like a simple mass-spring system and it is considered as critically damped.

$$c_{sp} = 2\sqrt{m_{sp}k_{sp}} \tag{25}$$

3.2.6 Dynamics of the Control Actuator

The geometry and the flow configuration of the control piston are shown in Figure 24. Flow against to the control piston, Q_{cc}, is given in Equation 22.

Leakage flow around the control piston is given in Equation 26. Leakage length, l_{c0}, is constant due to pump design. This yields the leakage as where pressure behind the control piston is defined as P_{ccm}, the diameter of control piston is d_c, and the radial clearance between control piston and sleeve is c_{cp}, with considering no eccentricity. Body forces of control piston mass are neglected.

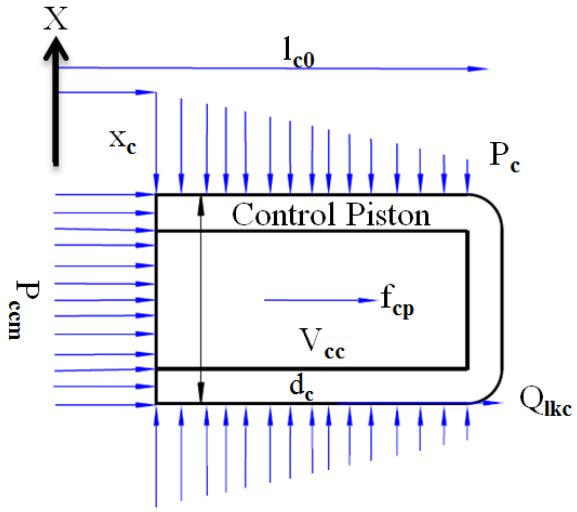

Figure 24: Free body diagram of the control actuator

$$Q_{lkc} = \frac{\pi d_c c_{cp}^3}{12 \mu l_{c0}} (P_{ccm} - P_c) \tag{26}$$

The pressure of the control actuator chamber is given in Equation 27. Displacement of control piston is denoted as x_c. The bulk modulus of fluid is defined as β and minimum volume of the control actuator piston is defined as V_{cc}.

$$\dot{P}_{ccm} = \frac{\beta}{V_{cc} + {d_c}^2 x_c(\pi/4)} \left(Q_{cc} - Q_{lkc} - (\pi/4)\,{d_c}^2 \dot{x}_c\right) \tag{27}$$

The viscous force, f_{cp}, acting on the control piston is given in Equation 28 according to the given relation in [14] where $\dot{x}_c$ is the velocity of the control piston. The total force acting on the control piston is defined in Equation 28.

$$f_{cp} = \frac{\mu\pi(d_c/2)l_{c0}\dot{x}_c}{c_{cp}} \tag{28}$$

$$FCP = (\pi/4)\,{d_c}^2(P_{ccm} - P_c) - f_{cp} \tag{29}$$

3.2.7 Dynamics of the Bias Actuator

The geometry and the flow pattern of the bias actuator are shown in Figure 25. Similar to the control actuator, pressure behind the bias piston is defined as P_{bcm} and leakage around the piston is defined as Q_{lkb}. The bias piston diameter is defined as d_b. The leakage length, l_{b0} - x_b, is variable depending on the displacement of the bias piston, x_b. Positive displacement direction of the bias piston is accepted as opposite direction with respect to the direction shown in Figure 25. While the pump is working below maximum full-flow pressure, displacement of the bias piston, x_b, is at the maximum limit. This yields the leakage as where the clearance between bias piston, the guide is defined as c_{rpc}, the diameter of the bias piston is d_b, and the bias actuator chamber pressure is denoted as P_{bcm}. Body forces of bias piston mass are neglected. Leakage flow around the bias piston, Q_{lkb}, is expressed in Equation 30. Additionally, there is a hole on the side wall of this bias piston. This hole helps the fluid to flow out from the bias piston chamber while unloading the pump. Flow through this hole, Q_{or}, is defined in Equation 31 where the diameter hole at the side wall is denoted as d_{obr}.

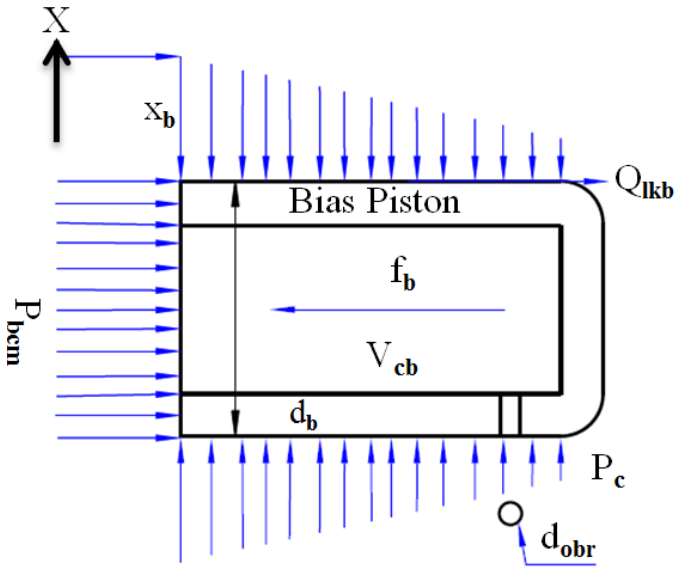

Figure 25: Free body diagram of the bias actuator

$$Q_{lkb} = \frac{\pi d_b c_{rpc}^3}{12\mu(l_{b0} - x_b)}(P_{bcm} - P_c) + \frac{\pi d_b c_{rpc}\dot{x}_b}{2} \tag{30}$$

$$Q_{or} = C_d \frac{\pi {d_{obr}}^2}{4}\sqrt{\frac{2(P_{bcm} - P_c)}{\rho}} \tag{31}$$

The pressure of the bias piston chamber is given in Equation 32, where the minimum volume of the bias actuator is defined as V_{cb}.

$$\dot{P}_{bcm} = \frac{\beta}{V_{cb} + (\pi/4)\,{d_b}^2 x_b}\left(-(\pi/4)\,{d_b}^2\dot{x}_b - Q_{lkb} - Q_{or}\right) \tag{32}$$

The bias piston is at maximum displacement, x_{b_max}, while the pump is not working. The viscous force, f_b, acting on the bias piston is given in Equation 33 according to the given relation in [14]. A compression spring is utilized inside the bias actuator chamber as shown in Figure 9. While the pump is not working, this spring, k_b, has a

pre-compression δ_b. The spring force, F_{spring}, on the bias piston is given in Equation 34 and total force acting on the control piston is defined in Equation 35.

$$f_b = -\frac{\mu\pi(d_b/2)(l_{b0} - x_b)\dot{x}_b}{c_{rpc}} \tag{33}$$

$$F_{spring} = k_b(\delta_b + (x_{bmax} - x_b)) \tag{34}$$

$$FB = F_{spring} + (\pi/4)\, {d_b}^2(P_{bcm} - P_c) + f_b \tag{35}$$

3.2.8 Dynamics of the i^{th} Pumping Piston

Figure 12 shows the control volume analysis of pressure development in a cylinder. Q_d is defined as instantaneous discharge flow out of a piston in Equation 36, where A_d is defined in Equation 16. The discharge pressure of the pump is defined as P_d. Q_s is defined as instantaneous suction flow through a piston in Equation 37, where A_s is defined in Equation 16. The pressure of the pump suction line is defined as P_s. Leakage terms are defined in the previous sections. Q_r represents the flow into and out from the piston chamber through the valve plate opening [32]. Definition of Q_{r_i} for the i^{th} piston is given in Equation 38.

$$Q_{d\_i} = C_d A_d \sqrt{\frac{2(P_i - P_d)}{\rho}} \tag{36}$$

$$Q_{s\_i} = C_d A_s \sqrt{\frac{2(P_s - P_i)}{\rho}} \tag{37}$$

$$Q_{r\_i} = Q_{d\_i} - Q_{s\_i} \tag{38}$$

Instantaneous volume, V_i, is given in Equation 39, where V_m is maximum cylinder volume. Instantaneous displacement of the i^{th} piston is denoted as x_i and piston area is denoted as A_p.

$$V_i = V_m - A_p x_i \tag{39}$$

Individual chamber volumes might be defined for each piston, which is assembled in a circular array inside the cylinder block at equal intervals around the x-axis. The pressure in the cylinder is derived in Equation 40, according to the control volume analysis.

$$\dot{P}_i = \frac{\beta}{V_i}\left(A_p \dot{x}_i - Q_{r\_i} - Q_{SB\_i} - Q_{SK\_i} - Q_{SG\_i} - Q_{SPHERE\_i}\right) \tag{40}$$

The angular position of the i^{th} piston is given in Equation 15. Pressure with respect to the angular position of the cylinder is given in Equation 41.

$$\frac{dP_i}{d\theta} = \frac{\beta}{\omega V_i}\left(A_p \dot{x}_i - Q_{r\_i} - Q_{SB\_i} - Q_{SK\_i} - Q_{SG\_i} - Q_{SPHERE\_i}\right) \tag{41}$$

The viscous force, F_{TK}, acting on the i^{th} piston is given in Equation 42 where $\dot{x}_i$ is the velocity of the i^{th} piston. The positive direction of the viscous force is considered as the direction against the positive direction of $\dot{x}_i$, which is shown in Figure 26. The engaged length between piston and cylinder block is shown l_i when x_i equals to zero.

$$F_{TK\_i} = \frac{\mu\pi(d_p/2)(l_i + x_i)\dot{x}_i}{h_k} \tag{42}$$

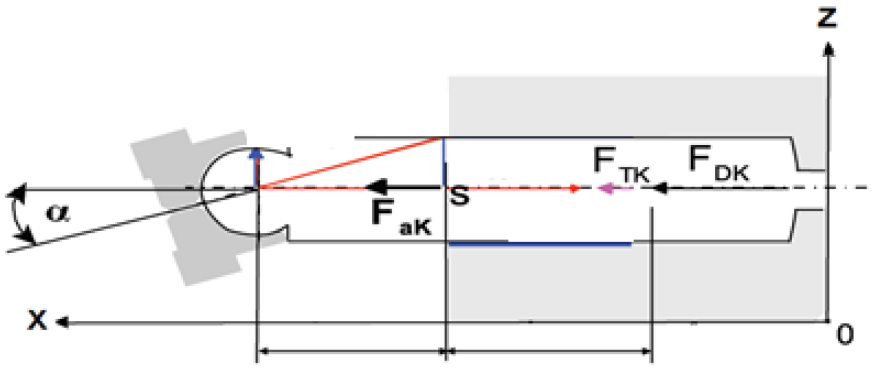

Figure 26: Forces acting on the i^{th} piston in the x-direction [32]

The inertia force, F_{aK}, acting on the i^{th} piston center of the piston-slipper group is given in Equation 43 where the mass of a piston and slipper group is defined as m_p.

$$F_{aK\_i} = m_p \ddot{x}_i \tag{43}$$

The pressure force, F_{DK}, acting on the i^{th} piston is given in Equation 44 where the area of a barrel piston is defined as A_P multiplied by differential pressure across the barrel piston.

$$F_{DKi} = A_P(P_i - P_c) \tag{44}$$

The total force acting on the i^{th} piston in the x-direction is given in Equation 45. Centrifugal force, $F_{\omega K}$, acts in the y-direction on the piston.

$$F_{AK\_i} = F_{aK\_i} + F_{DK\_i} + F_{TK\_i} \tag{45}$$

3.2.9 Dynamics of the Swash Plate Mechanism

Swivel torque due to pumping piston pressure is obtained by summation of the forces on each piston which are nested in the cylinder block as shown in Figure 27.

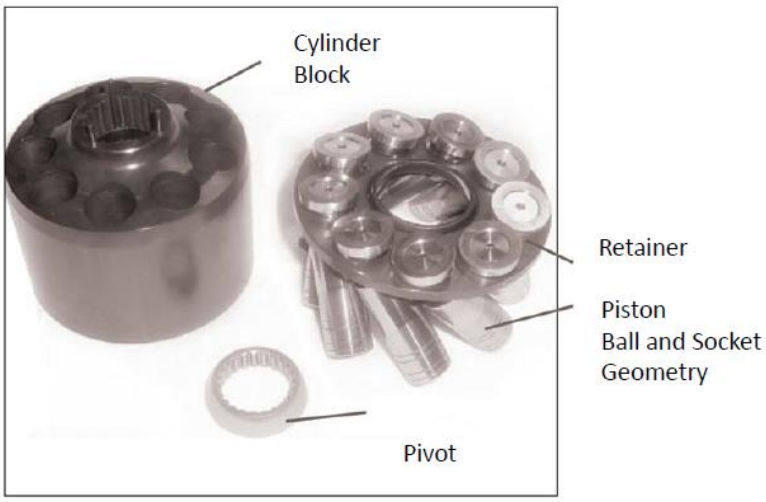

Figure 27: Cylinder block and multi-piston [23]

Swivel torque occurs due to the forces acting on each pumping piston and actuators. Figure 28 shows a diagram of forces exerted on the swash plate by a single piston [33]. Cylinder block center axis in x-axis and swivel axis of the swash plate (parallel to the y-axis) do not intersect as shown in Figure 28. The moment arm is defined in Equation 46. The axial total force in the x-direction is shown in Equation 45. The reaction of the i^{th} piston, F_{SK}, is defined in Equation 47.

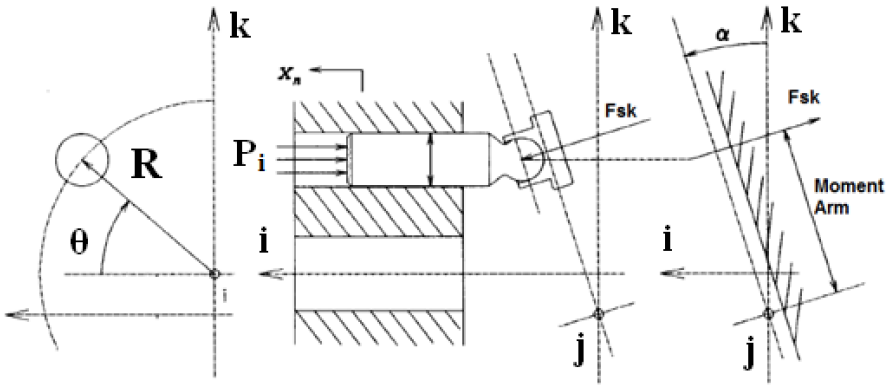

Figure 28: Swivel torque force diagram [33]

$$\text{Moment\_Arm} = \frac{R\sin(\theta) + (a - b)\sin(\alpha)}{\cos(\alpha)} \tag{46}$$

$$F_{SK\_i} = -\frac{F_{AK\_i}}{\cos(\alpha)} \tag{47}$$

The expression for torque applied to the swash plate, T_{y_i}, by the i^{th} piston is defined in Equation 48. The total torque applied to the swash plate in the y-direction by the pumping pistons is simply the summation as defined in Equation 49.

$$T_{y\_i} = F_{SK\_i}\text{Moment\_Arm} = -\frac{F_{AK\_i}}{\cos(\alpha)}\frac{(R\sin(\theta) + (a-b)\sin(\alpha))}{\cos(\alpha)} \tag{48}$$

$$T_y = \sum_{i=1}^{N} T_{y\_i} \tag{49}$$

Control actuator has to have the ability to overcome total torque applied to the swash plate in the y-direction in order to control the swash plate angle. Control actuator area has to be designed by considering this restriction.

Torque on the swash plate around x-direction and z-direction must be carried by swash plate bearings. The definition of these torques is explained with details in [5].

The force formed by the pressure, F_{DK}, is overpowering the other force sources at high pressures. The pressure in a barrel is being negative in a region on valve plate in a cycle. The total hydraulic torque applied to the swash plate in y-axis by the pumping pistons can be negative because of the pressure variations in a cycle. In order to have smooth operation Inequality 50 must be satisfied while discharge pressure is lower than the maximum full-flow pressure. Force constituted by the bias actuator, FB, is shown in Equation 35 and moment arm is defined as LR. By satisfying this condition, the total torque on the swash plate is being always positive. This is very important to eliminate oscillations of swash plate in a cycle while discharge pressure is lower than maximum full-flow pressure.

$$FB * LR > abs(min(0, T_y)) \quad (50)$$

Manring explained the various designed swash plate geometries in [7]. In this paper design of a trunning mounted, transverse servo swash plate is investigated as shown in Figure 29. Moment arms are the same for bias actuator and control actuator in this type of pumps.

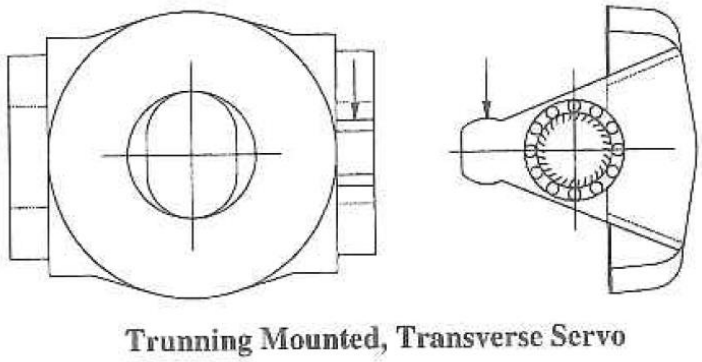

Figure 29: Geometry of the swash plate [7]

Schoenau et al [14] presented a complete pump model that includes individual torques on swash plate. An effective mass moment of inertia is defined which includes parameters apart from yoke assembly and variables related with operating conditions. This relation is handled by substitution of the input torques into complete pump model and grouping similar terms. In addition to the definition of effective mass moment of inertia, complete pump model coefficients are determined.

Manring and Johnson [34] presented a dynamic model of the pumping system. In this research, the equation of motion of the swash plate is presented by summing the moments at the pivot axis. By considering the results of this research, it is eligible to say that effects of the swash plate inertia and damping are negligible compared to the stiffness of the control actuator on system characteristics. This means that motion of the swash plate is highly dependent on the working conditions.

Manring [35] examined the control and containment forces acting on the swash plate. Total containment force acting on the swash plate bearings is shown analytically. As shown in the paper, the frequency of the forces is designated the number of pistons multiplied by pump shaft frequency. It is shown that frequency of the torque on the swash plate is twice of the force-frequency. Frequencies of the alternating forces and torques must be considered in order to determine right bearings, housings, and driving motor shaft.

Zhang et al presented a new swash plate damping model for hydraulic axial-piston pump [36]. An analytical expression is given which is a function of discharge pressure and swash plate angle.

The equation of motion of the swash plate mechanism around y-axis [34] is defined in Equation 51. Mass moment of inertia of the swash plate is defined as I.

$$I\ddot{\alpha} = (FB - FCP)LR + \sum_{i=1}^{N} T_y \tag{51}$$

The translational motion of the bias actuator and control actuator is in the opposite directions as shown in Figure 30. Motions of bias actuator and control actuator are defined in terms of swash plate angle in Equation 52 and Equation 53, respectively.

$$x_b = \alpha LR \tag{52}$$

$$x_c = -\alpha LR \tag{53}$$

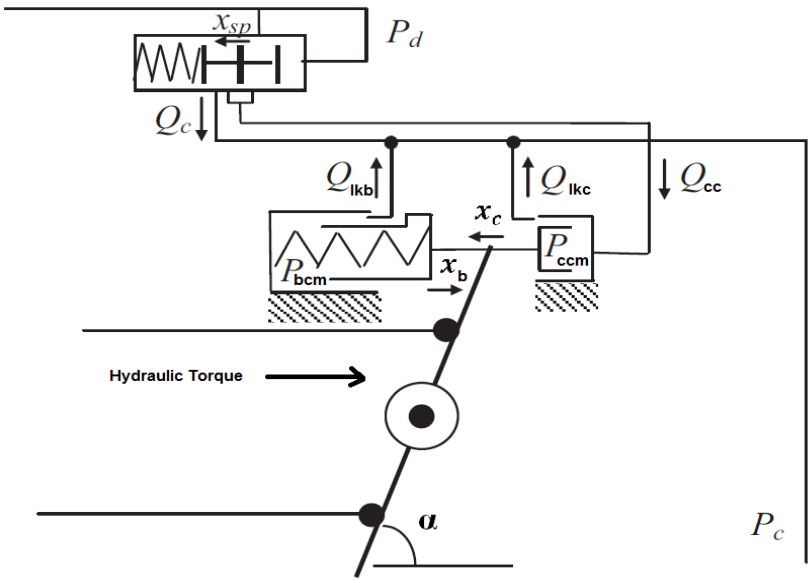

Figure 30: Schematic of a pressure compensator of an axial-piston swash plate pump [37]

3.2.10 Dynamics of the Pump

Pistons, which are coupled with ball and socket geometry, are arranged on the swash plate plain surface as shown in Figure 9 and the fundamental working principles are explained in Section 3.1. While a piston crosses over the suction port, it tends to increase fluid volume of the pumping piston chamber up to TDC by sliding on the inclined plane. The instantaneous suction flow of the pump is defined in Equation 54, where Q_{si} is defined in Equation 37.

$$Q_s = \sum_{i=1}^{N} Q_{si} \tag{54}$$

As a piston passes over the delivery port, it tends to decrease the fluid volume of the pumping piston chamber up to BDC by sliding on the inclined plane. This process occurs N times for each cycle of the pump. The instantaneous delivery flow of the pump is defined in Equation 55, where Q_{di} is defined in Equation 36.

$$Q_d = \sum_{i=1}^{N} Q_{di} \tag{55}$$

Watton [6] presented flow rate change of pump with respect to the angular position of a piston. It has been seen that flow rate has unique oscillation that resembles half sine wave at twice of the pump frequency (N x shaft frequency). Definition of flow rate change is shown for both odd and even piston pumps. Geometric oscillations for an axial piston pump for various piston numbers are shown in Table 2, where V_s is swept volume for a piston. Flow oscillation for a pump, whose piston number is odd, is the same for twice of this odd piston number. Because of this reason, an odd number of pistons are utilized in axial piston pumps generally.

Table 2: Geometric oscillation for an axial piston pump

N	3	4	5	6	7	8	9	10
$\frac{2\,\pi\,\delta Q}{N\,V_s\,\omega}$	0.14	0.325	0.05	0.14	0.0253	0.078	0.0153	0.05

3.2.11 Dynamics of the Test Bench

Ivantysynova presented various circuit diagrams in order to determine displacement volume in open circuit, displacement volume in closed circuit, efficiency test of a pump in open circuit, efficiency test of a pump in closed circuit and response time of a pressure controlled pump in [5].

Functional requirements and qualification tests are explained in detailed in [10]. In order to qualify a pump; dimensional check of principal parts, proof pressure test, determination of response time test, pressure oscillation test, cavitation test, etc. must

be done. In addition to these qualification tests, this document also consist acceptance tests.

The discharge pressure of the pump depends on the load condition of the hydraulic circuit. Flow through the orifice in the direction of the reservoir is defined in Equation 56, where reservoir pressure is defined as P_r and orifice opening area is defined as A_{od}.

$$Q_L = C_d A_{od} \sqrt{\frac{2(P_d - P_r)}{\rho}} \tag{56}$$

The discharge pressure of the pump is modeled using control volume approach. The control volume is defined as V_{md}, which covers from pump outlet to the needle valve. The discharge line of the pump is shown in Figure 31. The discharge pressure is given in Equation 57. Leakage term covers various flow paths, which are explained in Section 3.2.2. These flow paths are given for individual pistons. Total internal leakage of the pump is simply summation of these terms with leakage due to pressure compensator mechanism.

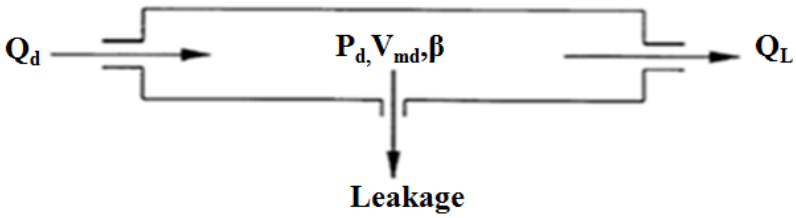

Figure 31: Determination of the delivery line for modeling discharge pressure of the pump

$$\dot{P}_d = \frac{\beta}{V_{md}} (Q_d - Q_L - \text{Leakage}) \tag{57}$$

As seen from Figure 32, a needle valve is utilized in order to load pump. Opening area, A_{od}, of this valve is controlled in order to control the discharge pressure of the pump. The hydraulic line between the test pump and the needle valve is constructed with a rigid pipeline to eliminate compensation of pressure oscillations on hoses. The pump is driven by a simple DC Motor at a constant speed. Technical details of the test bench hydraulic components are given in Appendix D. Pump test setup is shown in Figure 33.

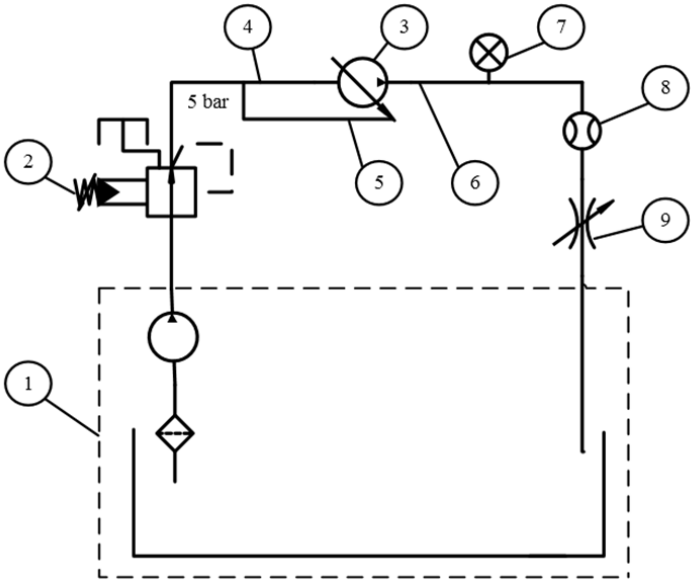

Part Number	Equipment
1	Hydraulic Test Unit
2	Pressure Reducing Valve
3	Test Pump
4	Suction Line
5	Leakage Line
6	Delivery Line
7	Pressure Sensor
8	Flowmeter
9	Needle Valve

Figure 32: Circuit diagram of the pump test bench

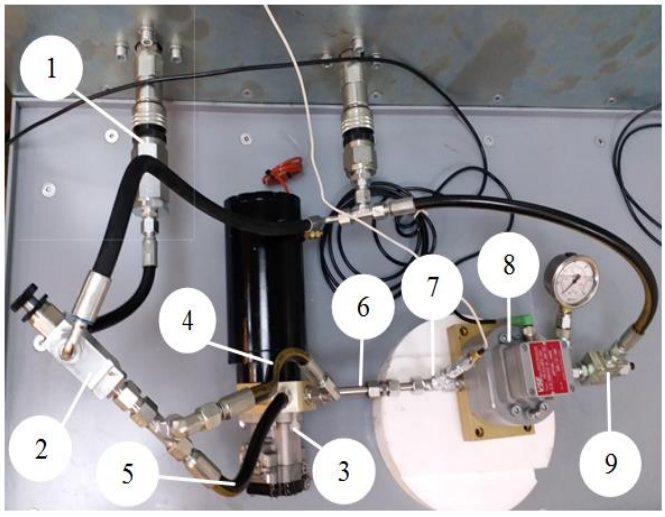

Part Number	Equipment
1	Hydraulic Test Unit
2	Pressure Reducing Valve
3	Test Pump
4	Suction Line
5	Leakage Line
6	Delivery Line
7	Pressure Sensor
8	Flowmeter
9	Needle Valve

Figure 33: Pump test bench

CHAPTER 4

SIMULATIONS AND EXPERIMENTAL RESULTS

The simulation model is built by considering physical relations given in the previous sections. Matlab/Simulink environment is used in order to model nonlinear equations given in the previous sections numerically.

The simulation and the experimental results of the pressure compensated axial piston pump are examined in this section. The evaluation of the performance of the pump is made in time-based.

It is important to mention that fixed-step ODE5 (Dormand-Prince) is used as solver in Matlab/Simulink simulations. The model is run several times by decreasing step size till achieve converged solutions in order to determine critical step size. Same results are handled by using step size equal or less than the critical value. It is found that critical step size is $10e^{-08}$ for these coupled equations by trial. Step size is used as $5e^{-08}$ in simulations in order to handle converged solutions.

4.1 Pump Model

4.1.1 Piston Model

The piston model uses the swash plate kinematics, discharge pressure, and angular position of piston, θ, as shown in Appendix A. The swash plate kinematics and angular position of piston, θ, determines the piston kinematics. Instantaneous delivery port area and suction port area are calculated due to angular position of piston. Delivery flow rate and suction flow rate are calculated by considering these areas, discharge pressure, and instantaneous pressure of the piston chamber. These

flows, piston kinematics, instantaneous swash plate angle, angular position of piston, instantaneous piston pressure are used in order to calculate delivery flow rate, hydraulic torque, leakages, and instantaneous piston pressure. The pump model contains multi-piston models with a phase difference, $2\pi/N$.

4.1.2 Compensation Section Model

The compensation section uses discharge pressure and hydraulic torque as shown in Appendix B. The discharge pressure powers the control actuator due its magnitude. Mechanical torque on the swash plate is calculated due to discharge pressure. Total torque on the swash plate is accumulated in the torque model section in order to model the swash plate kinematics. The bias actuator and the control actuator kinematics are also determined by Equation 52 and Equation 53 in the torque model section.

4.2 Test Bench Model

The pump test bench contains the pump and a needle valve as shown in Figure 32. This needle valve is used to adjust pump discharge pressure at various magnitudes. The load flow, Q_L, across the needle valve versus discharge pressure is measured experimentally. From these measurements, the opening area, A_{od}, versus the discharge pressure is calculated for the needle valve used in the test bench as shown in Appendix C. The test pressure is used as input to the simulation model by considering this relation.

4.3 Internal Dynamics Simulations

4.3.1 Kinematic Analysis

The kinematic relation of the displacement, velocity and acceleration of the i^{th} pumping piston are given in Equation 3, Equation 4 and Equation 5 respectively. Normalized kinematics of the i^{th} piston is given in Figure 34 for the case where

swash plate angle, α, is 16°, and secondary swash plate angle, η, is 2.5°. These angles are obtained values from the pump geometry.

The angles are given in Figure 34 by considering θ equals to the zero on discharge port in y-plane as shown in Figure 8. It is important to mention that BDC (where minimum cylinder volume occurs) is at 81.4° and TDC (where maximum cylinder volume occurs) is at 261.1° as seen in Figure 34. The angle between the axis of symmetry and BDC is named as the cross angle. The cross angle is 8.6° for this pump. These BDC and TDC points are so important to determine the indexing angle, δ, and the angle of kidney-shaped flow passage area on valve plate, ψ′, that are explained in Section 3.2.3. The variation of these points from quarter angles is due to superimposing of swash plate angles. This condition is valid when the discharge pressure is lower than rated pressure.

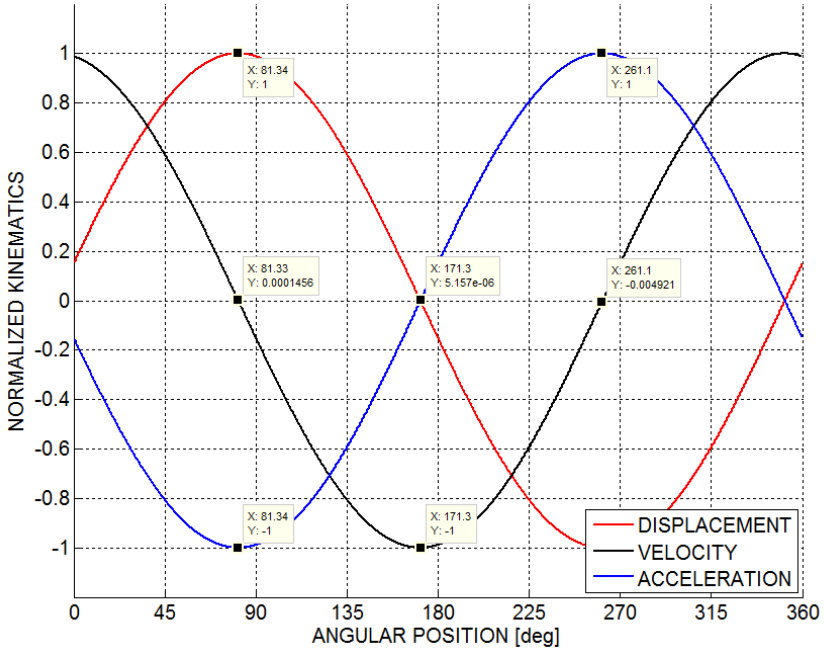

Figure 34: Motion of the ith piston in a cycle while α=16°, η=2.5°

The normalized motion of the ith pumping piston at rated pressure is shown in Figure 35. Swash plate angle, α, is equal to the minimum due to compensation of pressure mechanism and secondary swash plate angle, η, is equal to 2.5°. This secondary swash plate angle does not vary with the pump working conditions. As explained in

Section 3.1, the displacement of the i^{th} piston at rated pressure is designed in order for self-lubrication of the pump, decreasing excessive noise, improving the efficiency of the pump, and the flow requirement of pressure compensation mechanism. Because of the piston motion, extreme points are carried out near the middle of the suction port and discharge port, only half of this displacement volume can turn into flow. After the piston passes the extreme point at the discharge port approximately 360°, this piston is ready to suck fluid from pump discharge line. In other words, while the piston passes the extreme point at suction port approximately 180°, this piston is ready to discharge fluid to the reservoir line.

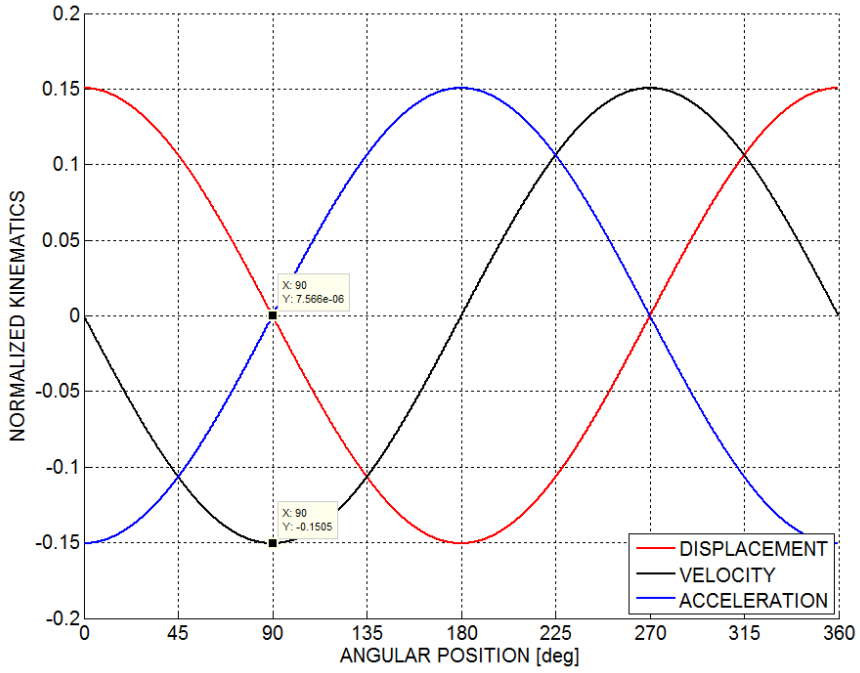

Figure 35: Motion of the i^{th} piston in a cycle while α=0°, η=2.5°

4.3.2 Simulation of Single Piston Discharge Pressure Profile on Valve Plate

The pressure profile of a piston on original valve plate at 100 bar in a cycle is shown in Figure 36. Saturation toolbox is used to determine the least pressure in the cylinder

block. $1e^{-12}$ Pa is used as minimum pressure limit. This pressure magnitude is obtained in a laboratory by researchers [38].

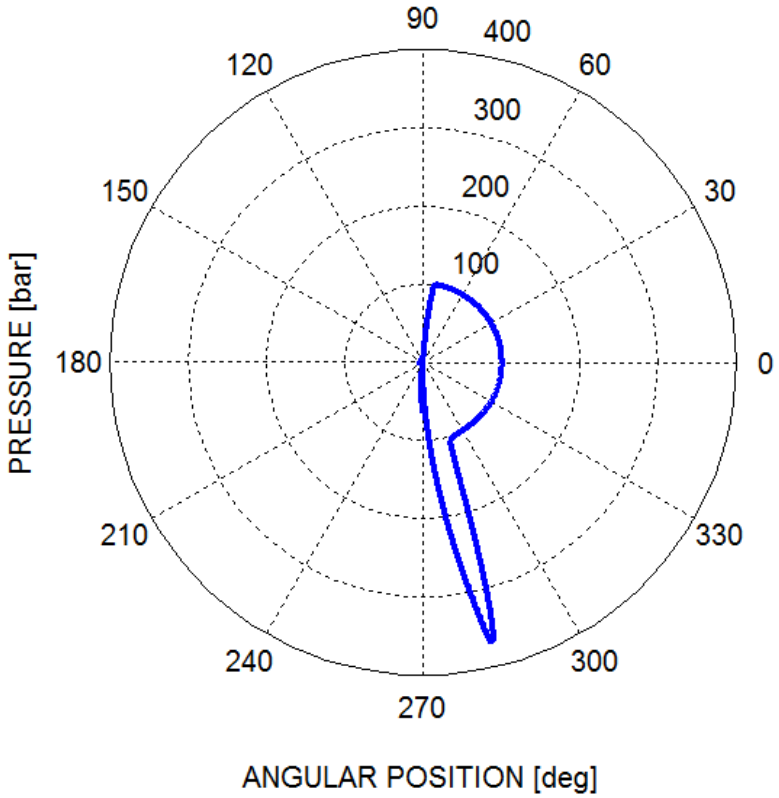

Figure 36: The chamber pressure, P_i, of a piston in a cycle when P_d=100 bar

It is seen that instantaneous pressure in trapping motion reaches through 368 bar while the pump/piston is working at 100 bar. It must be mentioned that the mechanical components are forced more than needed due to this jeopardization action. ψ' is measured 53.5° and indexing angle, δ, is measured 10.5° in this pump.

In order to decrease this pressure peak, a case study is done. In this study, the valve plate is designed in accordance with line to line porting where ψ' equal to ψ and the indexing angle, δ, equal to zero.

It is simulated that pressure peak can be minimized by utilizing line to line porting valve plate and changing indexing angle, δ, from 10.5° to the 0° as shown in Figure 37. The base method to control pressure peaks of the pump is optimizing dimensions of kidney ports on valve plate.

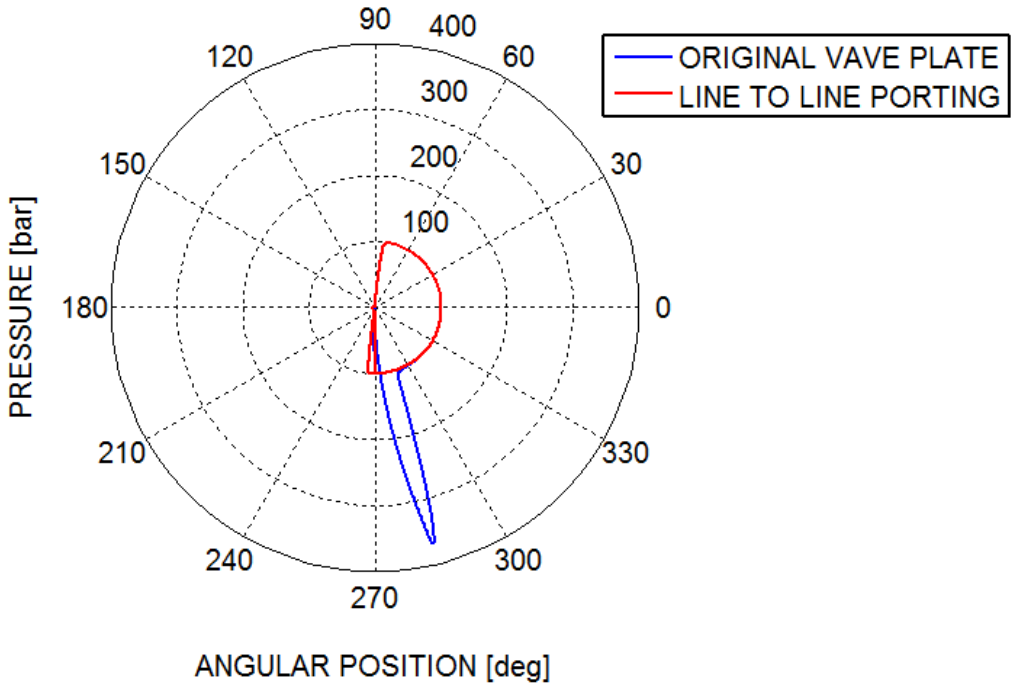

Figure 37: The chamber pressure, P_i, of a piston in a cycle with original valve plate and line to line porting design when P_d=100 bar

4.3.3 Simulation of Single Piston Delivery Flow Profile

The flow rate of a piston in a cycle on valve plate is shown in Figure 38 while the discharge pressure is at 100 bar. As seen from Figure 38, an initial flow peak occurs when the piston aligns with the discharge port due to over-compression between TDC and the angle that delivery flow begins. Then the flow rate decreases to a degree in accordance with the piston velocity. As shown in Figure 34, the maximum piston velocity happens when the piston is at the position where θ is between 340° and 350° during discharge pressure is lower than maximum full-flow pressure. The flow rate is the highest magnitude when the piston is at the maximum velocity which is shown in Figure 38, by ignoring flow peak. It is mentioned in Section 3.2.3 that Q_{web} might not be used around the region where maximum flow occurs.

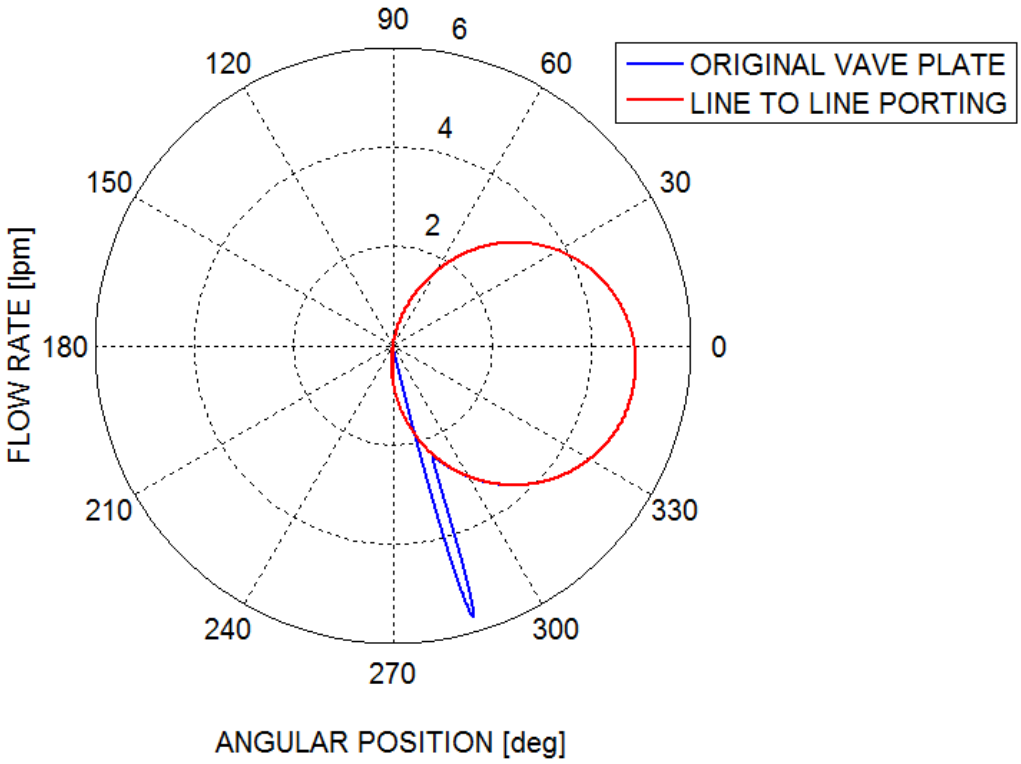

Figure 38: The delivery flow, Q_{di}, of a piston in a cycle on valve plate when P_d=100 bar

The case study is done in same conditions with the pressure profiles are given in Section 4.3.2. It is seen that the decrement in the pressure peak comes into account as a smooth flow rate variation in the discharge port.

The flow peak causes pressure fluctuations and vibration on the delivery line. This is very harmful to hydraulic pipes. According to the statistics, almost half of the reported failures of hydraulic systems on aircraft were due to the fracture of hydraulic pipes [39].

4.3.4 Simulation of Single Piston Delivery Flow Profile at Rated Pressure

The flow rate of a piston in a cycle on original valve plate is shown in Figure 39 while the discharge pressure is at rated pressure, 170 bar. As seen from Figure 39, an initial flow peak occurs when the piston aligns with the discharge port, due to the high pressure inside the piston. Then the flow rate decreases to the zero in accordance with the piston velocity. After piston crosses maximum displacement

point as shown in Figure 35, pumping piston chamber tends to increase while discharge area of the piston is open to the delivery line. Due to this reason, there exists backflow from delivery line to the pumping piston chamber.

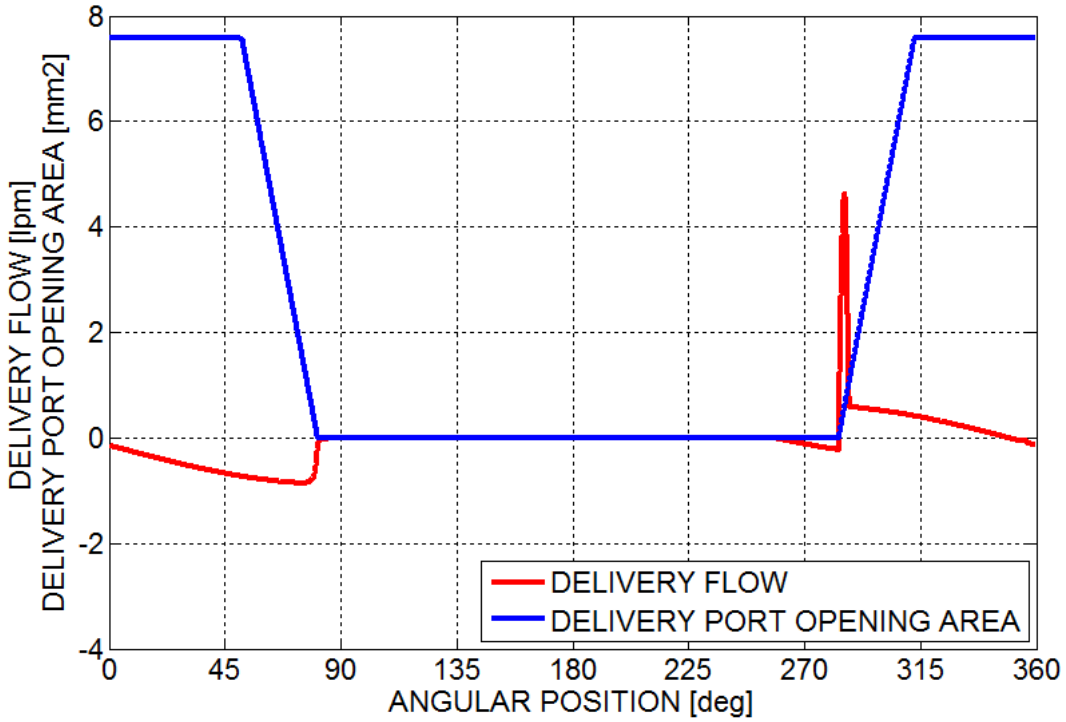

Figure 39: The delivery flow, Q_{di}, versus angular position, θ, at the rated pressure on the original valve plate

The flow rate of a piston in a cycle on line to line porting valve plate is shown in Figure 40 while the discharge pressure is at rated pressure, 170 bar. As seen in Figure 40, a backflow peak occurs when the piston tends to decrease the pumping piston chamber. Then delivery flow corresponds to piston velocity as shown in Figure 35.

Schematic of delivery flow, Q_{di}, the direction of a piston at rated pressure is given in Figure 41 in order to visualize the motion of the hydraulic fluid. Flow through to the inward plane means that hydraulic fluid in delivery line is fed by pumping piston. In adverse, flow through to the outward plane means that hydraulic fluid in the chamber of pumping piston is fed by pressurized delivery line.

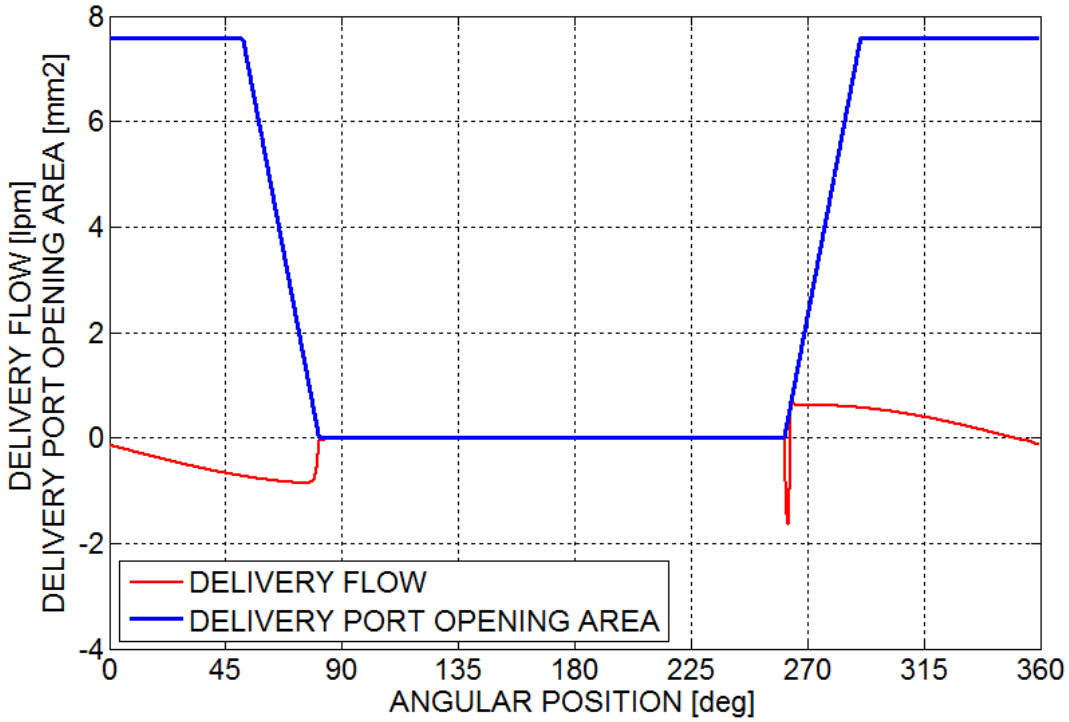

Figure 40: The delivery flow, Q_{di}, versus angular position, θ, at the rated pressure on the line to line porting

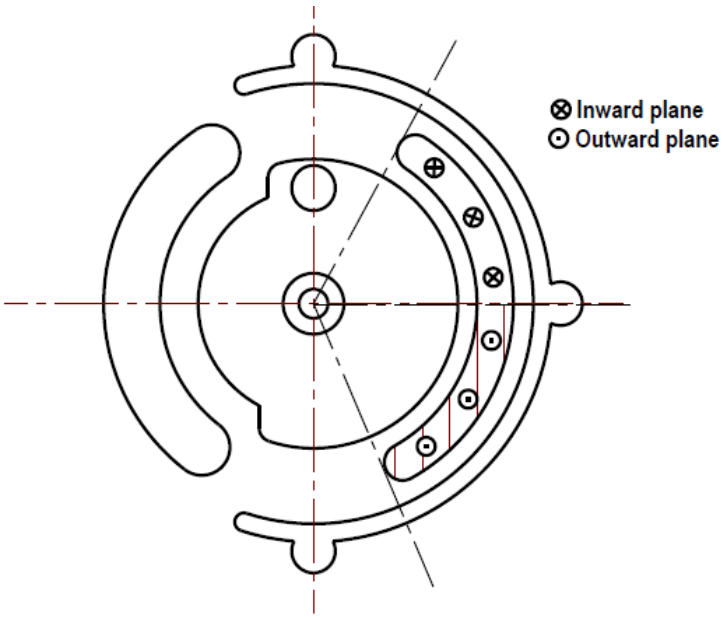

Figure 41: Schematic of delivery flow direction for a piston on valve plate at the rated pressure

4.3.5 Simulation of Single Piston Leakage Profiles

In this section, leakage flow sources are investigated related with a pumping piston. The definitions of these flows are shown in Section 3.2.2. The simulations of these leakage flows are studied in this section. In addition to original valve plate simulation, the leakage flow forms of the case studies are inspected. By eliminating pressure peak in the cylinder block chamber, the line to line porting designated valve plate improves the leakage flow to be smoother than other cases. Simulations show that leakage flow between the cylinder block and valve plate, and ball and socket joint leakage are the dominant part of the total leakage.

In addition to the simulation conditions explained in previous sections, a trapped design is studied. The simulation cases examined in this study are shown in Table 3.

Table 3: The simulation cases

Cases	The angle of the kidney-shaped port on cylinder block, Ψ	The angle of the kidney-shaped closed section between ports on valve plate, ψ'	Indexing Angle (δ)
Original Valve Plate	29.5°	53.4°	10.5°
Trapped Design	29.5°	40.1°	3.5°
Line to Line Porting	29.5°	29.5°	0°

4.3.5.1 Simulation of Leakage Flow between Cylinder Block and Valve Plate (Q_{SB})

The leakage flow between the valve plate and cylinder block (Q_{SB}) is explained in Section 3.2.2.2. As shown in Figure 42, this leakage flow around piston acts like pressure profile as shown in Figure 37. This result is valid while the gap between the valve plate and cylinder block, h_B, is constant.

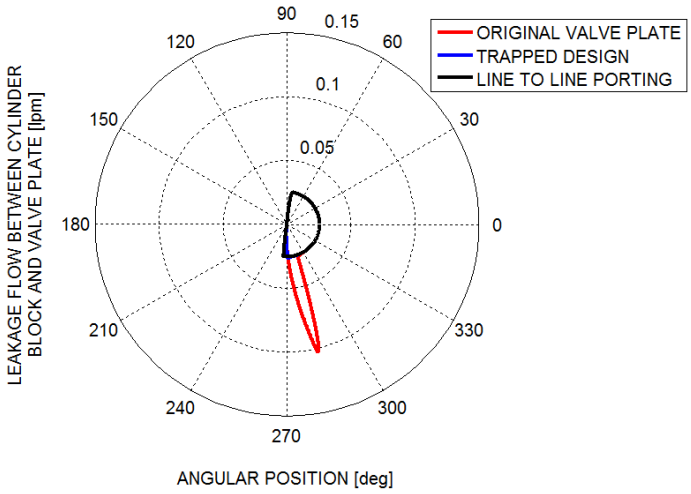

Figure 42: Leakage flow between the cylinder block and valve plate when P_d=100 bar

4.3.5.2 Simulation of Leakage Flow around a Piston (Q_{SK})

The leakage flow around a piston, Q_{SB}, is explained in Section 3.2.2.1. As shown in Figure 43, this leakage flow acts like pressure profile as shown in Figure 37. The shape of the leakage flow likes a half circle as shown in Figure 43. The center of half circle is located at a point which has an offset from the center point of axis system. This offset occurs due to the variation of instantaneous leakage flow path length, l_k. When the piston moves to the BDC, this flow path term increases. The leakage flow rate is inversely proportional to this term.

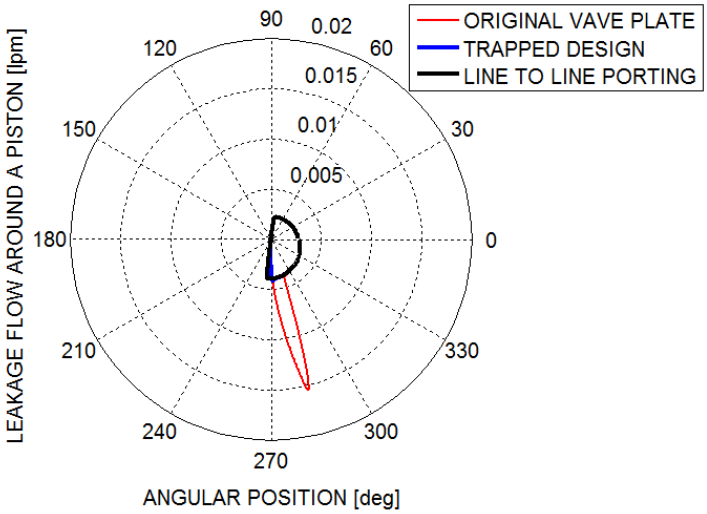

Figure 43: Leakage flow around a piston when P_d=100 bar

4.3.5.3 Simulation of Leakage Flow through the Slipper and Swash Plate (Q_{SG})

The leakage flow through the slipper and swash plate, Q_{SG}, is explained in Section 3.2.2.3. As shown in Figure 44, this leakage flow acts like pressure profile as shown in Figure 37. This leakage flow varies only with pressure variations. Although h_G varies depending on the pump operating conditions, in simulation h_G is assumed to be constant. The other terms in Equation 13 do not change with working conditions.

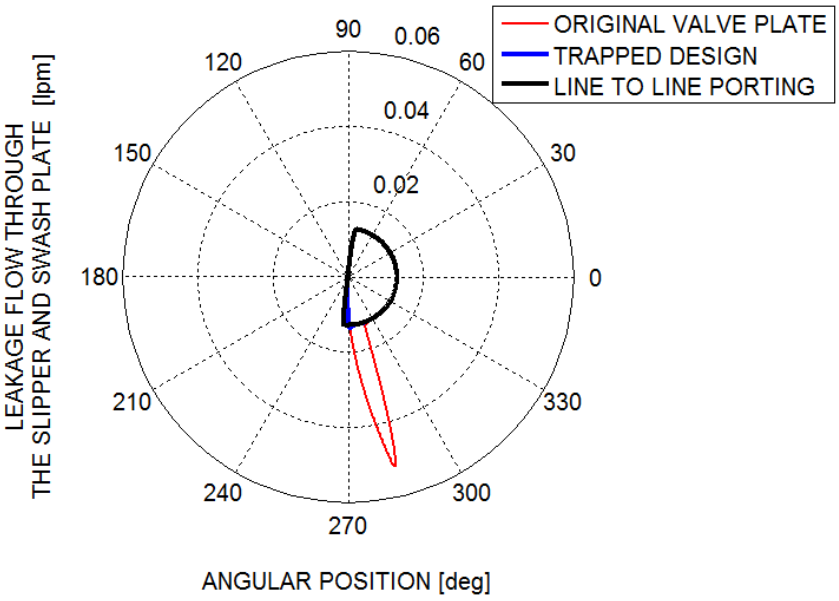

Figure 44: Leakage flow through the slipper and swash plate when P_d=100 bar

4.3.5.4 Simulation of Ball and Socket Joint Leakage Flow (Q_{SPHERE})

The leakage flow outward of the ball and socket joint, Q_{SPHERE}, is explained in Section 3.2.2.4. As shown in Figure 45, this leakage flow across the ball and socket joint is similar to the pressure profile shown in Figure 37. The magnitude of this flow changes with the pressure variations. The other terms in Equation 14 are related with joint design.

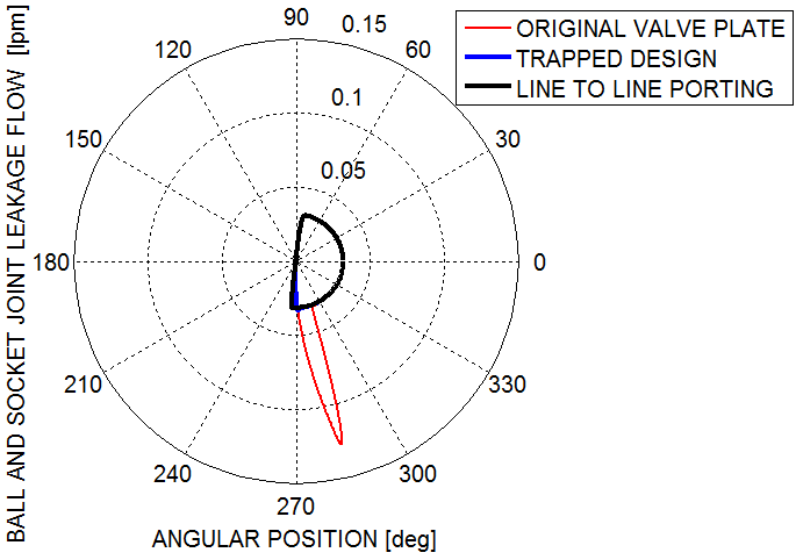

Figure 45: Ball and socket joint leakage flow when P_d=100 bar

4.3.6 Simulation of Hydraulic Torque on Swash Plate Applied by Single Piston

The sources of hydraulic torque on swash plate are explained in Section 3.2.9. The direction of the hydraulic torque changes when the piston passes swivel axis as shown in Figure 46 while the discharge pressure is 100 bar. This figure is given for original pump, whose maximum full-flow pressure is higher than 100 bar. The swash plate swivel axis is generally located away from the shaft axis in order to decrease the negative torque. This negative torque tries to decrease swash plate angle, α.

The torque peak is eliminated by employing line to line porting. This is very beneficial while the control actuator works for decreasing swash plate angle, α.

The torque sources are examined to determine dominating part of the total torque. The equation of pressure force acting on swash plate is defined in Equation 44. The torque due to the pressure force is shown in Figure 47. By considering maximum torque values of both valve plate designs, the torque due to pressure is the most dominant part of the total torque on the swash plate. The inertial and friction forces are equal for both conditions and negligible with respect to the pressure forces.

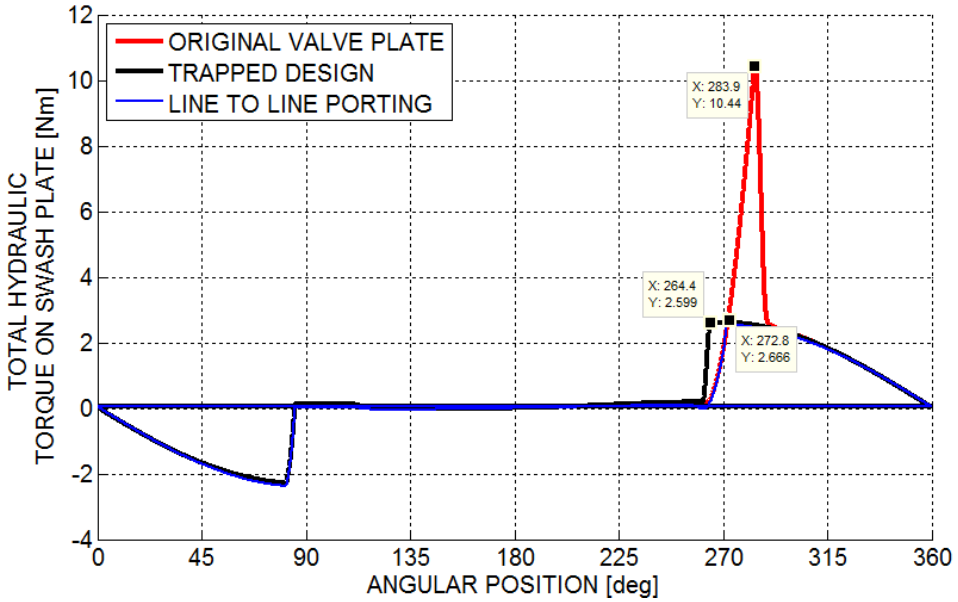

Figure 46: Hydraulic torque on swash plate due to a piston when P_d=100 bar

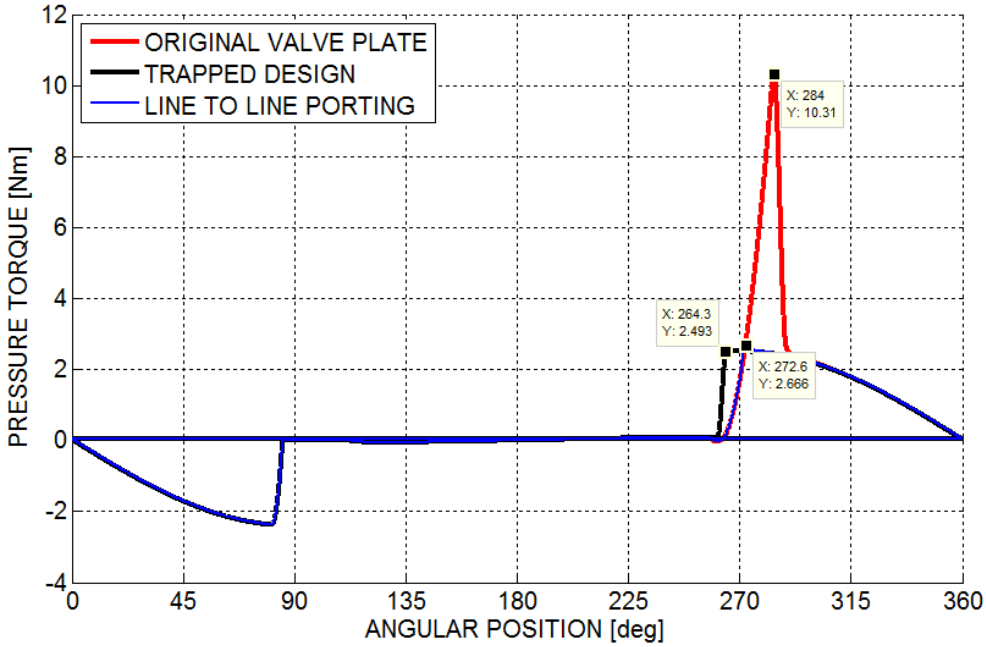

Figure 47: Hydraulic torque on swash plate due to pressure forces when P_d=100 bar

4.3.7 Simulation of Multi-Piston Pressure (P_d)

The multi-piston model is simulated by employing the single piston model with a phase shift. The phase shift, 2π/N, is determined by the number of pistons. A pump, which has nine pistons, is simulated in this study.

The discharge pressure profile of multi-piston model from start-up to 100 bar in a cycle for various valve plates is shown in Figure 48. The pressure oscillations magnitude is maximum on original valve plate. This pressure oscillations magnitude is decreased by utilizing trapped design. In line to line porting type valve plate, this magnitude is reduced to nearly zero.

Although the frequencies of pressure oscillations are different as shown in Figure 48, this is misleading. The second flow peak in 40° degrees travel of a piston at original valve plate is not seen clearly. The pump shaft frequency is multiplied by two times N (number of pistons) in order to determine pump discharge pressure frequency.

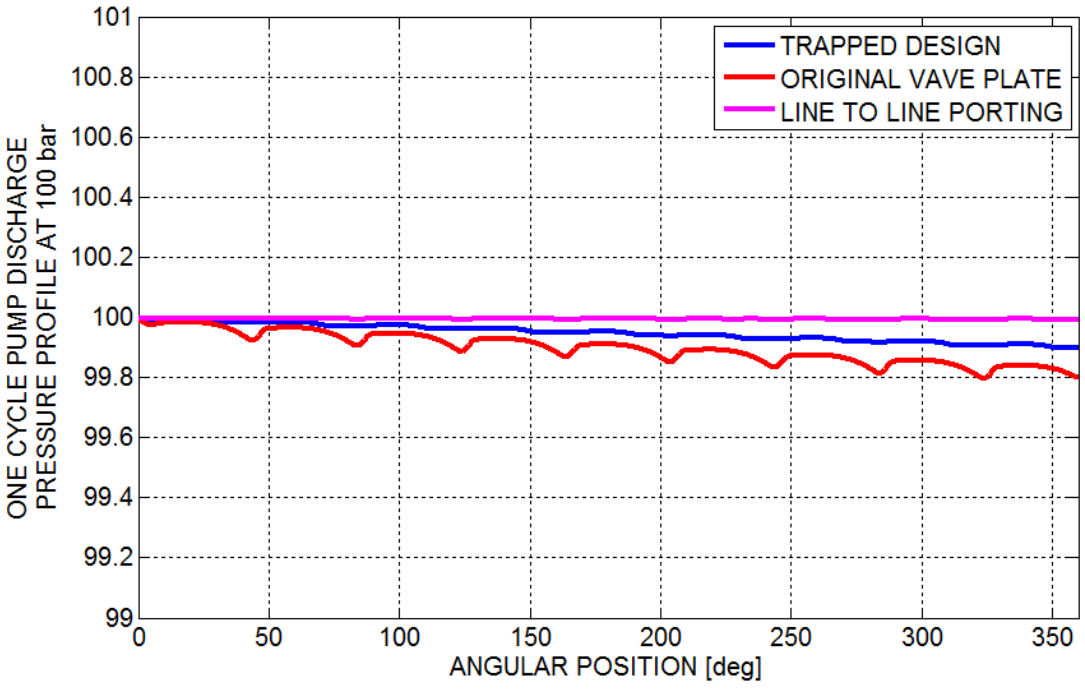

Figure 48: One cycle pump pressure profile at 100 bar

Gao utilized an attenuator in order to decrease the pressure and the flow oscillations in an aircraft pump [17]. It is shown that the maximum pressure fluctuations can be

reduced down to 80%. The relation between spring stiffness (attenuator component) and flow fluctuation amplitude is shown in this paper. Employment of the attenuator is similar to utilizing an accumulator on pressure line in industrial hydraulics. The amplitude attenuation rate is dependent on the ratio between the maximum flow rate of the pump and the attenuator volume.

4.3.8 Simulation of Multi-Piston Flow (Q_d)

One cycle delivery flow rate profile is shown in Figure 49 with same conditions given in Section 4.3.7. It is shown that instantaneous variations from the mean value, 14 lpm, are from 4 lpm to -2 lpm for the original valve plate. These instantaneous variations are reduced to 0.3 lpm in excessive flow and -0.4 lpm in insufficient flow in trapped design. In line to line porting type valve plate, these variations are reduced to 0.2 lpm in the excessive flow and -0.1 lpm in the insufficient flow.

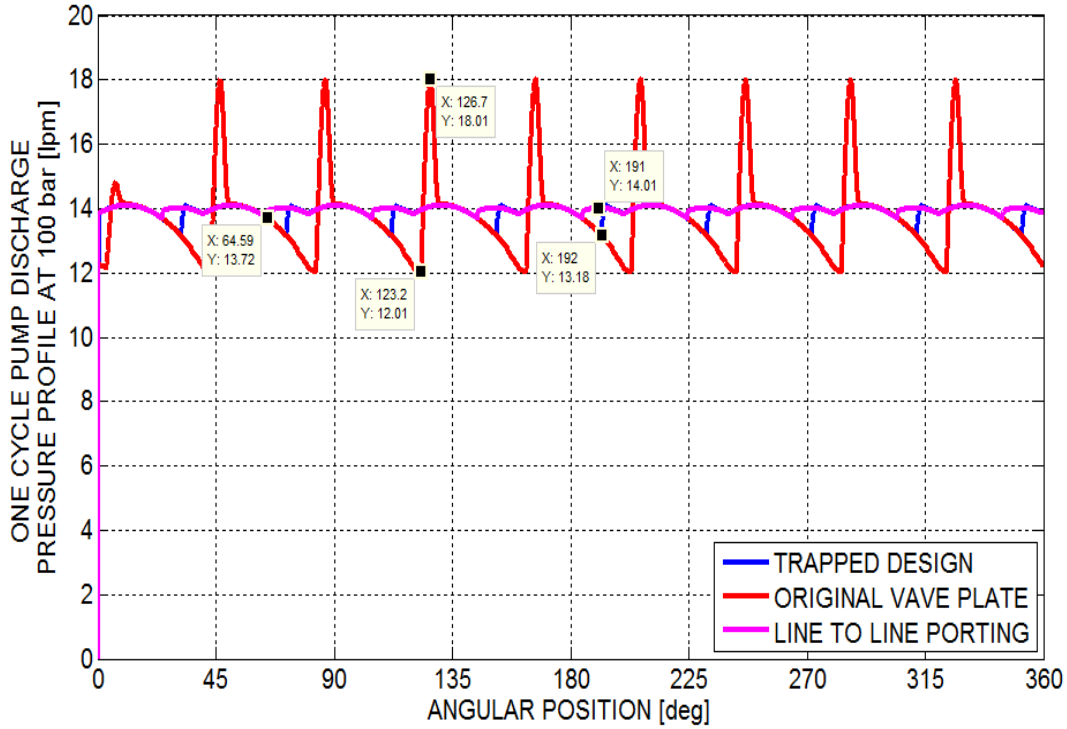

Figure 49: One cycle delivery flow rate, Q_d, profile from start-up to 100 bar

By the results of these simulations, it is shown that the delivery flow frequency is equal to the discharge pressure frequency. Similar to the discharge pressure profile

simulations, it seems that delivery flow frequency for original valve plate is different from others. It could be said that flow peak due to pressure peak is overpowering the other sources for original valve plate.

In order to deeply investigate the delivery flow, the individual delivery flow for each piston is plotted in Figure 50. Sharp variations exist in trapped valve plate at the angular displacement of a piston around 45°, 85°, 125°, etc. as shown in Figure 49. The reason of this result is shown in Figure 50 to examine individually contribution of delivery flow by each piston. The sharp variation in delivery flow for a piston increases the amplitude of delivery flow. The oscillation of instantaneous total delivery port area might be minimized in order to decrease pump delivery flow variation amplitude. The instantaneous total delivery port area is simply the summation of each pumping piston delivery area.

Ma et al [8] investigated a single cylinder and multi-cylinder model in order to present effects of cross angle and pre-compression angle on pressure peak and flow peak. This study is done on a non-over centered valve plate. The cross angle is defined as the angle between symmetry z-axis of valve plate as shown in Figure 8 and TDC by referencing cylinder block axis. Similarly, the pre-compression angle is defined as the angle between symmetry z-axis of the valve plate and BDC by referencing cylinder block axis. Model is run for various cross angles and pre-compression angles, in order to achieve best results. Although this study is very useful to optimize key parameters of the valve plate to minimize pressure peak and flow peak of the pump, no attention is paid on dynamics at rated pressure by variation of these parameters.

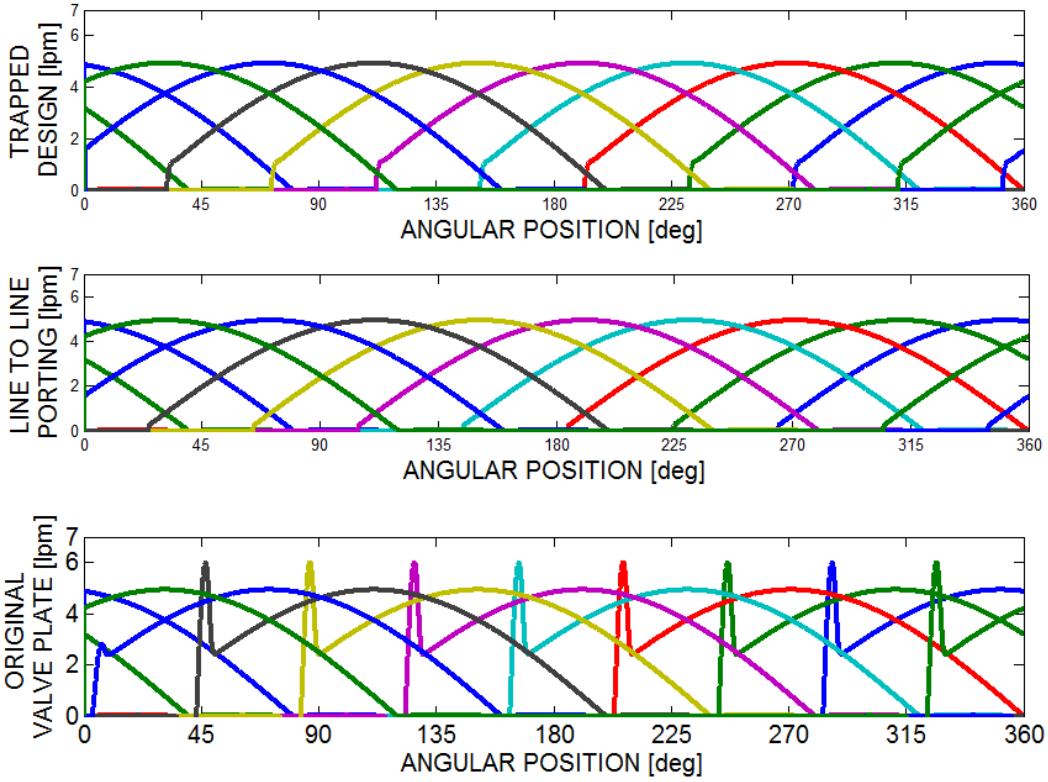

Figure 50: Individual delivery flows, Q_{di}, for each piston for various valve plate geometries from start-up to 100 bar

4.3.9 Simulation of Multi-Piston Flow, Q_d, at Rated Pressure

One cycle delivery flow rate profile is shown in Figure 51 while the discharge pressure is considered as the rated pressure.

It is shown that directions of flow peaks are different. The reason of this variation comes from different sources of the flows. Flow peaks at original valve plate and trapped design are related with the excessive pressure in the chamber of pumping piston. In contrary, flow peak at line to line porting occurs due to low pressure in the chamber of pumping piston with respect to the pressurized delivery line pressure at the closed system. Mean flow is nearly zero at each valve plates.

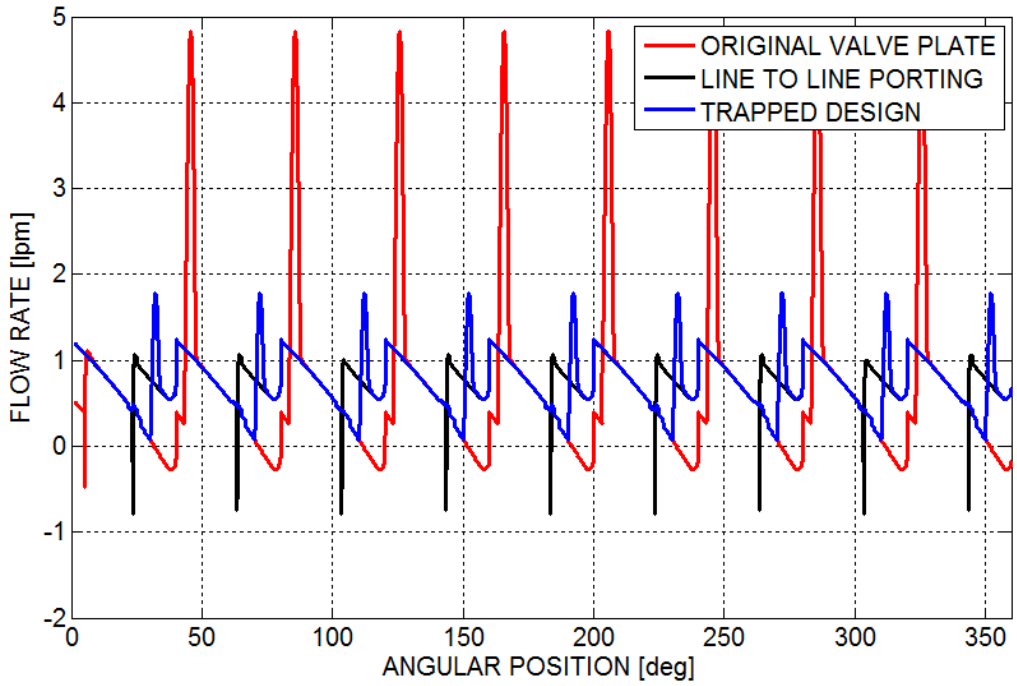

Figure 51: One cycle delivery flow rate, Q_d, profile at rated pressure, 170 bar

4.3.10 Simulation of Multi-Piston Hydraulic Torque on Swash Plate, T_y

Multi-piston model is simulated in order to calculate total hydraulic torque on swash plate due to pumping pistons with the same conditions given in the previous sections. There exists a tremendous difference in total hydraulic torque values as shown in Figure 52. Maximum hydraulic torque is shown as 9.87 N.m in the original valve plate. This value is decreased to the 2.65 N.m in valve plate with line to line porting. Minimum hydraulic torque is obtained in trapped designed valve plate as 2.53 N.m in these simulation conditions. In spite of the previous results, the best solution is reached at the trapped designed valve in given simulation conditions.

Minimizing the greatest hydraulic torque gives chance to minimize the control actuator area. Secondly, the total hydraulic torque on swash plate is always positive in Figure 52 when the discharge pressure is 100 bar. If hydraulic torque on swash plate is always positive for whole working range, this means that Equation 50 is satisfied without considering bias actuator force and pumping pistons are always trying to increase swash plate angle by itself. The bias actuator area and the control

actuator area can be decreased in order to reduce the total pump package volume, by optimization of hydraulic torque on the swash plate.

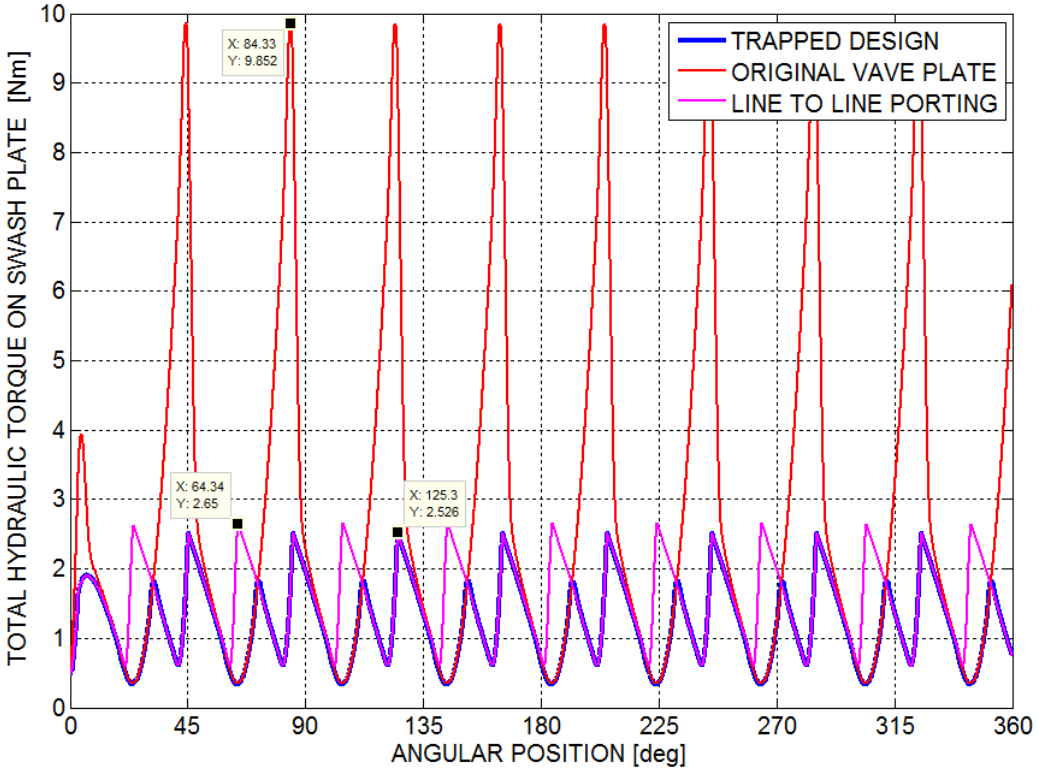

Figure 52: Total hydraulic torque on swash plate from start-up to 100 bar

In the view of these simulations, it is observed that hydraulic torque frequency is equal to the discharge pressure frequency. Similar to the discharge pressure profile simulations, it seems that hydraulic torque frequency at original valve plate is different from line to line porting and trapped design. Similar to the previous sections, torque peak is superior to other torque sources in 40° degree travel of a piston on original valve plate.

In order to deeply examine the hydraulic torque on swash plate, the individual torques of each piston are shown in Figure 53. There exists compensation of hydraulic torques on swash plate due to the mutual torque of pistons. Compensation is minimum at original valve plate, because of the individual maximum hydraulic torque is maximum at original valve plate. Although individual maximum hydraulic torque is minimum at valve plate with line to line porting, maximum total hydraulic

torque is minimum at trapped designed valve plate. This result is formed due to various valve timings. Valve timing and the length between the axis of the cylinder block and swash axis might be optimized in order to design hydraulic torque on swash plate.

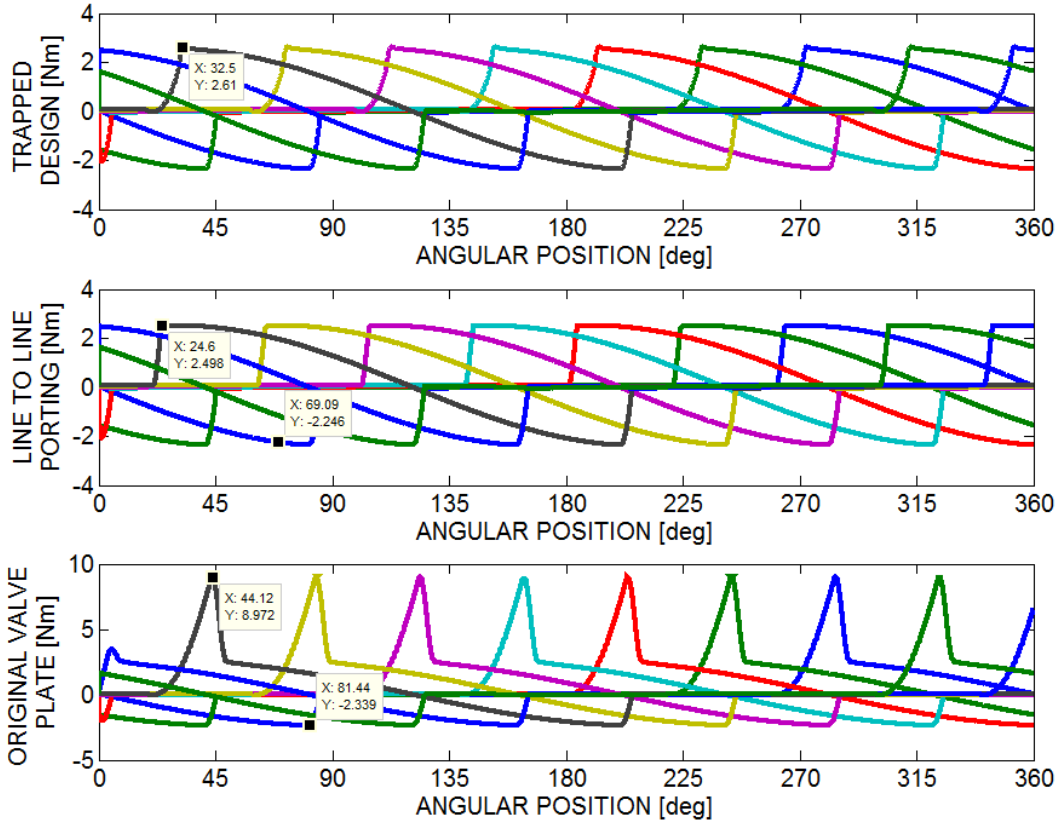

Figure 53: Individual hydraulic torque on swash plate (N.m) for various valve plate geometries at 100 bar

Manring [7] investigated that utilizing various indexing angle, δ, to alter carry-over angle. Carry-over angle, γ, is defined as the angle between z-axis on valve plate as shown in Figure 8 and beginning of discharge port at TDC with\without relief notch. The contribution of carry-over angle is presented in Equation 6.23 in [7] by averaging steady state operation variables. According to the Equation 6.23 in [7], the additional torque due to carry-over angle is linearly proportional to the magnitude of the carry-over angle. For this reason, the small values of carry-over angles are demanded. The negative indexing angle, δ, is utilized in order to reduce the carry-over angle, γ. Additional to this study, it is shown that transient torque peaks are

superior to determine pumping torque on swash plate in Figure 52 by using transient solution.

4.4 Simulations and Experimental Results

The simulations and the experiments are done in order to get the discharge pressure-delivery flow characteristics of the pump. The pump is modeled as explained in the previous sections. In order to obtain discharge pressure and delivery flow data on the entire working range of the pump, resistance on the delivery line is increased up to discharge pressure equal to the rated pressure by decreasing opening area magnitude of the needle valve. Experimental tests are done in test bench as shown in Figure 33. Similar to the simulations, the opening area of the needle valve is manually decreased down to get rated pressure on the delivery line.

4.4.1 Discharge Pressure Comparison of Test Results and Simulation Results

This test is performed with the hydraulic test circuit as shown in Figure 33. The pump suction line is pressurized to 5 bar with a booster pump. The discharge pressure data is gathered with a data acquisition at a sampling frequency of 50 kHz. The details of the data acquisition system are given in Appendix E. In this experiment and simulation, the volume between the delivery port of the pump and the load, V_{md}, is constructed as 300 cm^3. The chamber is decreased from 1000 cm^3 to 300 cm^3 to have less capacitance to visualize pressure oscillations at the delivery line clearly.

According to experimental results, the discharge pressure of the pump is approximately 48±15 bar. Oscillations of the discharge pressure are nearly at the same amplitude for both results as shown in Figure 54. The number of pressure peaks in a cycle is two times the number of piston. Although the first pressure peak is higher than the second peak in 40° degrees travel in simulation results, this condition is opposite in experimental results. The difference about discharge pressure trends is constituted due to differences in leakages related with the piston as explained in

Section 3.2.2. Although the shaft speed changes with respect to the load conditions, the shaft speed is assumed to be constant during the simulations. Due to this assumption, there exists a difference in the period of oscillations.

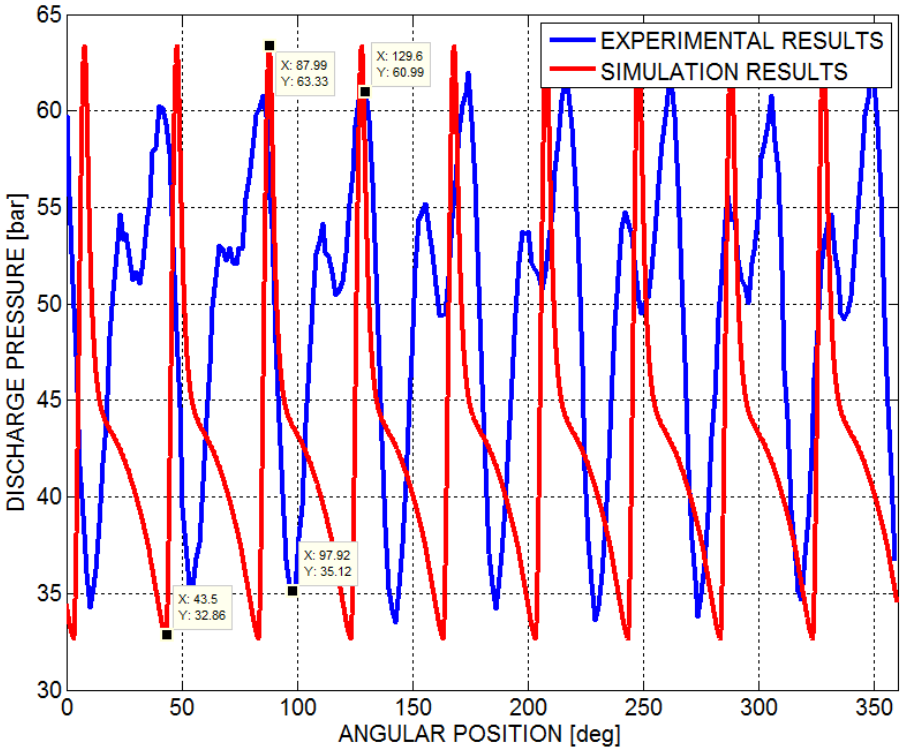

Figure 54: Discharge pressure of the pump at a cycle

4.4.2 Discharge Pressure-Delivery Flow Characteristics Comparison of Simulation Results and Experimental Results

The simulated and experimental results given in Figure 55 and Figure 56 are filtered for a window size, which is equal to the sampling frequency, 50 kHz. According to the simulation results, the maximum full-flow pressure of the pump is observed as 157.2 bar and the rated pressure is 172.8 bar. While the discharge pressure is lower than the maximum full-flow pressure, delivery flow oscillates about ±0.2 lpm in the simulation results.

Internal leakage due to increasing pressure is seen as a decrement in discharge flow rate in both cases. Additional to the pressure increment, the wear of the internal parts causes an increase of the clearances. As seen from Figure 55, internal leakages are

higher in test pump. This condition is probably formed due to wear of the internal parts. In adverse, model is run by using nominal manufacturing values.

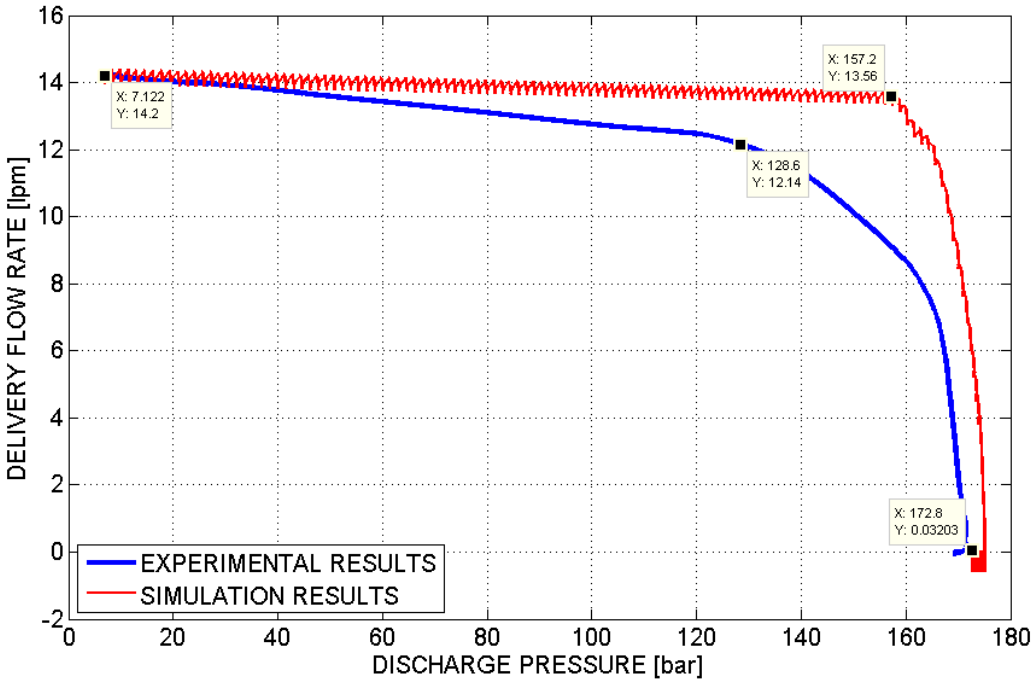

Figure 55: Pressure-flow characteristics of the pump

Although rated pressure values are approximately same in both cases, there exist differences in the maximum full-flow pressure values related with the determination of damping torque of swash plate or determination of the pressure compensation mechanism parameters.

4.4.3 Discharge Pressure-Delivery Flow Characteristics Comparison of Case Studies

In order to obtain the discharge pressure-delivery flow characteristics of various valve plated pumps, individual cases are implemented to the pump model. The attenuations of the delivery flow oscillation amplitudes for a unique discharge pressure magnitude are obtained by utilizing various cases as shown in Figure 56.

Flow rate oscillations are decreased by utilizing less trapping angle with respect to the original valve plate. This oscillation amplitude decreases to ±0.01 lpm in line to

line porting valve plates. The minimum leakage is achieved in line to line porting by obtaining smoother flow behavior as explained in Section 4.3.5. The decrease in the leakage leads to a higher flow rate at the same magnitude of discharge pressure.

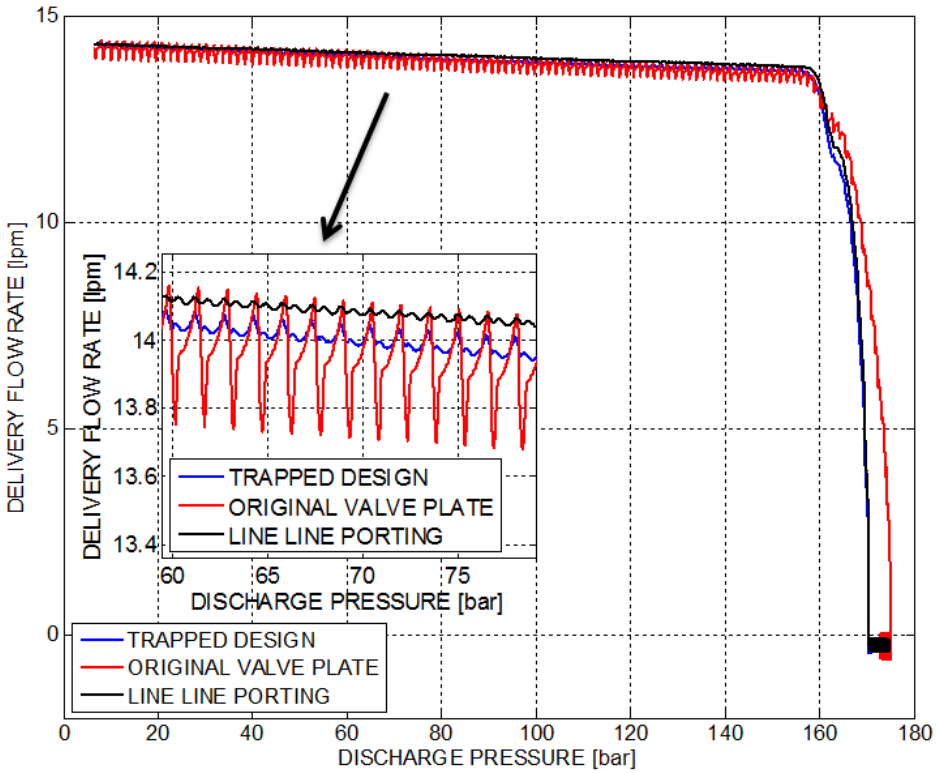

Figure 56: Discharge pressure-delivery flow characteristics curves of case studies

CHAPTER 5

SUMMARY, CONCLUSIONS, AND FUTURE WORK

5.1 Summary

In this thesis, dynamics of a pressure compensated axial piston pump is examined by deriving their linear and non-linear equations by modeling the pump in Matlab/Simulink environment. In this study, temperature variations in the hydraulic fluid are not considered. In order to obtain the discharge pressure-delivery flow characteristics of the pump, a test bench is constructed. The experimental results are compared with the simulation results. Various case studies are examined with different valve plate configurations in simulations. As a result, it is shown that the dynamic behavior of the pump can be improved by utilizing line to line porting type valve plate.

A detailed pump model is done in order to visualize the contribution of the functional components on the dynamics of the pump. Kinematics of the pumping pistons is modeled to determine the hydraulic torque on the swash plate. The hydraulic torque on the swash plate is studied by consideration of the pressure forces, the inertial forces, and the frictional forces. It is shown that dominant part of these sources is the pressure forces on the piston. The instantaneous pressure inside the pumping piston chamber is calculated by considering the piston kinematics, and the flow into and out of this volume. Within the pressure calculations, the compressibility of the hydraulic fluid is also taken into consideration.

Moving parts of the three-way valve are modeled as a simple spring-mass system. The valve activates the control spool by allowing flow into the control chamber when

the discharge pressure is higher than the maximum full-flow pressure. This flow allowed by the control spool increases the pressure in the control chamber. The rise in the pressure activates the control actuator which increases the negative torque exerted on the swash plate. When the resultant torque on the swash plate becomes negative, the swash plate tends to decrease the swash plate angle. By this motion, swept volume of the pump is minimized which results in a decrease in the delivery flow. In other words, pressure build-up capacity is limited by decreasing the delivery flow.

Leakage paths related with the pumping pistons, the three-way valve, the bias actuator, and the control actuator are modeled to obtain total internal leakage of the pump. The most significant leakage path is determined in order to handle the internal leakage problem more effectively.

5.2 Conclusions

As a result, it is possible to obtain the discharge pressure-delivery flow characteristics and internal dynamics of a newly designed pump. Different configurations can be implementable to the simulation model to analyze the effects of these variations on discharge pressure-delivery flow characteristics and internal dynamics of a new pump. The simulation model gives chance to a designer to project the pump dynamics for a given set of parameters, for example, the loads on the swash plate bearings, loads on the cylinder block bearings, and required input torque from the prime mover. By inverse approach, it is possible to determine the design parameters for a set of operational requirements. It is easy to design geometry of internal parts by using the parametric model.

It is shown that the amplitudes of the pressure oscillations are similar in simulated and experimental results. The simulation results show that utilizing various valve plate configurations can improve pressure oscillations in the delivery line as expected. The attenuation of the discharge pressure oscillations minimizes the oscillations amplitude of the delivery flow rate. In some applications where the control valve is mounted on the pump, minimizing the amplitude of the discharge

pressure oscillations is essential to control the actuator position precisely. In applications where the control valve is connected to the pump by a long piping, the discharge pressure oscillations cause fatigue in the pipes. This condition acts as a source of failure.

Although the rated pressure of the original pump is approximately 170 bar for the test pump, the instantaneous pressure of the pumping piston chamber can be much higher than the rated pressure. This study shows that the maximum pressure on the pumping piston can be nearly four times of the discharge pressure at original pump design. The peak pressure can be eliminated by utilizing line to line porting designated valve plate. Pressurizing piston chamber above the rated pressure causes wear problems especially on the cylinder block and pumping pistons.

Another outcome of the simulation results is that the resultant hydraulic torque on swash plate can be decreased by utilizing trapped or line to line porting designated valve plate. Reducing the maximum hydraulic torque on swash plate decreases the required control torque which changes swash plate angle. Smaller required control torque gives a possibility to employ smaller control actuator area which enables the designer to use a smaller volume for the pump.

In this study, discharge pressure oscillations of the pump are decreased by employing line to line porting valve plate instead of utilizing original valve plate. Internal leakage of the pump is decreased by smoother pressure regime acting on the components of the pump. This improvement increases the magnitude of the delivery flow rate for thr entire working range.

5.3 Future Work

Although the pump has been modeled down to the component level, the experiments have been performed on the pump as a whole. As a continuation of this work, the subcomponents of the pump can be experimentally verified in order to verify the entire simulation model.

The simulated case studies regarding the valve plate configurations in this thesis can be physically manufactured and tested. Experimental work on the case studies will give chance to cross-check the simulation results considering the whole pump model. For example, the pressure in the pumping piston chamber can be measured to compare with the simulation results. A single piston test bench can be constructed in order to measure various leakage paths to verify the simulation models.

The simulation model can be enhanced to include various numbers of pumping pistons, like 7, 11, 13.

REFERENCES

[1] Yücel, E., "Akışkan Gücü Kontrolü Teorisi", 1st Ed., Gazi University, Ankara, 1995.

[2] Manring, N.D., "Designing the Shaft Diameter for Acceptable Levels of Stress Within Axial-Piston Swash-Plate Type Hydrostatic Pump," Journal of Mechanical Design, vol. 122, pp. 553-559, 2000.

[3] Lewis, E., Stern, H., Design of Hydraulic Control, 1st Ed., McGraw-Hil Company Inc, New York & London, 1962.

[4] Blackburn, J.F., Reethof, G., and Shearer, J.L., Fluid Power Control, 1st Ed., MIT Press and John Wiley & Sons Inc., New York & London, 1960.

[5] Ivantsyn, J., Ivantsynova, M., Hydrostatic Pumps and Motors, 1st English Ed., Akademia Books International, New Delhi, 2001.

[6] Watton, J., Fundamentals of Fluid Power Control, 1st Ed., Cambridge University Press, Cambridge, 2009.

[7] Manring, N.D., Fluid Power Pumps & Motors, 1st Ed., Mc Graw Hill Education, New York, 2013.

[8] Ma, J., Fang, Y., Xu, B., Yang, H., "Optimization of cross angle based on the pumping dynamics model," Journal of Zhejiang University-Sci A (Appl. Phys. & Eng.), vol. 3, pp. 181-190, 2010.

[9] Parker Company, "Hydraulic Pump Basics," 02.02.2018.

[10] "IS0 8278 - Aerospace - Hydraulic, pressure compensated, variable delivery pumps - General requirements". 1986.

[11] Parker Hannifin, Pump & Motor Division Europe, "Axial Piston Pumps (HY30-32-3245/UK)," Chemnitz, Germany, 20215.

[12] Bosch Rexroth AG Mobile Applications, "Axial Piston Variable Pump A4VG," Elchingen, 2012.

[13] Kim, S.D., Cho, H.S., Lee , C.O., "A Parameter Sensitivity Analysis for the Dynamic Model of a Variable Displacement Axial Piston Pump," Proceedings of the Institution of Mechanical Engineers, vol. 201, pp. 235-243, 1987.

[14] Schoenau, G., Burton, R., Kavanagh, G., "Dynamic Analysis of a Variable Displacement Pump," Journal of Dynamic Systems, Measurement, and Control, vol. 112, pp. 122-131, 1990.

[15] Manring, N.D., "Valve-Plate Design for an Axial Piston Pump Operating at Low Displacements," Journal of Mechanical Design, vol. 125, pp. 200 - 207, 2013.

[16] Manring, N. D., Dong, Z., "The Impact of Using a Secondary Swash-Plate Angle Within an Axial Piston Pump," Journal of Dynamic Systems,

Measurement, and Control, vol. 126, pp. 65-74, 2004.

[17] Gao, F., Ouyang, X., Yang, H., Xu, X., "A novel pulsation attenuator for aircraft piston pump," Mechatronics, pp. 566-572, 2013.

[18] Manring, N. D., "Measuring Pump Efficiency: Uncertainty Considerations," Journal of Energy Resources Technology, vol. 127, pp. 280-284, 2005.

[19] Bergada, J.M., Kumar, S., Davies, D.LI., Watton, J., "A complete analysis of axial piston pump leakage and output flow ripples," Applied Mathematical Modelling, pp. 1731-1751, 2012.

[20] Bergada, J.M., Davies, D.J., Kumar, S., Watton, J., "The effect of oil pressure and temperature on barrel film thickness and barrel dynamics of an axial piston pump," Meccanica, pp. 639-654, 2012.

[21] Meyer, D., "Reynolds Equation for spherical bearings," vol. 125, pp. 203-206, 2003.

[22] Manring, N. D., Wray, C.L., Dong Z., "Experimental Studies on the Performance of Slipper Bearings Within Axial-Piston Pumps," Journal of Tribology, vol. 126, pp. 511-518, 2004.

[23] Eaton, "220 Piston Pump Service Manual E-PUMC-RR001-E2," February 2014.

[24] Kavanagh, G.P., "The Dynamic Modelling of an Axial Piston Hydraulic Pump," University of Saskatchewan, 1987.

[25] Likos, W. E., "Hydraulic Test Loop For Nonflammable Hydraulic Fluid," Southwest Research Institute, San Antonio, 1998.

[26] Manring, N. D., "The Improved Volumetric-Efficiency of an Axial-Piston Pump Utilizing a Trapped-Volume Design," Journal of Dynamic Systems, Measurement, and Control, vol. 123, pp. 479 - 487, 2001.

[27] Xu, B., Zhang, J., Yang, H., "Simulation research on distribution method of axial piston utilizing pressure equalization mechanism," Journal of Mechanical Engineering Science, vol. 227, pp. 459-469, 2012.

[28] Manring, N.D., "Tipping the Cylinder Block of an Axial-Piston Swash-Plate Type Hydrostatic Machine," Journal of Dynamic Systems, Measurement, and Control, vol. 122, pp. 216 - 221, 2000.

[29] Manring, N. D., "Scaling the Speed Limitations for Axial-Piston Swash-Plate Type Hydrostatic Machines," Journal of Dynamic Systems, Measurement, and Control, vol. 136, pp. 1-8, 2014.

[30] Mandal, N.P., Saha, R., Mookherjee, S., and Sanyal, D., "Pressure Compensator Design for a Swash Plate Axial Piston Pump," Journal of Dynamic Systems, Measurement, and Control, vol. 136, pp. 1-12, 2014.

[31] Merritt, H. E., Hydraulic Control Systems, New York, London, Sydney: John Wiley & Sons, Inc, 1967.

[32] Ivantysynova, M., "Design and Modeling of Fluid Power Systems Lecture 12," Indiana, 02.02.2018.

[33] Manring, N. D., Johnson, R. E., "Swivel Torque within a Variable-Displacement Pump," in Proceedings of the 46th National Conference on Fluid Power, Milwaukee, 1994.

[34] Manring, N.D., Johnson, R.E., "Modeling and Designing a Variable-Displacement Open-Loop Pump," Journal of Dynamic Systems, Measurement, and Control, vol. 118, pp. 267-271, 1996.

[35] Manring, N. D., "The Control and Containment Forces on the Swash Plate of an Axial Piston Pump," Journal of Dynamic Systems, Measurements, and Control, vol. 121, pp. 599-605, 1999.

[36] Zhang, X., Cho, J., Nair S.S., Manring N.D., "New Swash Plate Damping Model for Hydraulic Axial-Piston Pump," vol. 123, pp. 463-470, 2001.

[37] Mandal, N.P., Saha, R., Sanyal, D., "Design and Performance Analysis of a Pressure Compensator for a Swash Plate Type Variable Displacement Axial Piston Pump," in Proceedings of the 37th National & 4th International Conference on Fluid Mechanics and Fluid Power, Chennai, 2010.

[38] "Hypertextbook,"[Online].Available: https://hypertextbook.com/facts/1998/RobertSaronson.shtml.[Accessed 11.02.2018].

[39] Changbin, G., Zongxia J., Shouzhan, H., "Theoretical study of flow ripple for an aviation axial-piston pump with damping holes in the valve plate," Chinese Journal of Aeronautics, vol. 27, pp. 169-181, 2013.

APPENDICES

A. Matlab/Simulink Model of the Cylinder Block (Single Piston)

Matlab/Simulink model of the cylinder block for a single piston is given in Figure A.1.

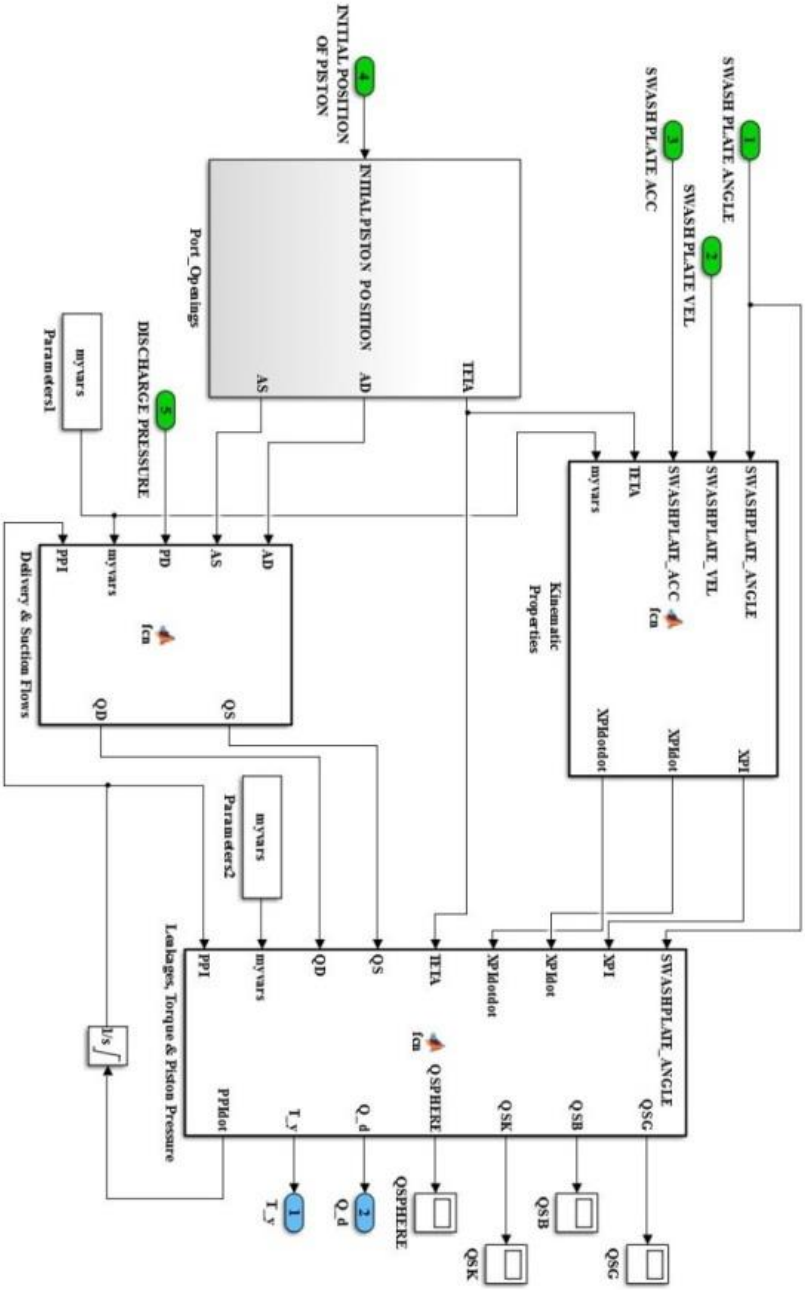

Figure A.1: Matlab/Simulink model of cylinder block (single piston)

B. Matlab/Simulink Model of the Compensation Section

Matlab/Simulink model of the compensation section is given in Figure B.1.

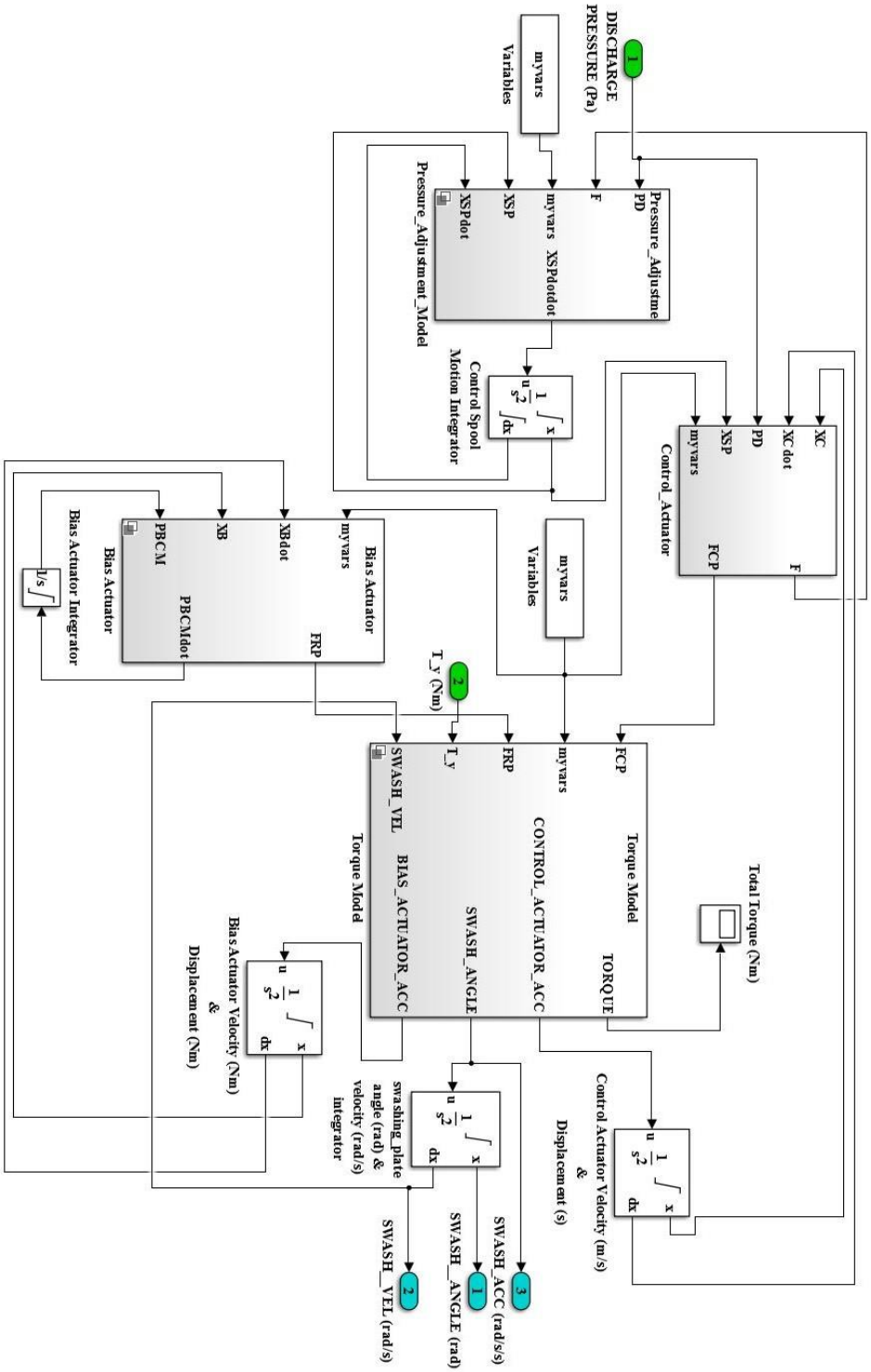

Figure B.1: Matlab/Simulink model of the compensation section

C. Matlab/Simulink Model of the Test Bench

Matlab/Simulink model of the test bench is given in Figure C.1.

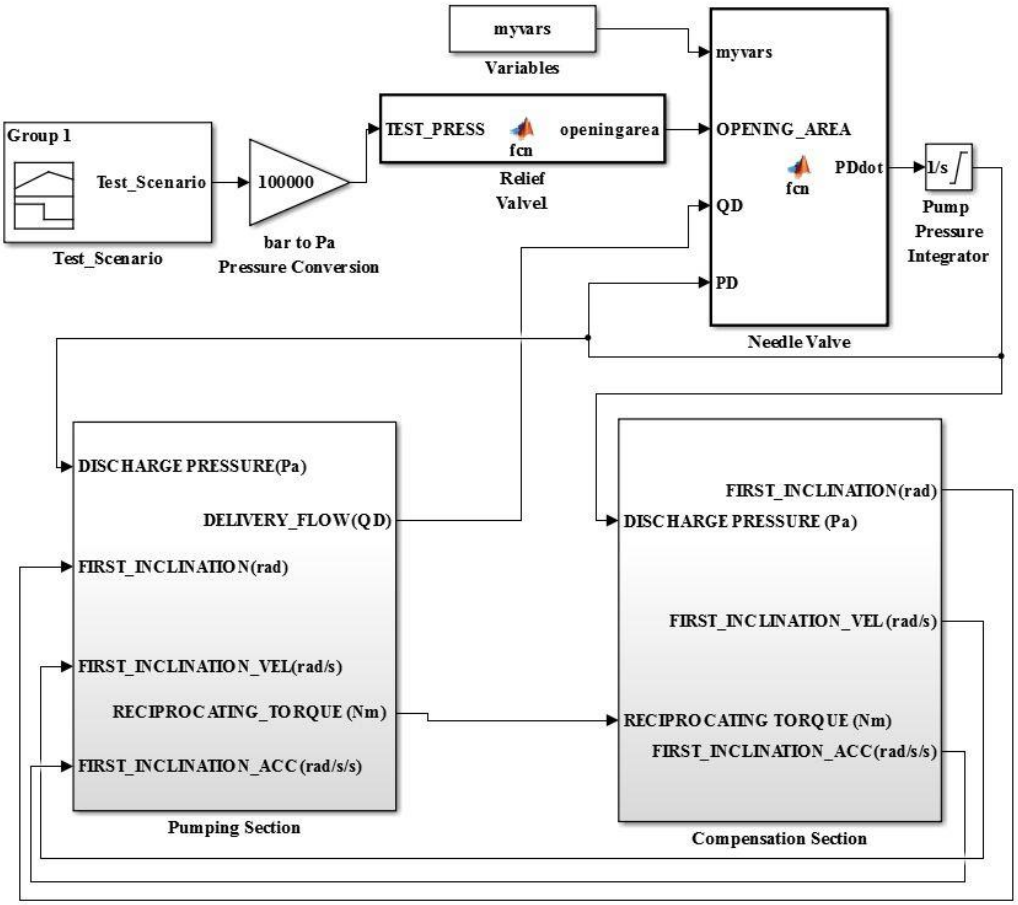

Figure C.1: Matlab/Simulink model of the test bench

D. Technical Properties of the Test Bench

A simple hydraulic test unit is used in order to pressurize the suction and drain line of the pump. PRH082K10N coded pressure reducing valve (manuf. PARKER company) is used to control the inlet pressure of the test pump. Technical details of the needle valve are shown in Figure D.1. Hoses used in the test system are produced according to the SAE 100R16. Dash size of the hoses is 5. 10-L fittings according to the ISO 8434-1 are used in order to join the components. Stainless steel tubes are used in delivery line whose material number is 1.4571. Outer and inner diameters of the tubes are 10 mm and 8 mm, respectively. XPC10 coded pressure sensor (manuf. TE Connectivity company) is used to measure discharge line pressure. Technical details of the pressure sensor are shown in Table D.1. VS 10 coded flowmeter (manuf. VSE company) is used to measure delivery flow. Technical details of the flowmeter are shown in Table D.2. J02A2ZN coded needle valve (manuf. PARKER company) is employed in order to load the pump. Technical details of the needle valve are shown in Figure D.2.

Table D.1: Performance specifications of the pressure sensor (XPC 10)

Parameters	Non amplified [1]	A1	Notes
Power supply	1 to 10 Vdc regulated	10 to 30 Vdc	
Sensitivity "FSO"	See previous table	4 V ±0.2 V	Signal 0.5 - 4.5V for A1 option
Zero Offset	±1 mV	0.5 V ±0.2 V	
Combined Non-Linearity & Hysteresis	±0.5%FS ±0.3%FS ±0.25%FS		FS ≤ 10 bar 10 bar < FS < 100 bar 100 bar ≤ FS
Operating Temperature (OTR)	-40 to 220°C (-40 to 428°F)	-40°C to 120°C (-40°F to 250°F)	
Compensated Temperature (CTR)	0 to 150°C (32 to 300°F)	0 to 80°C (32°F to 170°F)	
Thermal Zero Shift in CTR (TZS)	< ±1%FS/50°C		
Thermal Sensitivity Shift in CTR (TSS)	< ±1% of reading /50°C		
Input Impedance or consumption	500 Ω nom.	< 50 mA	
Output Impedance	350 Ω nom.	1000 Ω	
Ingress Protection	IP50 IP67		Standard or SC option P7 option
Media – Pressure Port	Fluids compatible with stainless steel		

Table D.2: Performance specifications of the flowmeter (VS 10)

Accuracy	± 0.3 % of measured value at viscosity > 20 cSt (< 20 cSt reduced accuracy)		
Repeatability	± 0.05 % under same operating conditions		
Materials	**Body** EN-GJS-400-15 (EN 1563) Stainless Steel 1.4305	**Bearings** Ball / Plain / Plain (Copper-free) depend on liquid	**Seals** FPM (standard) NBR, PTFE, EPDM
Max. operating pressures	**Cast iron** 315 bar/4,568 psi	**Stainless steel** 450 bar / 6,526 psi	
Medium temperature	Standard Ex-design High temperature	–40 ≤ ... 120° C –20 ≤ ... 100° C –40 ≤ ... 210° C	
Viscosity ranges	1...100,000 cSt		
Mounting positions	Unrestricted, on subplate with side or bottom connections		
Filtering for ball bearing type	VS 0.02/0.04/0.1 10 µm VS 0.2/0.4 20 µm VS 1/2 50 µm VS 4 50 µm	**Exceptions** Flow meters with special clearance on request.	
Noise level	Max. 72 dB(A)		
Preamplifier	10 to 28 Volt (DC)		

General Description

Pilot Operated Pressure Reducing Valve. For additional information see Technical Tips on pages PC1-PC6.

Features

- Hardened, precision ground parts for durability
- Low profile adapter for minimal space requirements
- Fully guided pilot for more consistent reseat
- Steel adapters are coated with yellow zinc dichromate for protection from salt spray
- Polyurethane "D"-Ring eliminates backup rings and prevents hydrolysis
- Internal screening protects pilot spring from debris

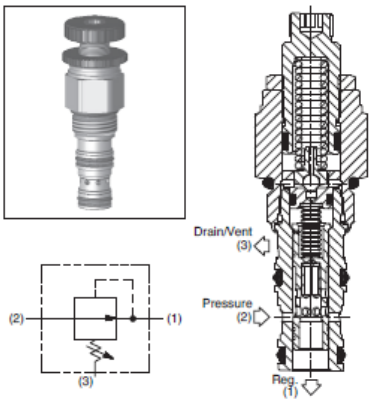

Specifications

Rated Flow	30 LPM (8 GPM)
Maximum Inlet Pressure	380 Bar (5500 PSI)
Maximum Pressure Setting	350 Bar (5000 PSI)
Maximum Tank Pressure	350 Bar (5000 PSI)
Maximum Drain Flow	0.56 LPM (0.15 GPM)
Cartridge Material	All parts steel. All operating parts hardened steel.
Operating Temp. Range/Seals	-45°C to +93.3°C ("D"-Ring) (-50°F to +200°F) -31.7°C to +121.1°C (Fluorocarbon) (-25°F to +250°F)
Fluid Campatibility/ Viscosity	Mineral-based or synthetic with lubricating properties at viscosities of 45 to 2000 SSU (6 to 420 cSt)
Filtration	ISO Code 16/13, SAE Class 4 or better
Approx. Weight	.11 kg (.25 lbs.)
Cavity	C08-3 (See BC Section for more details)
Form Tool	Rougher NTF08-3R Finisher NFT08-3F

Performance Curves

Flow vs. Pressure (Through cartridge only)

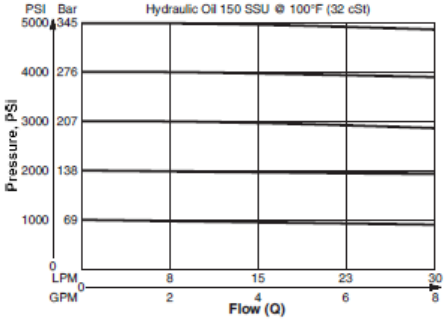

Flow vs. Pressure Drop (Through cartridge only)

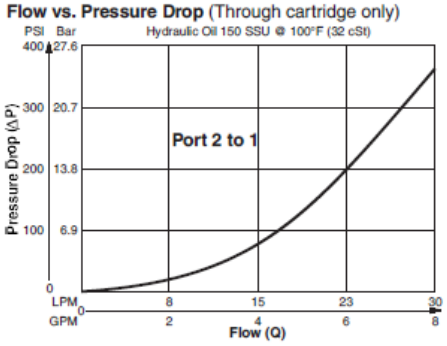

Figure D.1: Performance specifications of the pressure reducing valve (PRH082K10N)

General Description

Cartridge Style Needle Valve. For additional information see Technical Tips on pages FC1-FC4.

Features

- Shuts off to a very low leakage level
- High flow capacity from a small cavity
- Good adjustment sensitivity - ideal for fine control
- Good contamination tolerant
- Adjustable and tamperproof versions available
- All external parts zinc plated

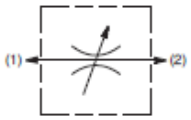

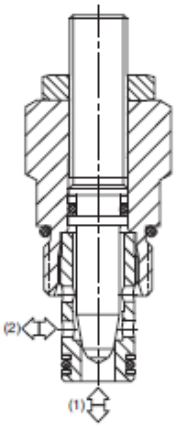

Specifications

Rated Flow	45 LPM (12 GPM)
Maximum Inlet Pressure	420 Bar (6000 PSI)
Cartridge Material	All parts steel. All operating parts hardened steel.
Operating Temp. Range/Seals	-40°C to +93.3°C (Nitrile) (-40°F to +200°F) -31.7°C to +121.1°C (Fluorocarbon) (-25°F to +250°F)
Fluid Compatibility/ Viscosity	Mineral-based or synthetic with lubricating properties at viscosities of 45 to 2000 SSU (6 to 420 cSt)
Filtration	ISO Code 16/13, SAE Class 4 or better
Approx. Weight	.11 kg (.24 lbs.)
Cavity	C08-2 (See BC Section for more details)
Form Tool	Rougher None Finisher NFT08-2F

Performance Curves (Through cartridge only)

Low Pressure Drop vs. Flow 1 to 2 & 2 to 1

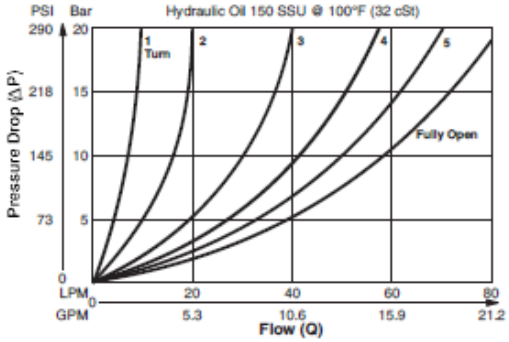

High Pressure Drop vs. Flow 1 to 2 & 2 to 1

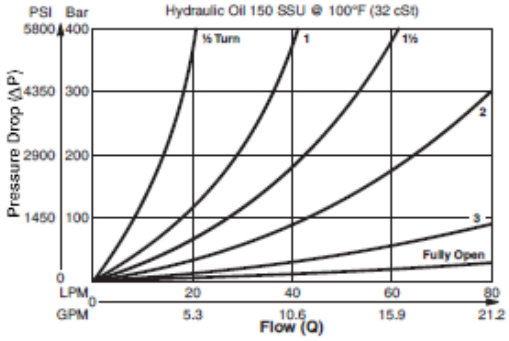

Figure D.2: Performance specifications of the needle valve (J02A2ZN)

E. Data Acquisition System Hardware

For data acquisition, National Instruments (NI) products are used to measure data. It is important to mention that measurements are saved at 50 kHz with NI components. NI 9188 chassis tool is used to collect data taken from I/O modules. Maximum input or output frequency of this tool is 1 MHz. This property is much higher than the sampling frequency of experiments, 50 kHz. Timing resolution of this component is 12.5 ns and timing resolution is 50 ppm of sample rate. NI 9218 is built-in support for voltage measurements. In the experiments, this module is used in order to gather data taken from pressure sensor. This tool can collect data up to 13.1072 MHz. SEG 1060 tool, is produced by Hydrotechnik, is used to convert PWM data taken from flowmeter, VS 10, to the voltage output. The scan rate of this tool is limited with 100 Hz. Because limitation of this component, flow measurements are taken up to 100 Hz. NI 9215 tool is preferred in order to measure data taken from SEG 1060.